Synthetic studies towards benzo-RvD1$_{n\text{-}3\ DPA}$

Nora Dotterud Lerstad

Thesis for the degree Master of Pharmacy

45 credits

Section for Pharmaceutical Chemistry

Department of Pharmacy

Faculty of Mathematics and Natural Sciences

UNIVERSITY OF OSLO

May 2020

Synthetic studies towards benzo-RvD1$_{n\text{-}3\ DPA}$

Nora Dotterud Lerstad

Thesis for the degree Master of Pharmacy

45 credits

Department of Pharmacy

Faculty of Mathematics and Natural Sciences

UNIVERSITY OF OSLO

May 2020

2020

Synthetic studies towards benzo-RvD1$_{n\text{-}3\ DPA}$

Nora Dotterud Lerstad

http://www.duo.uio.no/

Acknowledgements

This thesis has been based on the work I have done spanning from August 2019 to May 2020, during my master degree in Pharmaceutical Chemistry, Department of Pharmacy, University of Oslo.

I would like to express my deepest appreciation to Professor Trond Vidar Hansen and Associate professor Anders Vik for allowing me to take part in such an inspiring academic group, the LIPCHEM group. A special thank you to my supervisors Professor Trond Vidar Hansen, Associate professor Anders Vik and Master of Pharmacy Amalie Føreid Reinertsen. Thank you for sharing your knowledge and being an inspiration during this year, and thank you for all the time you have spent proofreading my work.

A special mention goes to Dr. Jørn E. Tungen and Master of Pharmacy Amalie Føreid Reinertsen for doing the work that this thesis is based on. A big thank you goes to Master of Pharmacy Amalie Føreid Reinertsen and Dr. Karoline Primdahl. Master of Pharmacy Amalie Føreid Reinertsen has been of great help with my work in the lab and with my writing. Dr. Karoline Primdahl has been of great help in teaching me lab techniques and answering all my questions. I have really enjoyed the time I have spent in the lab. I would really like to thank all the members of the LIPCHEM group for all the help you have provided, and for a great working environment. I really enjoyed being a part of your group.

Finally, I would like to thank my family and my partner Magnus Hagelund, who has truly been a great support during this year. I could not have done it without any of you.

Oslo, May 2020

Nora Dotterud Lerstad

Abstract

The focus of this thesis has been to develop a total synthesis of benzo-RvD1$_{n\text{-}3\ DPA}$, which is an analog of the specialized pro-resolving lipid mediator (SPM) named RvD1$_{n\text{-}3\ DPA}$.

The synthetic methods towards the α-fragment of benzo-RvD1$_{n\text{-}3\ DPA}$ are based on previously published work performed by the LIPCHEM group. New reactions introduced in this thesis work include a Tebbe olefination reaction to yield a terminal alkene, a Heck-Mizoroki reaction to insert the benzo-group, and a Barbier reaction to afford an acetylene in the molecule.

Inflammation is the body`s natural protective response to injury and invading pathogens. Resolution of inflammation is an active process, governed by SPMs. Both biological and synthesized SPMs exert potent anti-inflammatory and pro-resolving actions in inflammation, by ceasing the infiltration of polymorphonuclear leukocytes, increasing macrophage efferocytosis and phagocytosis and promoting tissue repair. They are able to resolve inflammation without suppressing the immune response. Therefore, these pro-resolving mediators could potentially be a new wave in treatment of certain inflammatory diseases, such as neurodegenerative diseases, asthma, atherosclerosis and rheumatoid arthritis.

Unfortunately, due to the limited timeframe for this study, and the Covid-19 situation, a total synthesis was not completed. The work reported in this thesis may be the fundament for further synthetic studies towards making benzo-analogs of RvD1$_{n\text{-}3\ DPA}$.

Graphical abstract

Synthesis of the α-fragment

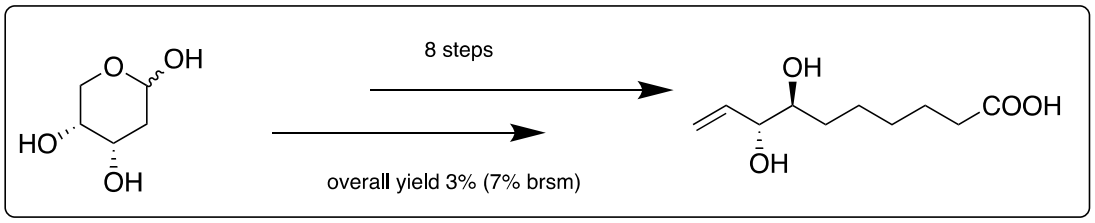

Completion of the total synthesis

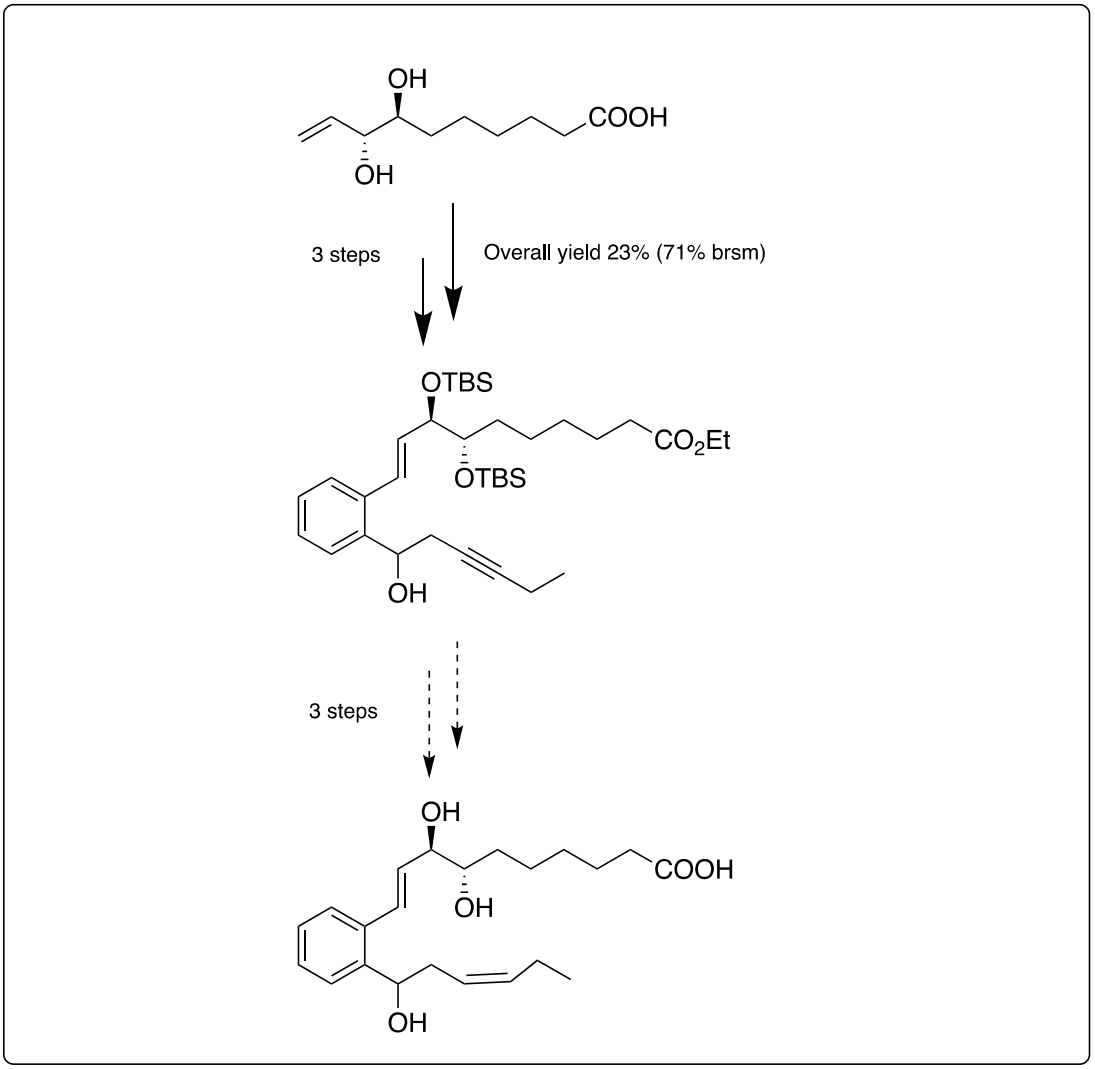

List of abbreviations

AA	arachidonic acid
ALA	alpha-linoleic acid
ALX/FPR2	lipoxin A_4 receptor
AT	aspirin-triggered
BLT1	leukotriene B_4 receptor 1
brsm	based on recovered starting material
CAM	cerium-ammonium-molybdate
CC	chemokine proteins with two adjacent cysteines
ChemR23/ERV1	resolvin E1 receptor
COX	cyclooxygenase
CXC	chemokine proteins with an amino acid between two cysteines
DAMP	disease-associated molecular pattern
DHA	docosahexaenoic acid
DMARD	disease-modifying anti-rheumatic drug
DMP	Dess-Martin periodinane
DRV1/GPR32	resolvin D1 receptor
DRV2/GPR18	resolvin D2 receptor
EC_{50}	half maximal effective concentration
EPA	eicosapentaenoic acid
ERV/ChemR23	resolvin E1 receptor
Et_2O	diethyl ether
Et_3N	triethylamine

EtOAc	ethyl acetate
EtSH	ethanethiol
GPCR/GPR	G-protein coupled receptor
HPLC	high-performance liquid chromatography
HRMS	high-resolution mass spectrometry
ICAM-1	intercellular adhesion molecule-1
IL-6	interleukin-6
K_d	dissociation constant
LA	linoleic acid
LOX	lipoxygenase
LT	leukotriene
LX	lipoxin
Mac-1	macrophage-1 antigen
MaR	maresin
MCTR	maresin conjugates in tissue regeneration
MeOH	methanol
MS	mass spectrum
n-3 DPA	n-3 docosapentaenoic acid
NAHMDS	sodium *bis*(trimethylsilyl)amide
NBS	*N*-bromosuccinimide
NF-κB	nuclear factor κ B
NO	nitrogen oxide
NPD1/PD1	neuroprotectin D1
NSAIDs	non-steroidal anti-inflammatory drugs

o(tolyl)$_3$P	*tri*-(*o*-tolyl) phosphine
Pael-R/GPR37	protectin D1 receptor
PCTR	protectin conjugates in tissue regeneration
PAMP	pathogen-associated molecular pattern
PD	protectin
PG	prostaglandin
PGI_2	prostacyclin
PLA_2	phospholipase A_2
PMN	polymorphonuclear leukocytes
PPM	parts per million
PRR	pattern recognition receptor
PTSA	*p*-toluenesulfonic acid
PUFA	polyunsaturated fatty acid
RCTR	resolvin conjugates in tissue regeneration
R_f	retardation factor
ROS	reactive oxygen species
RT	room temperature
RvD	resolvin of the D-series
RvE	resolvin of the E-series
RvT	13-series resolvins
SAR	structure-activity relationship
SPM	specialized pro-resolving mediator
TBAF	tetra-n-butylammonium fluoride
TBSOTf	*tert*-Butyldimethylsilyl triflate

THF	tetrahydrofuran
TLC	thin layer chromatography
TLR	toll-like receptor
TNFα	tumor necrosis factor α
TRPV	transient receptor potential V
TXA	thromboxane

Table of Contents

1 Introduction

1.1 Aim of study

The aim of this master thesis was to synthesize benzo-RvD1$_{n\text{-}3\ DPA}$ (Figure 1), a synthetic analog of the specialized pro-resolving lipid mediator (SPM) RvD1$_{n\text{-}3\ DPA}$. Benzo-RvD1$_{n\text{-}3\ DPA}$ holds a benzo-fused ring system, instead of the *E,E,Z,E*-tetraene moiety present in RvD1$_{n\text{-}3\ DPA}$. Benzo-RvD1$_{n\text{-}3\ DPA}$ is considered a chemically more stable analog of RvD1$_{n\text{-}3\ DPA}$, because the *E,E,Z,E*-tetraene bond moiety in RvD1$_{n\text{-}3\ DPA}$ is susceptible to isomerization when exposed to light, heat and acids.[1] The benzo-group mimics the *E,Z,E*-triene of the mentioned tetraene. This analog is easier to prepare and will give the compound increased chemical stability, as well as reduced metabolism, as was seen with the benzo-lipoxin A$_4$ analogs synthesized by Petasis *et al*.[2]

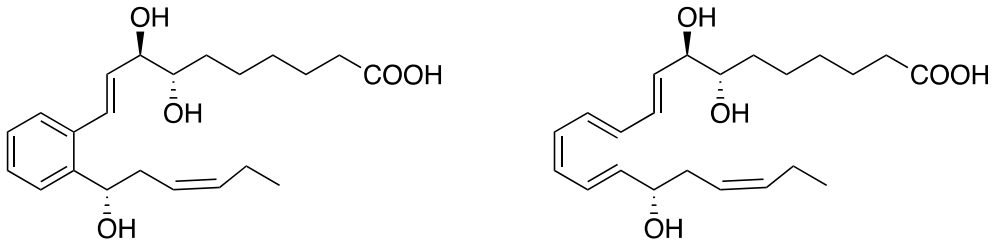

Benzo-RvD1$_{n\text{-}3\ DPA}$ (**1**) RvD1$_{n\text{-}3\ DPA}$ (**2**)

Figure 1: The structures of benzo-RvD1$_{n\text{-}3\ DPA}$ and the biological compound RvD1$_{n\text{-}3\ DPA}$.[3, 4]

In 2019, Reinertsen tried to prepare benzo-RvD1$_{n\text{-}3\ DPA}$, and was not far from the goal.[5] The studies presented in this thesis are based on the synthetic strategies used by Tungen *et al*.[3] to make RvD1$_{n\text{-}3\ DPA}$, which was further developed by Reinertsen in her efforts in synthesizing the benzo-RvD1$_{n\text{-}3\ DPA}$ analog.[5]

It is of interest to synthesize benzo-RvD1$_{n\text{-}3\ DPA}$ in order to investigate if this analog displays similar biological activities as RvD1$_{n\text{-}3\ DPA}$. Hence, when available, benzo-RvD1$_{n\text{-}3\ DPA}$ will be subjected to *in vitro* studies and enzymatic studies with eicosanoid oxidoreductase enzymes in

collaboration with Professor Charles N. Serhan at Harvard Medical School. *In vivo* biological testing will be performed with international collaborators to test the biological activities of this SPM analog.

Figure 2 presents the retrosynthetic analysis of the synthetic approach taken in this thesis. The first part of the synthesis is synthesizing the α-fragment **7** earlier prepared by Dr. Jørn E. Tungen.[3] Further synthetic approaches involves a Tebbe olefination reaction to afford compound **6**, a Heck reaction to afford compound **4** and a Barbier reaction, with further reduction of the alkyne moiety, deprotection of the alcohols and hydrolysis of the ester to afford benzo-RvD1$_{\text{n-3 DPA}}$ (**1**). Compound **3** and **5** are commercially available.

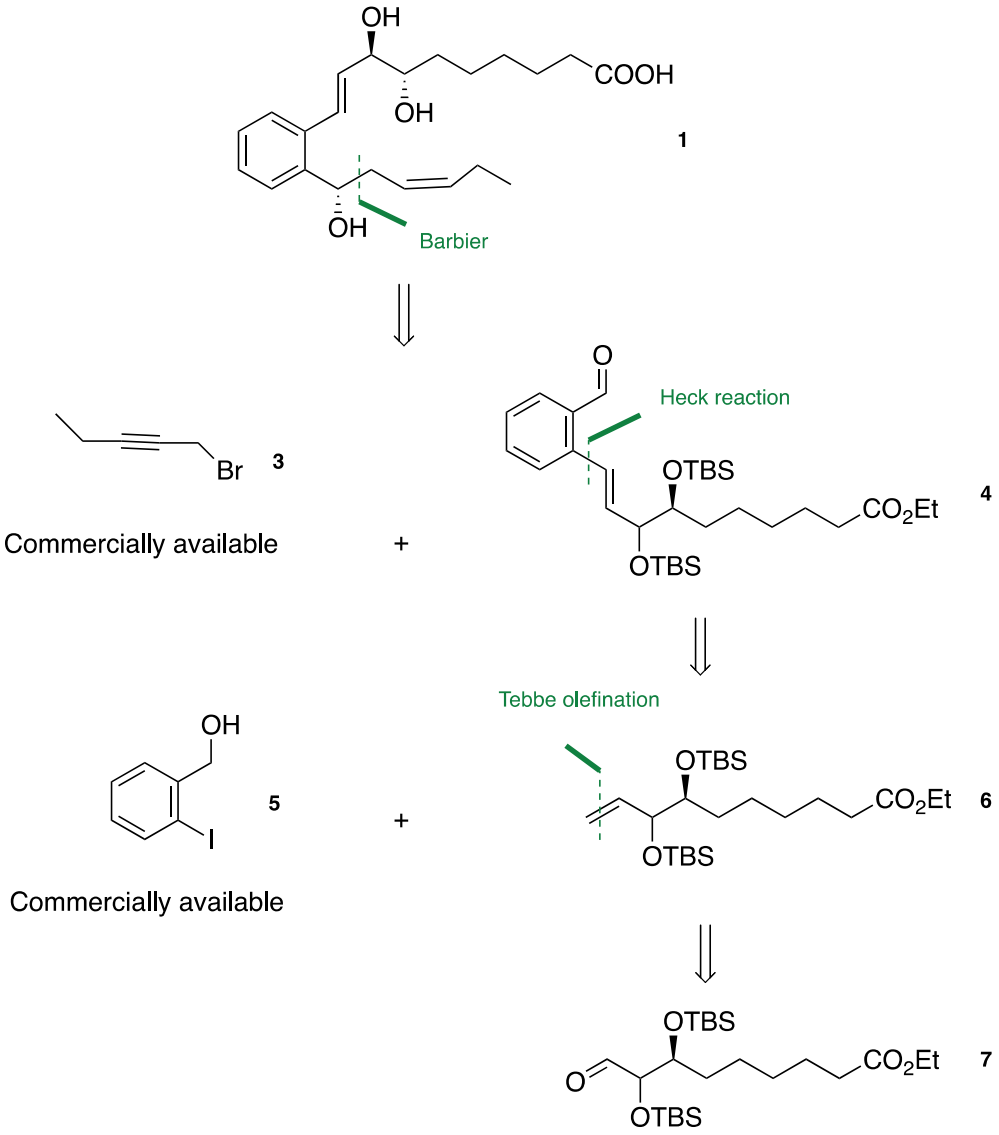

Figure 2: Retrosynthetic analysis of benzo-RvD1$_{\text{n-3 DPA}}$.

1.2 Inflammation and resolution of inflammation

Inflammation is the body`s natural protective response to physical injury and invading pathogens. The aim of the immune response is to repair damaged tissue and surmount the infection. This response is a strictly controlled and finely tuned process, which is driven by immune cells and pro-inflammatory mediators.[6]

Until recently, the resolution of inflammation was regarded to be a passive process. By self-resolving exudate experimental models, resolution mechanisms could be studied, and is now considered an active process brought on by pro-resolving mediators.[7]

The term anti-inflammatory may be translated to suppression of the inflammatory pathways. This is a property of a treatment or substance that reduce inflammation or swelling, such as inhibiting the chemotaxis of neutrophils, vascular permeability and generation of reactive oxygen species, as well as platelet aggregation and neutrophil-endothelial interactions. Anti-inflammatory actions can reduce the protection against physical injury and invading pathogens. Pro-resolving actions consist of increasing macrophage clearance by phagocytosis of bacteria and efferocytosis of cellular debris, in addition to upregulation of prostacyclin. These actions return the tissue to homeostasis.[8]

Inflammation may be divided into acute and chronic inflammation. The cardinal signs of inflammation is redness, heat, swelling and pain accompanied by loss of function.[9] Acute inflammation begins with leakage of neutrophils, fluid and proteins from the blood vessels to the vascular compartment, and contains a series of cellular responses that lasts for the first few hours after injury or infection. Chronic inflammation is defined by the presence of lymphocytes, macrophages and plasma cells in the inflamed tissue, and has little to do with the duration of the inflammatory process.[10]

1.2.1 Acute Inflammation

Following an injury or infection, the endothelial cells are activated by different factors, such as ischemia, trauma, cytokines and toxins.[11] These factors express damage-associated molecular patterns (DAMPs) or pathogen-associated molecular patterns (PAMPs), which interact with pattern recognition receptors (PRR) on the cell surface, such as the toll-like receptors (TLR).[12] The response to this is expression of adhesion molecules such as P-selectin, E-selectin and ICAM-1 on the outer surface of the endothelial cells, and the release of pro-inflammatory cytokines and chemokines, as well as pro-inflammatory eicosanoids such as prostaglandins and leukotrienes.[13, 14] These pro-inflammatory agents attract especially one type of neutrophils, namely the polymorphonuclear leukocytes (PMNs). The mechanisms and pathways of inflammation and resolution of inflammation are summarized in figure 3. The PMNs adhere to the endothelium through interaction between its adhesion molecule Mac-1 and the endothelium ICAM-1, and transmigrate to the inflamed tissue through PMN rolling and diapedesis.[10, 15] The PMNs are gradually replaced by macrophages, which are differentiated from monocytes.[16] Both PMNs and macrophages are phagocytes, meaning they ingest pathogens and cell debris from the tissue. These cells are also responsible for releasing hydrolytic and proteolytic enzymes and reactive oxygen species (ROS) to neutralize invading pathogens, all of which can culminate in tissue damage.[17] The leakage of water and salt is due to opening of the tight junctions between the endothelial cells, which causes edema.[10]

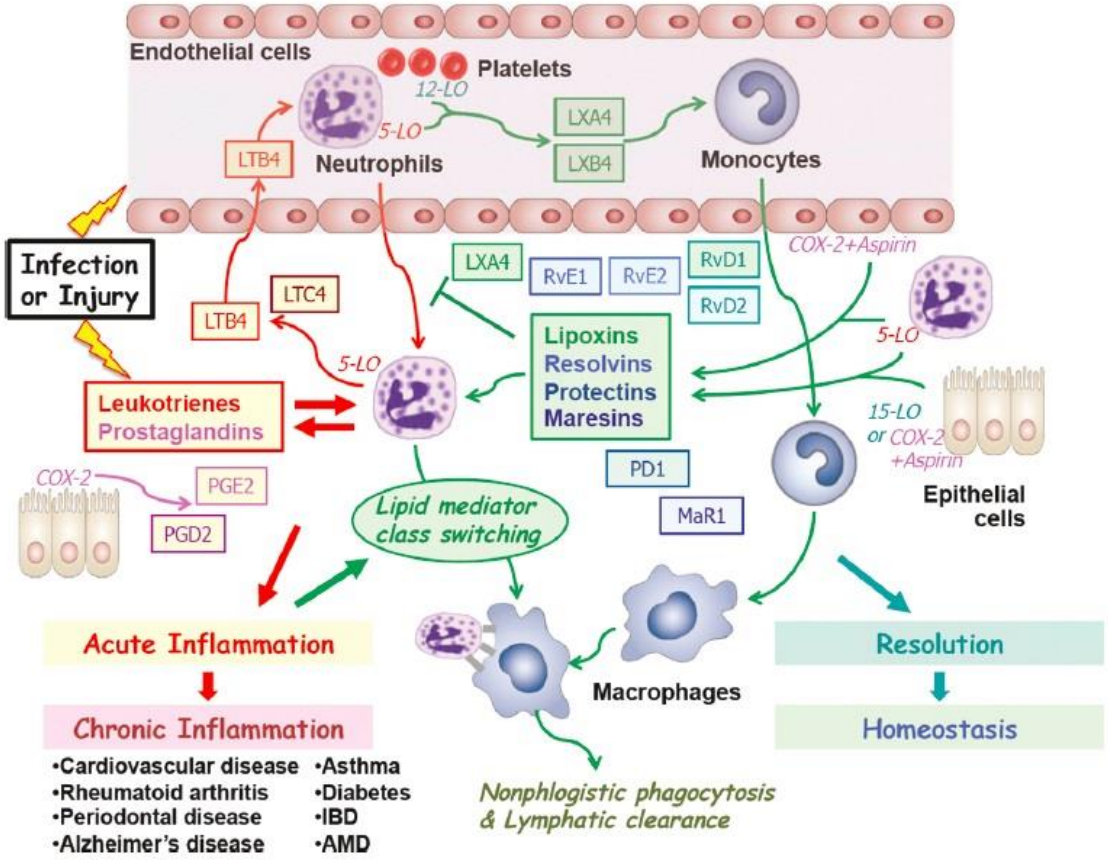

Figure 3: An overview of the mechanisms for inflammation and resolution of inflammation. SPMs play a significant part in the resolution phase of inflammation. The failure to resolve inflammation may lead to chronic inflammation and different disease states. This figure is taken from a published article of Serhan *et al.*[18]

The PMNs attract additional leukocytes to the inflamed tissue. Conversion from prothrombin to thrombin activates the platelets, leading to platelet aggregation and platelet adhesion to the endothelium. Normally, the PMNs are carried by the blood flow in the vascularity, and do not engage with the endothelial wall. This deviant aggregation and adhesion can result in intravascular thrombosis. Inflammation can also cause hemorrhage due to damage of the endothelium. A certain sign of hemorrhage is the localization of red blood cells in the tissue.[10]

The events of acute inflammation are all reversible. Apoptosis and phagocytosis clear the PMNs, and the lymphatic system drains the fluids and pro-inflammatory mediators back to the blood flow. Additionally, activation of the fibrinolytic system clears the thrombosis.[10]

1.2.2 Chronic Inflammation

The continuous engagement of the innate and acquired immune system withholds the immune response.[12, 16] Specific expression of certain adhesion molecules on the surface of the endothelium adheres to lymphocytes and monocytes that result in transmigration of these cells into the inflamed tissue. Once present in the tissue, the lymphocytes and monocytes release factors that stimulate the production of collagen. This increase in collagen production boosts the inflammatory response and gives scarring of the tissue. When it is excessive scarring, the tissue will not go back to the pre-injured state, and this event is not reversible.[10]

1.2.3 Resolution of inflammation

Resolution of inflammation is an active process orchestrated by numerous pro-resolving mediators, such as the specialized pro-resolving mediators (SPMs). The SPMs stop the invasion of PMNs and increase efferocytosis and phagocytosis by macrophages.[19] Resolution prevents tissue injury and the further development into chronic inflammation and autoimmunity. Figure 4 depicts an ideal inflammation and resolution of inflammation situation. Failed resolution can develop into a chronic inflammatory disease.[8] Rheumatoid arthritis, asthma and atherosclerosis are examples of disease states with an underlying chronic inflammation.[20-22]

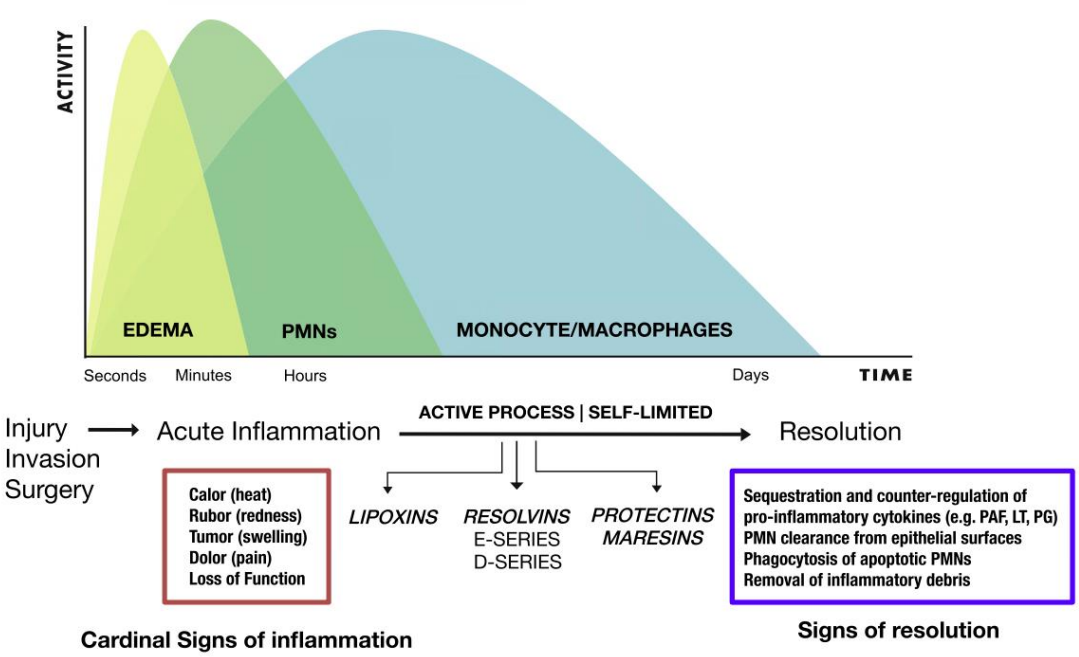

Figure 4: A timeline for an ideal inflammation and resolution from the start of the inflammatory process to the resolution commences and the inflammation resolves. The figure is taken from a published article of Chiang *et al.*[23]

A successful resolution is dependent on a neutralization of the source of inflammation and the successful clearance of the inflamed site. The neutralization step involves catabolism of the pro-inflammatory mediators, which will stop the invasion of leukocytes and edema.[16, 19]

The resolution phase commences when the PMNs are gradually replaced by macrophages. The interaction between interleukin-6 (IL-6) and its receptor initiates the switch between these cell types, due to a chemokine shift from CXC chemokines to CC chemokines.[16] CXC chemokines is a family of chemokines who plays a major part in chemotaxis of leukocytes, while the CC chemokines chemically attract monocytes.[24] This shift reduces the recruitment of PMNs. Anti-inflammatory mediators remove the cytokines and chemokines from the inflamed tissue.[16]

PMNs will either be recirculated or undergo apoptosis and further efferocytosis by macrophages. When macrophages ingest apoptotic PMNs, they change to a phenotype that promotes resolution by production of SPMs. If the apoptotic cells are not cleared by

phagocytosis, they will undergo secondary necrosis, releasing their toxic content into the tissues. This release will do further damage to the tissues, and could cause a prolonged inflammatory response. To prevent further damage from the macrophages, they either undergo apoptosis or adhere to mesothelial cells to enable drainage through the lymphatic system.[16]

1.2.4 Treatment of inflammation

COX (cyclooxygenase)-inhibitors, glucocorticoids and disease-modifying anti-rheumatic drugs (DMARDs) are some of the medicinal agents used in the treatment of inflammatory diseases today. Inflammation is a necessary tool for host protection. All of these treatments are anti-inflammatory, by inhibiting the inflammatory response. The inhibition of inflammation can reduce the progression of inflammation, and hence delay resolution. These leads to suppression of the immune system, which makes the body more susceptible to injury and invading pathogens.[25] SPMs are able to resolve inflammation without suppressing the immune response. Therefore, these pro-resolving mediators could potentially be a new wave in treatment of certain inflammatory diseases, such as neurodegenerative diseases, asthma, atherosclerosis and rheumatoid arthritis.[22, 26-29]

1.2.4.1 COX-inhibitors

COX-inhibitors, termed non-steroidal anti-inflammatory drugs (NSAIDs) exert their effect through inhibition of the cyclooxygenase (COX) enzymes, inhibiting the formation of prostaglandins, prostacyclin and thromboxane. NSAIDs are widely used as painkillers, and therapeutic agents in the treatment of several different inflammatory conditions.[30] COX-inhibitors only treat the symptoms, not the underlying cause of inflammation. In addition, there are serious potential adverse reactions from COX-inhibitors, due to inhibition of the formation of prostanoids. They can lead to gastric ulcers and gastric bleeding.[31]

1.2.4.2 Glucocorticoids

Glucocorticoids are naturally occurring endogenous substances, which are common treatment for several severe inflammatory disorders.[32] Glucocorticoids suppress the production of cytokines by acting on receptors to downregulate their gene expression.[33] Glucocorticoids

affects several signaling pathways, leading to side effects such as osteoporosis, inhibited wound repair, immunosuppression, hypertension, metabolic disturbances and growth retardation in children. Therefore, prolonged therapy with glucocorticoids is not recommended.[32]

1.2.4.3 DMARDs

DMARDs are drugs used in the treatment of inflammatory diseases such as rheumatoid arthritis and psoriasis, by inhibition of pro-inflammatory mediators. The most frequently used DMARDs attack the pro-inflammatory cytokine tumor necrosis factor α (TNFα). TNFα is a cytokine and a chemoattractant for PMNs, which is also responsible for recruiting other cytokines and chemokines.[24, 25] Uncontrolled and excessive production of TNFα is linked to inflammatory disorders.[33] The suppression of TNFα has shown to increase the risk of infections.[34]

1.3 Polyunsaturated Fatty Acids (PUFAs)

Arachidonic acid (AA), eicosapentaenoic acid (EPA) and docosahexaenoic acid (DHA) are essential fatty acids that must be supplied through dietary intake. Their molecular structures are presented in Figure 5. AA is an ω-6 PUFA. The ω-6 nomenclature is based on the last double bond in the carbon chain, counting six carbon atoms from the methyl group. EPA and DHA are ω-3 PUFAs, having the last double bond three carbon atoms from the methyl group. All of these PUFAs are elevated in plasma levels during inflammation.[4]

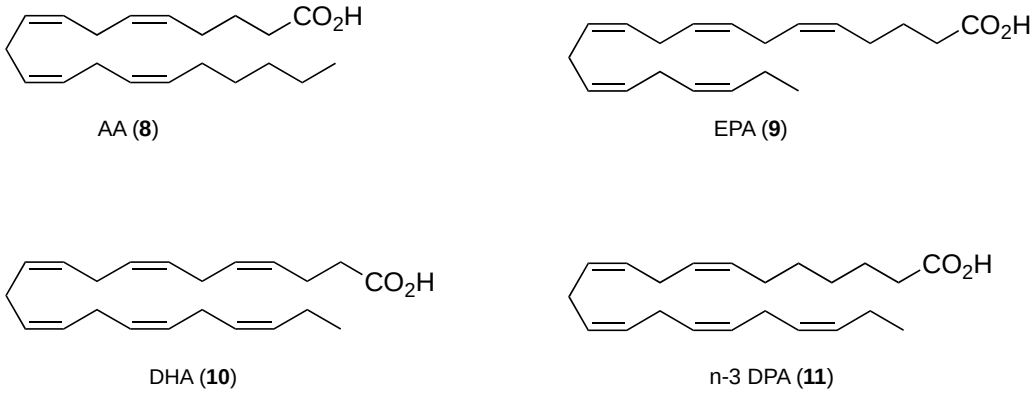

Figure 5: Molecular structures of the PUFAs AA, EPA, DHA and n-3 DPA.[18]

1.3.1 Arachidonic Acid

Arachidonic acid, synthesized from linoleic acid (LA), is a precursor for pro-inflammatory prostanoids and leukotrienes, termed eicosanoids; and the pro-resolving lipoxins. The cyclooxygenase (COX)-enzymes converts AA to prostanoids, and the lipoxygenase (LOX)-enzymes 5- and 15-LOX convert arachidonic acid to leukotrienes and lipoxins. AA is usually bound to phospholipids on the cell membrane through an ester bond. Phospholipase A_2 (PLA_2) cleaves the ester bond to release free AA. The free form of AA can be converted to eicosanoids.[35]

1.3.2 EPA, DHA and n-3 DPA

Alpha-linolenic acid (ALA) is converted by elongation and desaturation to EPA and then further to DHA. An intermediate in the formation of DHA from EPA is n-3 docosapentaenoic acid (n-3 DPA) consisting of 22 carbons and five *Z*-double bonds.[36] These PUFAs are present in the same amounts in the blood stream, brain, retina of the eye and the heart.[4, 37]

EPA and DHA are the lipid constituents in fish oil and ω-3 supplements. The European Food Safety Authority recommends an intake of 250-500 mg of ω-3 fatty acids daily for the average European adult, to reduce cardiovascular events.[38] ω-3 supplements show beneficial effects on immune modulation.[39] They have shown to improve survival rate in patients with heart failure.[40] Supplementation of ω-3 PUFAs has also demonstrated an effect on reducing inflammation in rheumatoid arthritis, atherosclerosis and asthma.[41-43]

A diet rich in ω-3 PUFAs reduces the amount of pro-inflammatory mediators from AA, due to competition with the converting enzymes. In this scenario, the production of less potent eicosanoids, the 5-series leukotrienes and the 3-series prostaglandins, derived from EPA will reduce the amount of the more potent AA derived eicosanoids.[44] This could be one of the reasons for the anti-inflammatory effects of ω-3 PUFAs. It is now postulated that the beneficial anti-inflammatory effects exerted by the ω-3 PUFAs are due to their hydroxyl-substituted metabolites, coined SPMs.[45]

1.3.3. The eicosanoids

The eicosanoids consist of the prostanoids and the leukotrienes. Figure 6 presents some of the prostanoid molecular structures derived from AA. The prostanoids are further divided into prostaglandins, prostacyclin and thromboxane. Prostaglandins mediate vasodilatation and regulation of blood flow to protect the gastric mucosa, myocardium and the renal parenchyma, as well as activation of pro-inflammatory cells and generating fever. Furthermore, they induce a switch between lipid mediators from pro-inflammatory to anti-inflammatory and pro-resolving mediators.[31, 46] Prostacyclin and thromboxane coordinate platelet activation and thrombogenesis.[31] Leukotrienes generate superoxide and mediate leukocyte chemotaxis and lymphocyte migration.[47, 48] The leukotrienes initiate bronchoconstriction of the airways involved in asthma and contribute to the vascular permeability during inflammation.[31, 49, 50]

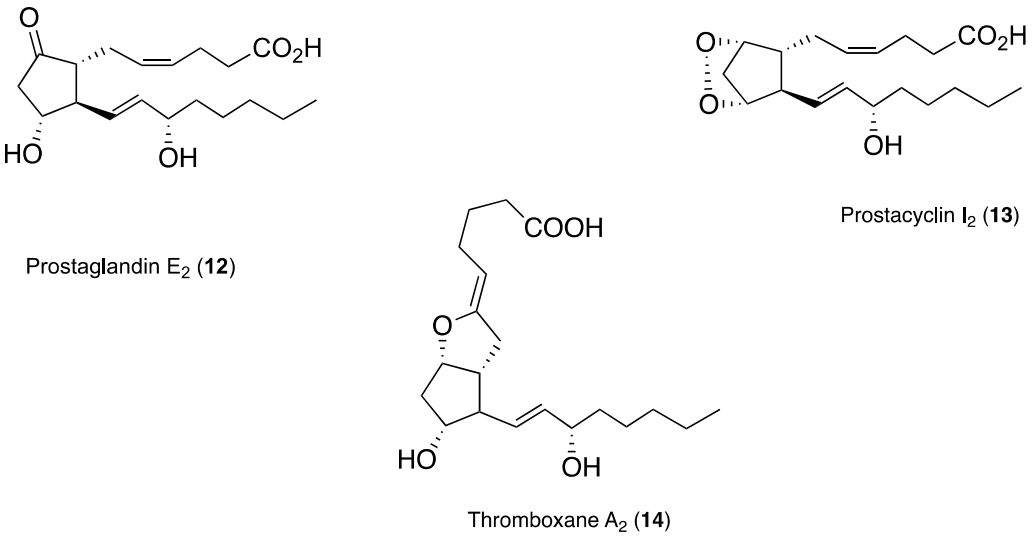

Figure 6: The structures of PGE_2, prostacyclin I_2 and thromboxane A_2, AA derived prostanoids.[31]

1.4 The specialized pro-resolving mediators

Endogenous pro-resolving mediators are a diverse group, containing different proteins and peptides, gaseous mediators such as hydrogen sulphide and carbon monoxide, adenosine, neuromodulators, cytokines and lipid mediators termed SPMs.[8, 51-57] All of these mediators orchestrate the resolution of inflammation. SPMs are the focus of this thesis.

SPMs are a group of potent endogenous anti-inflammatory lipid mediators, which act locally, after which they are inactivated. They exert their effect in the nanogram range.[58] Their predecessors are polyunsaturated fatty acids (PUFAs), such as AA, EPA, DHA and DPA. An overview of these PUFAs and their respective SPM derivatives are presented in Figure 7. During inflammation, these PUFAs are mobilized and converted to their corresponding SPMs.[4] Arachidonic acid is converted to lipoxins. E-series resolvins derive from EPA. D-series resolvins, protectins, maresins, as well as their sulfido-conjugated analogs derive from DHA.[18] n-3 DPA derivatives are n-3 DPA resolvins, protectins and maresins, as well as 13-series resolvins.[4 59]

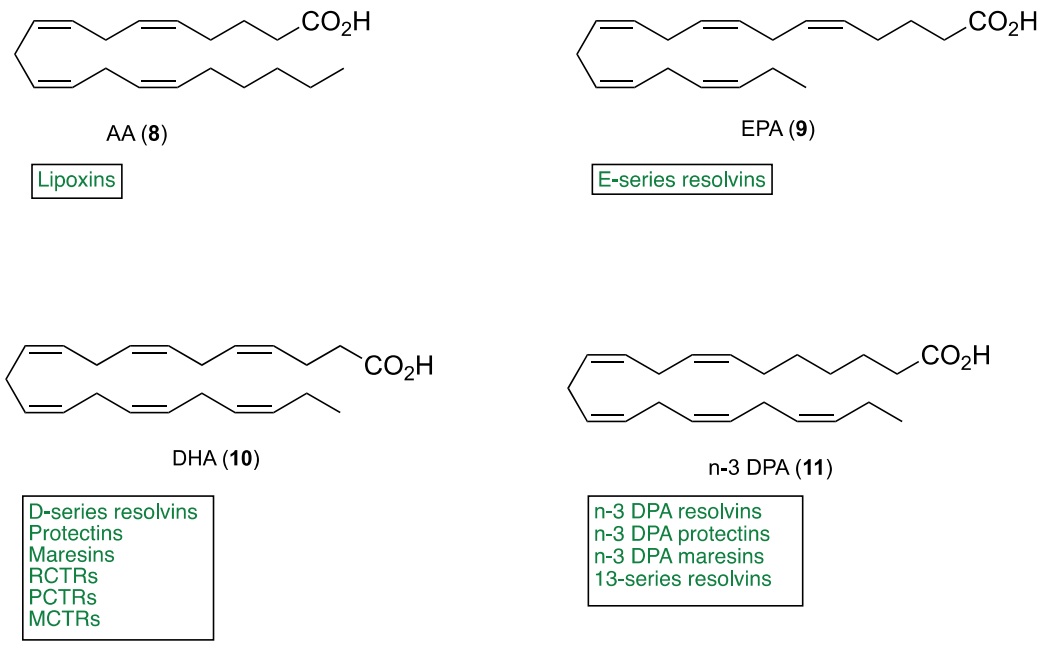

Figure 7: The PUFAs AA, EPA, DHA and n-3 DPA with their individual SPM families. Arachidonic acid is converted to lipoxins (LX). EPA is converted to the E-series resolvins (RvE). DHA is converted

to the D-series resolvins (RvD), protectins (PD) and maresins (MaR), while n-3 DPA is converted to the corresponding n-3 DPA SPMs.[60]

The SPMs have two important tasks in the process of resolution: 1) Stop infiltration of neutrophilic adhesion and chemotaxis, 2) increase the efferocytosis of apoptotic PMNs and cellular debris, and increase the phagocytosis of the invading pathogen by macrophages and accelerate their clearance.[19, 26, 61] The SPMs have also shown to promote tissue repair and regeneration, and reduce inflammatory pain.[45, 62, 63] Lower doses of antibiotics are required to clear an infection, when SPMs are administered concomitantly.[61]

The SPMs are generated at different stages in the resolution phase, which indicates that they have different resolution tasks. They are biosynthesized in exudates from leukocytes and macrophages, through transcellular or intracellular biosynthesis. SPMs exert their effects through interaction with G-protein coupled receptors (GPCRs), which activate resolution pathways.[64]

1.4.1 SPM receptors

Seven receptors are hitherto identified to interact with SPMs, all of which are GPCRs.[64] SPMs are agonists on these receptors, with the exception of the BLT1 receptor. These receptors interact stereoselectively with different SPMs, and the interactions seem to be concentration-dependent.[58] Figure 8 present an overview of the SPM interactions with the main SPM receptors.

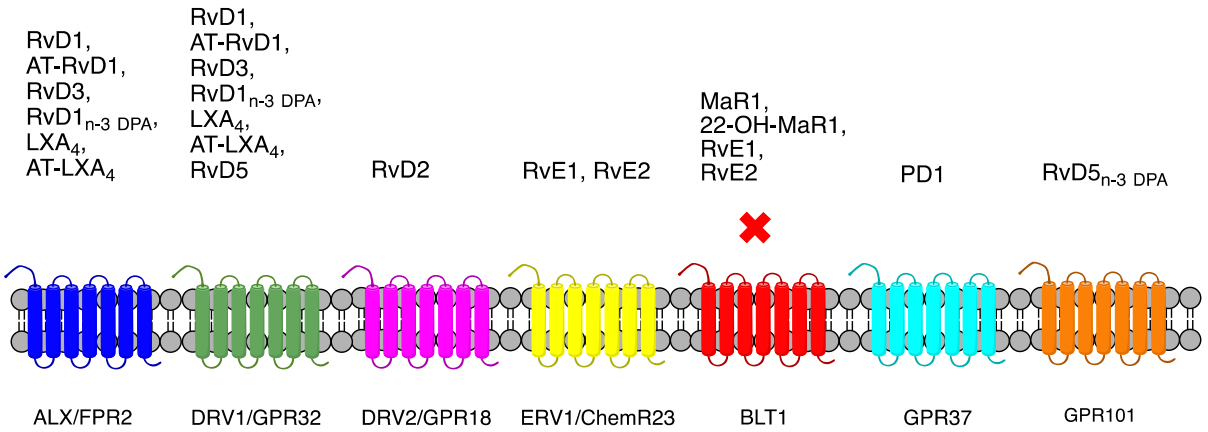

Figure 8: The main receptors on which the SPMs exert their effects. The SPMs are agonists on their receptors, with the exception on BLT1, the leukotriene B_4 (LTB_4) receptor. Some SPMs act as partial agonists on BLT1, and block or dampen the effects of LTB_4.[64-66]

1.4.1.1 ALX/FPR2

ALX is a lipoxin A_4 receptor. The ALX receptor is expressed in myeloid cells, as well as in lymphocytes, dendritic cells, endothelial cells and epithelial cells, where it mediates anti-inflammatory and pro-resolving effects. ALX can interact with a wide variety of proteins and peptides, as well as lipoxins and other SPMs. In addition to LXA_4, RvD1, 17*R*-RvD1 and $RvD1_{n\text{-}3\ DPA}$ have shown agonistic effects to this receptor.[3, 58] The expression of ALX dictates the scope and duration of the inflammatory response.[67] When PMNs are activated, they rapidly mobilize ALX receptors on the cell surface.[68]

1.4.1.2 DRV/GPR32

The DRV/GPR32 receptor is expressed on leukocytes in the vascularity.[8] In contrast to the ALX receptors, GPR32 is not upregulated during PMN activation, which could indicate that the effects mediated through GPR32 are more maintenance and homeostatic effects.[68] Activation of GPR32 enhances macrophage phagocytosis and reduces the production of cytokines and chemokines.[61] RvD1, 17*R*-RvD1, RvD3, RvD5 and $RvD1_{n\text{-}3\ DPA}$ has shown agonistic effects on this receptor, and their affinity and potency for GPR32 is similar as for their affinity (dissociation constant (K_d)) and half maximal effective concentration (EC_{50}) for the ALX receptor.[3, 8, 58] GPR32 plays a role in self-resolving inflammation, speeding up phagocytosis of amyloid-β, which can prevent the onset of Alzheimer`s disease.[69]

1.4.1.3 ERV/ChemR23

RvE1 and 18*S*-RvE1 are agonists on ChemR23, while RvE2 is a partial agonist. These interactions reduce the number of PMNs and protect the host from osteoporosis.[58] ChemR23 is expressed on leukocytes, the gastrointestinal tract, prostate, heart, brain, kidneys and lungs. Also, the receptor is abundantly present in monocytes, neutrophils and T lymphocytes. The expression of ChemR23 is upregulated in the presence of pro-inflammatory cytokines such as TNFα.[70]

1.4.1.4 BLT1

BLT1 is a LTB_4 receptor, but several SPMs have shown partial agonistic action on this receptor, inhibiting the effects of LTB_4.[58] Among these are MaR1, RvE1 and RvE2.[64]

1.4.1.5 ERV2/GRP18

The discovery of RvD2 receptor was reported by Chiang *et al.* in 2015.[71] This GPCR is expressed on human leukocytes. The pro-resolving actions of RvD2 were mediated through its interactions with the ERV2/GRP18 receptor, reducing PMN infiltration and enhancing phagocytosis of bacteria.[71]

1.4.1.6 Pael-R/GPR37

NPD1 has shown to exert its effects through activation of the G protein-coupled receptor Pael-R/GPR37. This activation leads to an increase in macrophage phagocytosis and a shift from pro-inflammatory cytokines to anti-inflammatory cytokines, which reduces inflammatory pain.[65]

1.4.1.7 GPR101

Another receptor recently discovered, is the GPR101 receptor. This receptor has shown to mediate the effects of $RvD5_{n\text{-}3\ DPA}$, which dampens inflammation in psoriasis and infection.[66]

1.4.2 Aspirin-triggered SPMs

Aspirin-triggered (AT)-analogs are formed in the presence of aspirin, by the COX-2 enzyme.[72] Low-dose aspirin exerts its anti-inflammatory role through the activity of the SPM AT-lipoxin (ATL). Aspirin acetylates COX-2, which shifts its enzyme activity to producing lipoxins.[73, 74]

The AT-analogs differ from the analogs generated by lipoxygenases with an opposite configuration of one of the hydroxyl groups. They are epimers of the SPMs generated by LOX-enzymes. Serhan *et al.* first reported the AT-resolvins in 2002. The effects and potency of the AT-analogs coincide with what is demonstrated with their lipoxygenase-generated epimers.[75, 76]

1.4.3 Lipoxins

The lipoxins are SPMs derived from AA, which stop chemotaxis of neutrophils and inhibit eosinophil recruitment.[47, 77] Lipoxins also stimulate the clearance of apoptotic leukocytes and macrophages.[78] Lipoxins and their analogs have demonstrated pro-resolving effects in eczema, rheumatoid arthritis, colitis, atherosclerosis, sepsis, protection from boneloss and fibrosis.[22, 28, 79-83] The structures of lipoxin A_4 (LXA_4) and lipoxin B_4 (LXB_4) are presented in Figure 9.

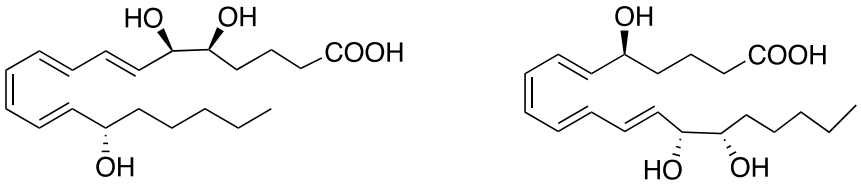

LXA_4 (**15**) LXB_4 (**16**)

Figure 9: The structures of lipoxin A_4 (LXA_4) and lipoxin B_4 (LXB_4).[84]

1.4.4 SPMs derived from EPA

1.4.4.1 E-series resolvins

The resolvins were discovered by Serhan *et al.* in 2002, and termed resolvins because of their potent pro-resolving actions.[75] The E-series resolvins are formed by the insertion of molecular oxygen at carbon 18 by 5-LOX. The second step affords the resolvins RvE1, RvE2 and RvE3.[44] The structures of RvE1 and RvE2 are presented in Figure 10.

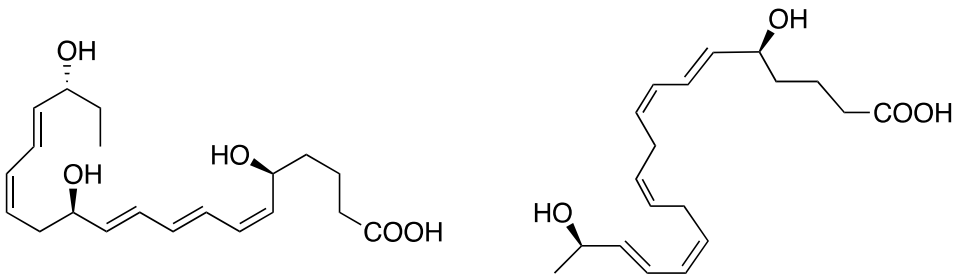

Figure 10: The structures of RvE1 and RvE2, the most studied E-series resolvins.[23]

Resolvin E1

The effects of RvE1 are mediated through a specific agonist action on the ChemR23 receptor, with a K_d of 11.3 ± 5.4 nM, and a partial agonist action on the BLT1 receptor with a K_d of 45 nM.[70, 85] The interaction with ChemR23 inhibits the formation of fibrosis.[86] In a murine model of psoriasis, RvE1 has demonstrated an effect in reducing inflammatory cell infiltration and epidermal hyperplasia through the antagonistic interaction with the BLT1 receptor.[87]

RvE1 is currently being tested in clinical trials for the treatment of corneal inflammation and dry eye syndrome, with promising results.[88, 89] This SPM has been demonstrated to be just as potent as a high-dose dexamethasone in stopping PMN infiltration.[70] RvE1 reduces osteoclast mediated bone destruction in periodontitis, indicating a potential effect in stopping the development of osteoporosis.[90] Furthermore, RvE1 plays a part in allergic reactions by the suppression of interleukin-23 and interleukin-6.[91]

1.4.5 SPMs derived from DHA

1.4.5.1 D-series resolvins

The D-series resolvins are formed from DHA by the initial insertion of molecular oxygen in carbon 17 position by 15-LOX.[75] There are hitherto discovered six D-series resolvins, namely RvD1, RvD2, RvD3, RvD4, RvD5 and RvD6, as well as the sulfido-conjugated resolvins 7*S*,8*R*,17*S*-RCTR1, 7*S*,8*R*,17*S*-RCTR2 and 7*S*,8*R*,17*S*-RCTR3.[18, 92] The structures of resolvins RvD1-5 are presented in Figure 11.

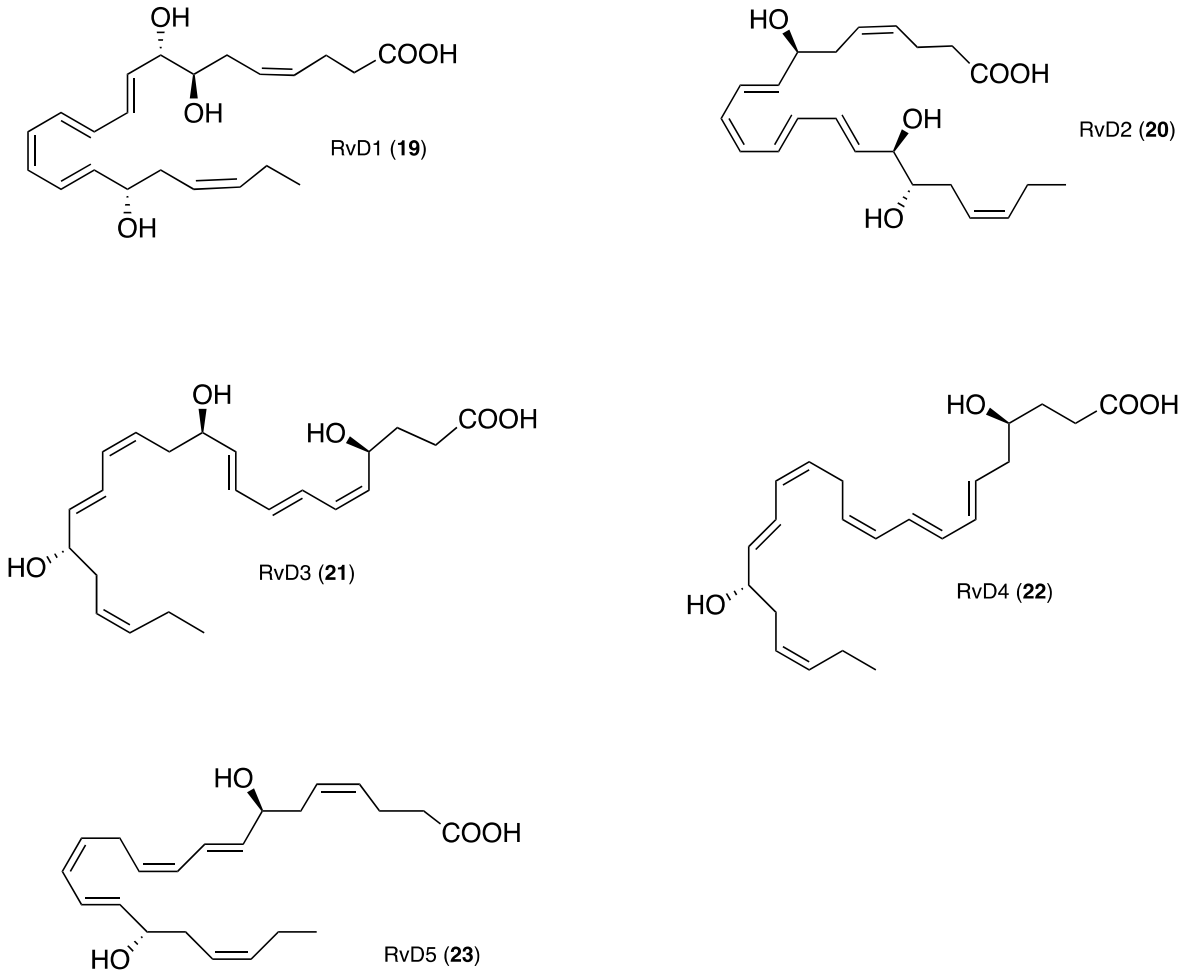

Figure 11: Structures of the resolvins RvD1, RvD2, RvD3, RvD4 and RvD5.[23]

Resolvin D1

RvD1 has demonstrated the same potency as indomethacin in stopping PMN infiltration. It plays a role in reducing pain, improving metabolic syndrome and insulin sensitivity increasing the healing of diabetes wounds, increasing phagocytosis of amyloid-β implicated in Alzheimer`s disease, and improving the function of salivary glands and gastrointestinal tract.[69, 93-98]

RvD1 and AT-RvD1 has demonstrated a marked reduction in lung eosinophilia and other pro-inflammatory mediators, as well as clearance of macrophages from the lungs and reducing fibrosis. Analogs of these SPMs could be potential novel therapies for allergic reactions and asthma.[21, 99] AT-RvD1 reduces pain by blocking transient receptor potential V 3 (TRPV3) and has also demonstrated an effect against arthritis pain in rats.[100, 101] In a murine model, AT-RvD1 has shown to prevent cognitive decline.[102] RvD1 together with RvD2 has shown to exert pro-resolving actions in inflamed adipose tissue in obesity.[103] RvD1 and AT-RvD1 have exerted EC_{50} values of approximately 50 nM on reducing transmigration of PMNs.[18]

Resolvin D2

RvD2 generates nitrogen oxide (NO) in small amounts, which has an antiadhesive effect, but were not generated in pro-inflammatory amounts. This SPM has demonstrated to reduce the deadliness of sepsis in mice by reducing PMN-endothelium interaction and downregulate the production of cytokines.[104] Furthermore, RvD2 has shown an antithrombotic effect and the prevention of dermal necrosis, and speeds up the phagocytosis of bacteria.[104, 105] RvD2 has demonstrated a positive effect on re-epithelization of the skin, an effect also seen in a murine model of diabetes.[96, 106]

Furthermore, RvD3 has demonstrated anti-inflammatory effects in an arthritis model.[107] RvD5 was identified in synovial fluids of joints in rheumatoid arthritis patients, and has demonstrated to inhibit pro-inflammatory cytokines such as nuclear factor κ B (NF-κB) and TNF-α, and increase macrophage phagocytosis of *Escherichia coli* through the activation of GPR32.[28, 61]

1.4.5.2 Protectins

Protectins have shown promising immunoresolving effects both *in vitro* and *in vivo*. Protectins consist of PD1/NPD1 (presented in Figure 12) and the sulfido-conjugated protectins 16*R*,17*S*-PCTR1, 16*R*,17*S*-PCTR2 and 16*R*,17*S*-PCTR3.[108]

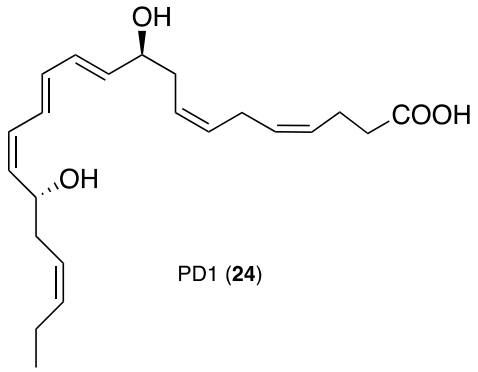

PD1 (**24**)

Figure 12: Structure of PD1/NPD1.[18]

Protectin D1/Neuroprotectin D1

PD1 is also termed neuroprotectin D1 (NPD1), as it was first found in neuronal systems.[109] PD1 binds to neutrophils presumably at two different binding sites, due to very different affinities, K_d, of 25 nM and 200 nM.[8] PD1 binds to GPR37 with a K_d of 1 pmol per protein and an EC_{50} value of 1 nM.[65] This SPM is highly expressed in the brain and the retina.[110] In an *in vivo* murine model of stroke, PD1 and AT-PD1 have shown to exert neuroprotective effects by inhibiting the infiltration of leukocytes after ischemia and reperfusion.[111, 112] PD1 reduces cytokine IL-1β production in glioma cells, which prevents cell death and plaque formation. This has shown to be important factors in Alzheimer`s disease.[113] PD1 is now being tested on Alzheimer`s disease in humans.[110] *In vitro*, PD1 has demonstrated a protective effect on photoreceptor cells in the retina, by inhibiting apoptosis.[114, 115] PD1 was found to interact with the GPR37 receptor, and this interaction increases macrophage phagocytosis, shifts cytokines towards pro-resolving cytokines and reduces inflammatory pain.[65] PD1 plays a role in asthma by reducing eosinophilic infiltration, both in murine models and in healthy subjects.[27, 110, 116] PD1 has also shown to have a role in atherosclerosis and pain.[117] PD1 exert an effect in wound healing through proliferation of epithelial cells.[118] An isomer of PD1, PDX, reduces platelet aggregation and thrombogenesis *in vitro*.[119]

1.4.5.3 Maresins

Maresins are produced in macrophages, and exert potent pro-resolving effects, hence the name maresins.[120] Maresins are produced from DHA by 12-LOX, through the insertion of molecular oxygen in carbon 14 position.[121] In addition to MaR1 and MaR2, whose structures are presented in Figure 13, the recently discovered sulfido-conjugated maresins (MCTRs) consist of MCTR1, MCTR2 and MCTR3.[63, 122]

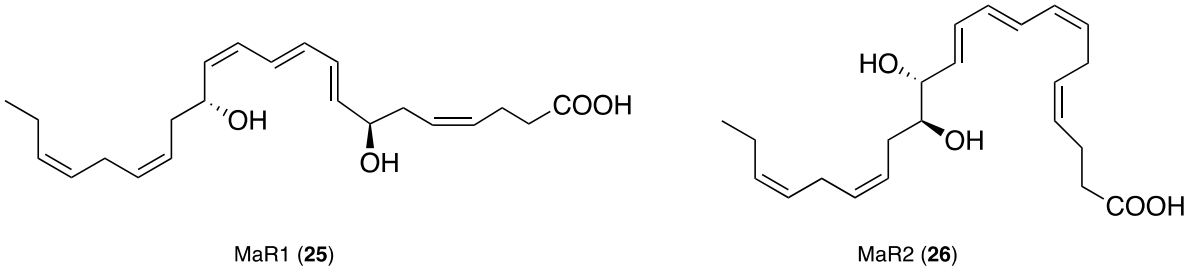

MaR1 (**25**) MaR2 (**26**)

Figure 13: The structures of MaR1 and MaR2.[23, 121]

Maresin 1

MaR1 reduces the accumulation of PMNs in tissues, as well as stimulating the regeneration of tissue by macrophage efferocytosis.[120, 121] MaR1 has tissue protective and restorative properties, and increases the rate of regeneration in planaria.[62, 120] It is also potent in reducing neuropathic and inflammatory pain by blocking the TRPV1 currents in mice with an half maximal inhibitory concentration (IC_{50}) of 0.5 nM.[62] MaR1 was identified in human synovial fluids, which indicates that this SPM exert pro-resolving actions in inflammation of joints in rheumatoid arthritis.[28] In mice, MaR1 has demonstrated protective actions in colitis and bronchial epithelial cells, by reducing cytokine production.[123, 124] The epoxy-precursor for MaR1 has shown to stimulate the phenotype switch from M1 to M2 macrophages, which is a pro-resolution phenotype.[125]

1.4.5.4 Sulfido-conjugates

Recently reported novel SPMs are the sulfido-conjugates, namely the resolvin conjugates in tissue regeneration (RCTR), the protectin conjugates in tissue regeneration (PCTR) and the

maresin conjugates in tissue regeneration (MCTR).[126, 127] They are all metabolites of DHA.[128] The sulfido-conjugates are produced by macrophages through 17-lipoxygenation, and have shown to be especially important in tissue regeneration, accelerating the regeneration of tissue in planaria.[122, 128, 129]

1.4.5 SPMs derived from n-3 DPA

1.4.5.5 n-3 DPA analogs

n-3 DPA SPMs were first reported by Dalli *et al.* in 2013.[4] The first n-3 DPA analogs reported was PD1 $_{\text{n-3 DPA}}$, PD2 $_{\text{n-3 DPA}}$, RvD1 $_{\text{n-3 DPA}}$, RvD2 $_{\text{n-3 DPA}}$ and RvD5$_{\text{n-3 DPA}}$, and are presented in Figure 14. n-3 DPA analogs are generated enzymatically by LOX-enzymes from n-3 DPA during acute inflammation.[4] This is evidenced by the hydroxyl group, which is primarily in the *S*-configuration (about 80%).[130] Several *in vitro* studies and *in vivo* murine models have been conducted with these SPMs. n-3 DPA analogs demonstrate protective effects against secondary organ damage, reduced lunge tissue damage, reduced amounts of infiltrated leukocytes and reduced amounts of platelet-leukocyte aggregates, which is an indication for systemic inflammation.[4, 131] The n-3 DPA analogs significantly reduced the prostanoid synthesis.[4] There is also seen a correlation between the amounts of n-3 DPA in red blood cells and atherosclerosis.[132] The pro-resolving effects of the n-3 DPA analogs on inflammation in humans remain to be studied.

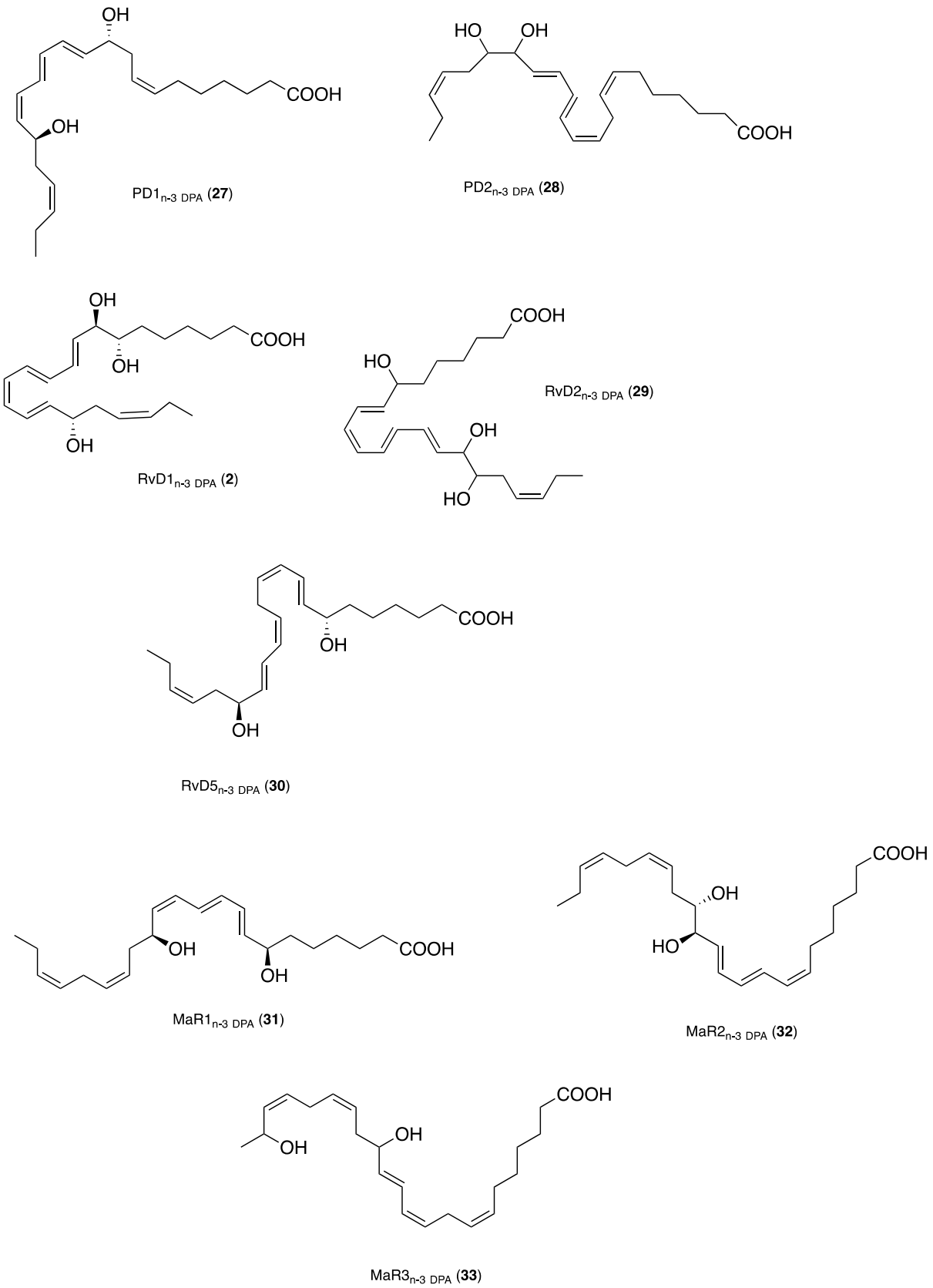

Figure 14: The structures of the known n-3 DPA analogs.[4] The absolute configuration is presented where established.

$PD1_{n\text{-}3\ DPA}$ and $RvD5_{n\text{-}3\ DPA}$ are upregulated in the intestine of patients with irritable bowel disease (IBD). These two SPMs demonstrated protective effects in the intestine of mice, by the reduction of neutrophil adhesion to the epithelium, suggesting a therapeutic strategy towards intestinal inflammation.[133] $PD1_{n\text{-}3\ DPA}$ and $MaR1_{n\text{-}3\ DPA}$ have shown to potently increase macrophage phagocytosis and efferocytosis.[134, 135] $PD1_{n\text{-}3\ DPA}$ has also shown neuroprotective actions by resolving neuro-inflammation in epileptogenesis.[136] $RvD5_{n\text{-}3\ DPA}$ binds to GPR101 with a K_d of approximately 6.9 nM, which leads to upregulation of intracellular cAMP, phagocytosis by leukocytes and macrophages, and clearance of cell debris. The effects exerted by this interaction is implicated in inflammatory arthritis.[66]

The n-3 DPA analogs are generated at different stages during the inflammation process, just as the DHA and EPA analogs. $RvD1_{n\text{-}3\ DPA}$ peaked during the neutrophil infiltration and in the later part of the resolution phase. The same was true for $PD2_{n\text{-}3\ DPA}$. $PD1_{n\text{-}3\ DPA}$. $MaR2_{n\text{-}3\ DPA}$ and $MaR3_{n\text{-}3\ DPA}$ peaked four hours into the inflammation, and gradually decreased over the course of 20 hours. $RvD2_{n\text{-}3\ DPA}$ peaked at the onset of resolution, while $RvD5_{n\text{-}3\ DPA}$ gradually increased and peaked late in the resolution phase. $MaR1_{n\text{-}3\ DPA}$ peaked in the late stage of the resolution phase.[4] The time lines for exudate levels of the n-3 DPA analogs are shown in Figure 15.

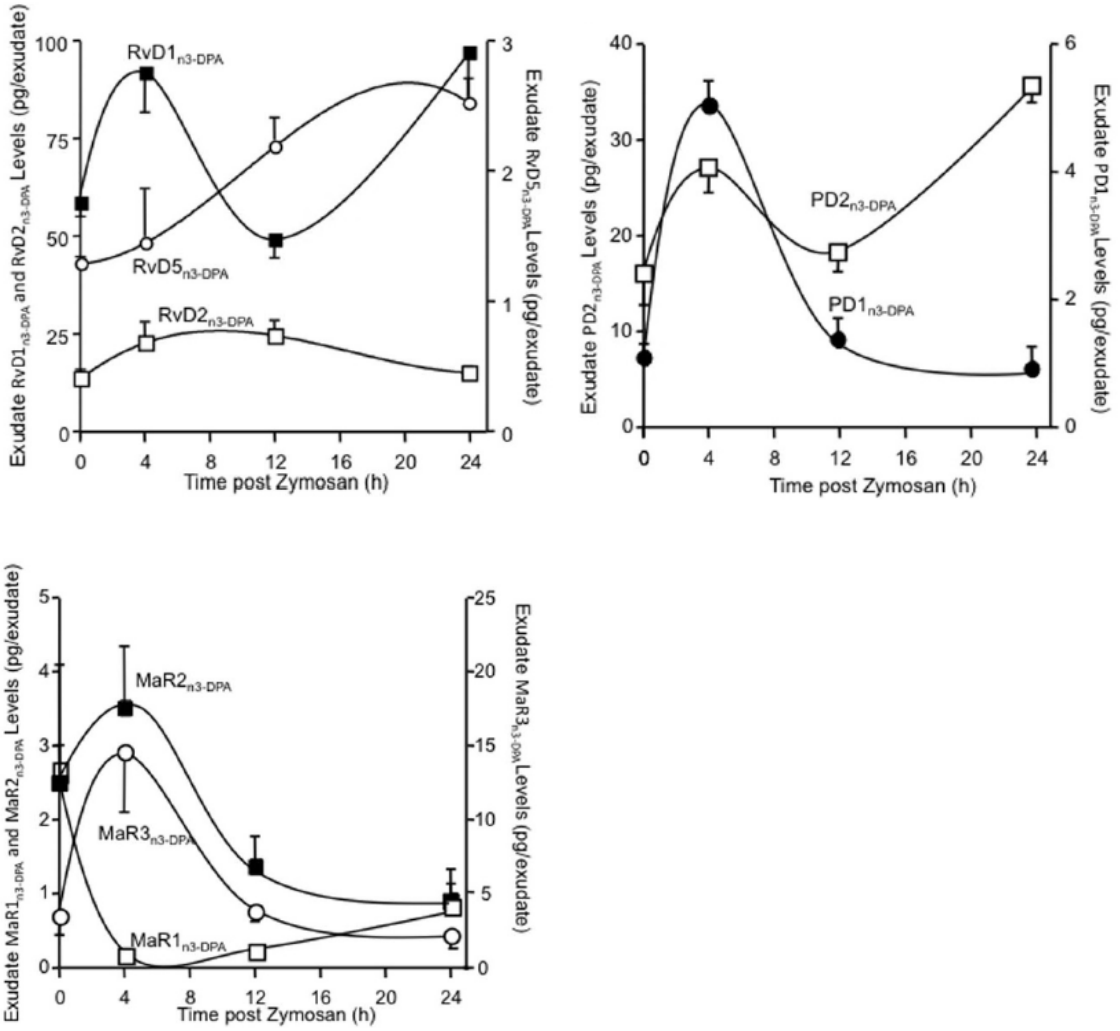

Figure 15: The figure is adapted from Dalli *et al.* and illustrates the exudate levels of $RvD1_{n\text{-}3\ DPA}$, $RvD2_{n\text{-}3\ DPA}$, $RvD5_{n\text{-}3\ DPA}$, $PD1_{n\text{-}3\ DPA}$, $PD2_{n\text{-}3\ DPA}$, $MaR1_{n\text{-}3\ DPA}$, $MaR2_{n\text{-}3\ DPA}$ and $MaR3_{n\text{-}3\ DPA}$ during resolution of inflammation.[4]

1.4.5.6 13-series resolvins

The 13-series resolvins (RvTs) are a newly discovered class of SPMs derived from n-3 DPA. These SPMs have demonstrated an increase in mice survival during infections. These SPMs are biosynthesized by COX-2 enzymes in inflammatory exudates. There are hitherto four reported RvTs, namely RvT1, RvT2, RvT3 and RvT4.[59]

1.5 Resolvin $D1_{n\text{-}3\ DPA}$

Benzo-$RvD1_{n\text{-}3\ DPA}$, which is the focus of this thesis, is an analog of $RvD1_{n\text{-}3\ DPA}$. Tungen *et al*. established the configurational assignment of $RvD1_{n\text{-}3\ DPA}$ in 2019, and proved the presence of an *E,E,Z,E*-tetraene. The allylic hydroxyl groups in carbon 7 and carbon 8 position are in an *anti*-configuration.[3] The molecular structure of $RvD1_{n\text{-}3\ DPA}$ is presented in Figure 16.

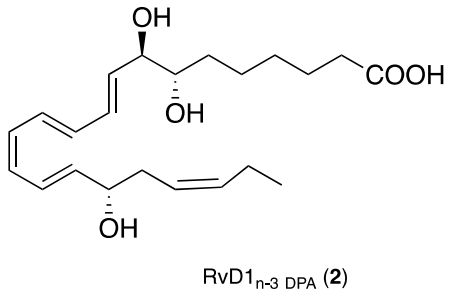

Figure 16: The molecular structure of $RvD1_{n\text{-}3\ DPA}$.[3]

$RvD1_{n\text{-}3\ DPA}$ is quite similar in structure to RvD1, only lacking a *Z*-double bond in carbon 4-5 position. Therefore, it can be assumed that the biosynthesis, effects and metabolism also is quite similar.[4] $RvD1_{n\text{-}3\ DPA}$ has shown to act on the same G protein-coupled receptors, namely human ALX/FPR2 and DRV1/GPR32 receptors.[137] Both $RvD1_{n\text{-}3\ DPA}$ and RvD1 activate the receptors in a nanomolar range. The potency of $RvD1_{n\text{-}3\ DPA}$ on these receptors are equivalent to the potency demonstrated by RvD1 according to Tungen *et al*. (Figure 17A and 17B).[3]

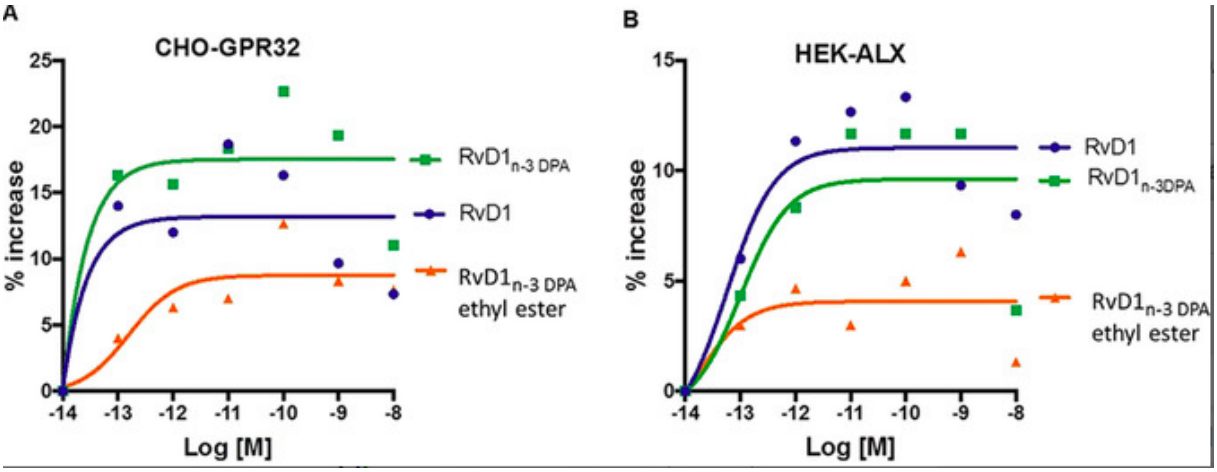

Figure 17: Interaction of $RvD1_{n\text{-}3\ DPA}$ with the receptors GPR32 (A) and ALX (B), compared to RvD1 and $RvD1_{n\text{-}3\ DPA}$ ethyl ester. The graphs demonstrate that $RvD1_{n\text{-}3\ DPA}$ have a comparable affinity for the GPR32 and ALX receptors as RvD1. The ethyl ester of $RvD1_{n\text{-}3\ DPA}$ has a slightly lower affinity. The figure is adapted from Tungen *et al.*[3]

1.5.1 Biological effects of $RvD1_{n\text{-}3\ DPA}$

In vitro, synthetic $RvD1_{n\text{-}3\ DPA}$ demonstrated an increased macrophage ingestion of apoptotic cells (Figure 18A) and bacteria (Figure 18B). *In vivo* mice studies with $RvD1_{n\text{-}3\ DPA}$ have also demonstrated a reduction of leukocytes in inflammatory exudates (Figure 18C) and an increase in phagocytosis of bacteria (Figure 18D).[3] In a murine model of epilepsy, $RvD1_{n\text{-}3\ DPA}$ reduced the amounts of seizures and shortened the duration of seizures even after discontinuation of treatment.[136]

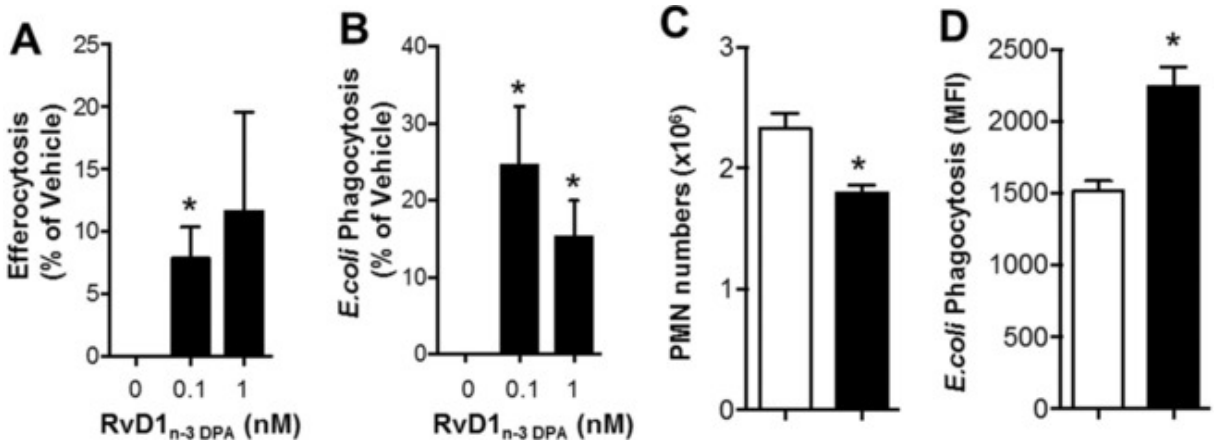

Figure 18: *In vitro* effects of $RvD1_{n\text{-}3\ DPA}$ on macrophage efferocytosis and phagocytosis, as well as *in vivo* effects on PMN infiltration and phagocytosis have been demonstrated. The figure is adapted from Tungen *et al.*[3]

1.5.2 Biosynthesis of $RvD1_{n\text{-}3\ DPA}$

The anticipated biosynthesis of $RvD1_{n\text{-}3\ DPA}$ is initiated by two lipoxygenase-mediated reactions, as shown in Scheme 1. The first steps afford a peroxide in carbon 17 position, and then in carbon 7 position. Then 7,17-dihydroxy(peroxy)-DPA is further biosynthesized to the 7,8-epoxy-17-hydroxy-DPA, which is finally converted to $RvD1_{n\text{-}3\ DPA}$ by ring opening of the epoxide.[138]

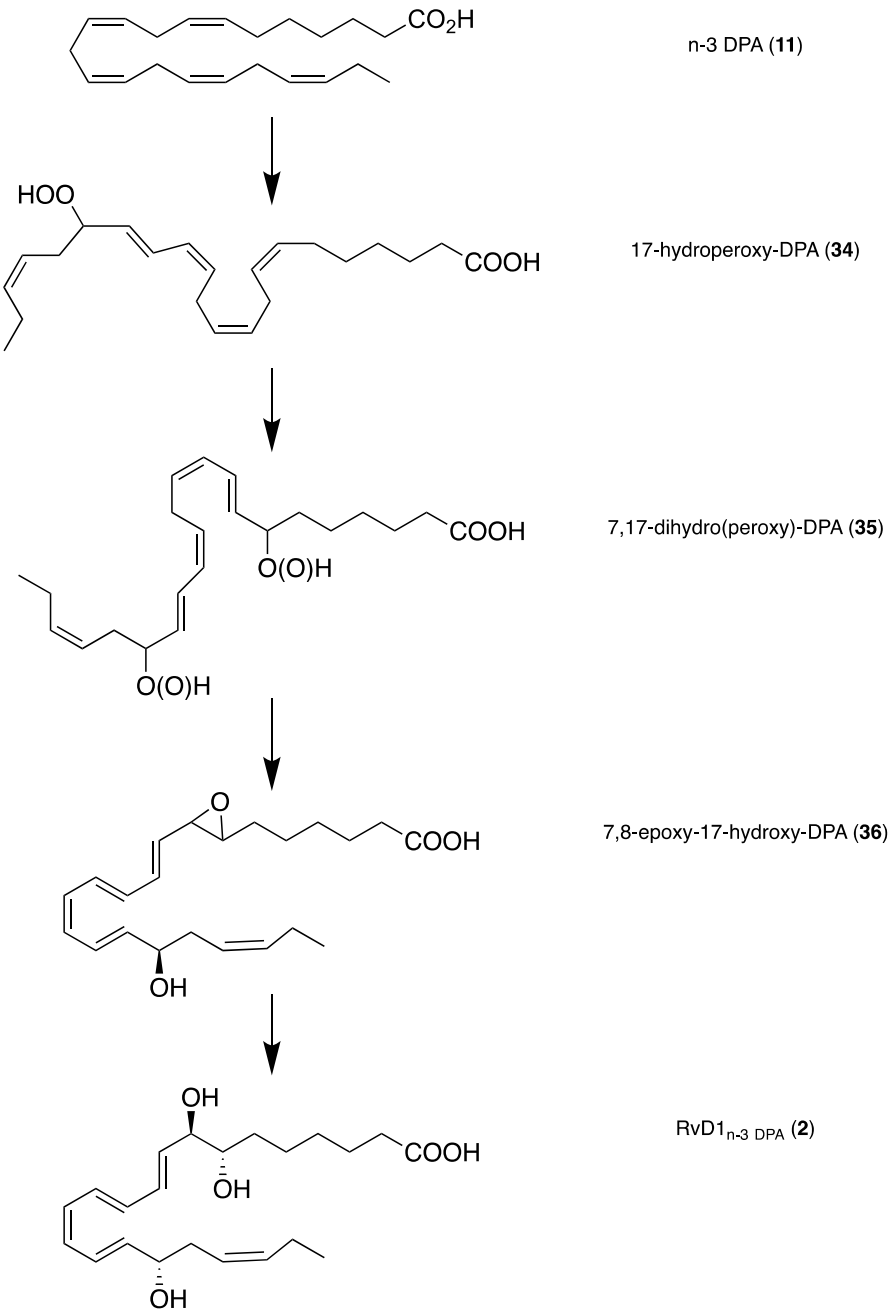

Scheme 1: Anticipated biosynthesis of $RvD1_{n\text{-}3\ DPA}$ from n-3 DPA.[138]

1.5.3 Metabolism of RvD1$_{n\text{-}3\ DPA}$

The assumed metabolism of RvD1$_{n\text{-}3\ DPA}$ is presented in Scheme 2. This assumption is based on the metabolic pathway of RvD1. RvD1$_{n\text{-}3\ DPA}$ is oxidized in either carbon 8 or carbon 17 position to 8-oxo-RvD1$_{n\text{-}3\ DPA}$ and 17-oxo-RvD1$_{n\text{-}3\ DPA}$, respectively. 8-Oxo-RvD1 has shown to exert the same potency as RvD1, and 17-oxo-RvD1 has shown to be inactive *in vivo*. Therefore, it can be assumed that 8-oxo-RvD1$_{n\text{-}3\ DPA}$ is an active metabolite, and 17-oxo-RvD1$_{n\text{-}3\ DPA}$ is the inactivation product of RvD1$_{n\text{-}3\ DPA}$.[18]

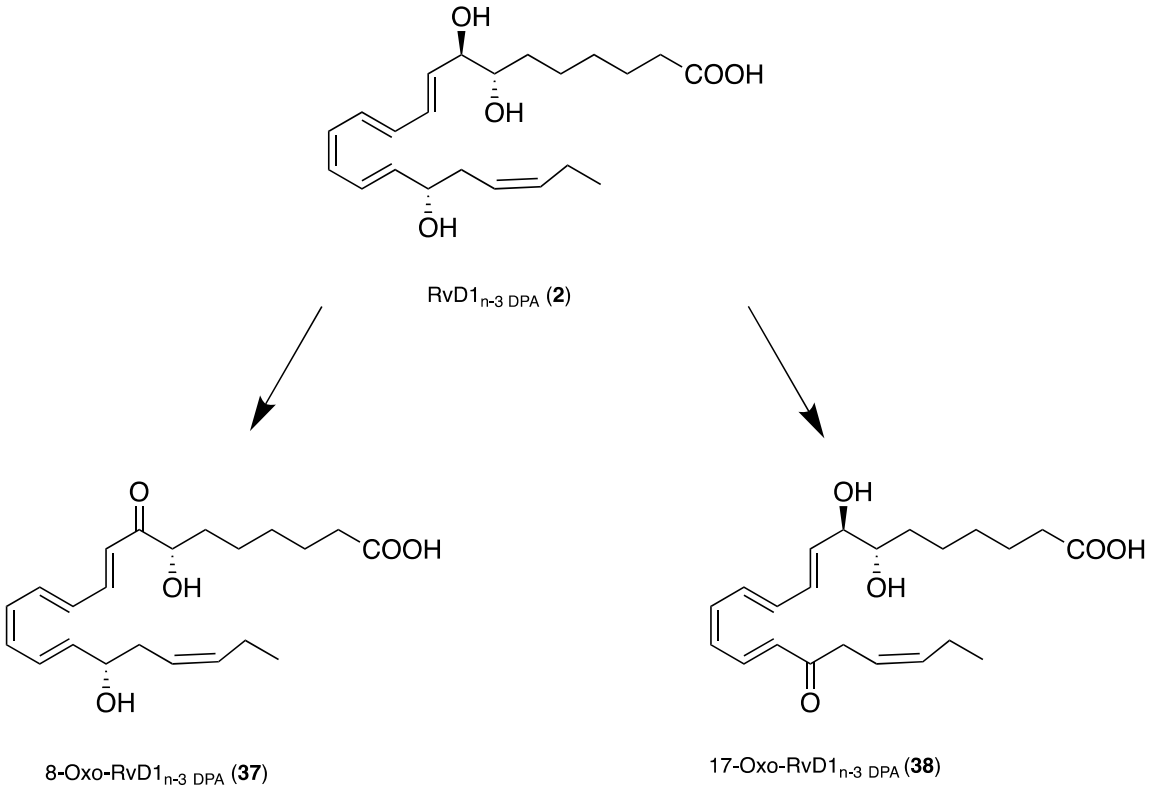

Scheme 2: The anticipated metabolic pathway for RvD1$_{n\text{-}3\ DPA}$ based on the proposed metabolic pathway for RvD1 reported by Serhan.[18]

1.5.4 Structure-activity relationships of RvD1$_{n\text{-}3\ DPA}$

The *E,E,Z,E* –tetraene moiety is chemically labile, susceptible to light, heat and acids, and could easily isomerize to a mixture of geometrical isomers.[3, 139] To retain the pro-resolving properties

of RvD1$_{n\text{-}3\ DPA}$, the *E*-double bond at C_9-C_{10} and the *Z*-double bond at C_{19}-C_{20} must remain in the same configuration.[140] Replacing this tetraene moiety with a benzo-group could potentially mimic the *E,E,Z,E*-tetraene, and the molecule gains structural rigidity. Structural rigidity may be an advantage because EORs, which are mainly responsible for the inactivation *in vivo*, are dependent on a certain conformation for substrate recognition, as seen with LXA_4-analogs. Furthermore, the benzo-group does not isomerize as the *E,E,Z,E*-tetraene moiety.[141] The ethyl ester of RvD1$_{n\text{-}3\ DPA}$ has significantly lower affinity for the receptors GPR18 and ALX-receptor than RvD1$_{n\text{-}3\ DPA}$.[3] Therefore, the carboxylic acid may be important for binding to the receptors.

The configuration of the stereogenic centers with the secondary alcohols at 7*S*, 8*R* and 17*S* are important for the structure-activity relationship (SAR) of RvD1, and therefore assumed to be important for the SAR of RvD1$_{n\text{-}3\ DPA}$. The 17-hydroxy-group is important for retaining the pro-resolving actions of RvD1, as the 17-deoxy-metabolite is the inactivation product of RvD1.[1] The 17*R*-epimer of RvD1$_{n\text{-}3\ DPA}$ may potentially be pro-resolving, as it is analogous to the AT-derived epimers of the D series resolvins, which exert corresponding potency and affinity to the receptors.[1, 72] The 17*R*-epimer of RvD1 has shown to resist rapid enzymatic inactivation by EORs to 17-deoxy-RvD1.[1] This may also be the case for 17*R*-RvD1$_{n\text{-}3\ DPA}$, which could be an interesting lead for further research on more enzymatically stable n-3 DPA-analogs. A structure highlighted with the anticipated SAR for RvD1$_{n\text{-}3\ DPA}$ is presented in Figure 19.

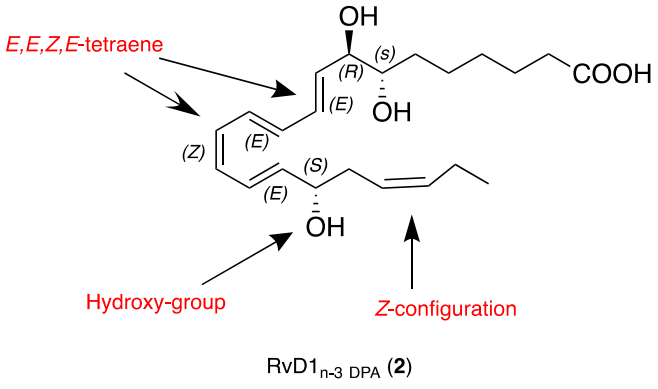

Figure 19: Some of the important structural features are highlighted for RvD1$_{n\text{-}3\ DPA}$.

1.6 Total synthesis of SPMs

There has been great interest in making SPMs and SPM analogs by total synthesis, which could lead to potential new therapeutics and lead compounds. Several efforts have been reported on the total synthesis of SPMs. The first total syntheses of RvD2 and RvD5 were reported in 2004 and 2005, respectively.[142, 143] Rodriguez and Spur reported the first total synthesis of RvD6 [144] in 2012. In 2014, the structure, biosynthesis, *in vivo* bioactions and stereochemistry of $PD1_{n\text{-}3\ DPA}$ was elucidated,[134] while $MaR1_{n\text{-}3\ DPA}$ was prepared and structural assigned in 2014.[135] Recently, Sønderskov *et al.* reported the structural elucidation and the first total synthesis of $MaR2_{n\text{-}3\ DPA}$.[145] Tungen *et al.* reported the first total synthesis of $RvD1_{n\text{-}3\ DPA}$ in 2019. The retrosynthetic analysis of this total synthesis is illustrated in Figure 20.[3]

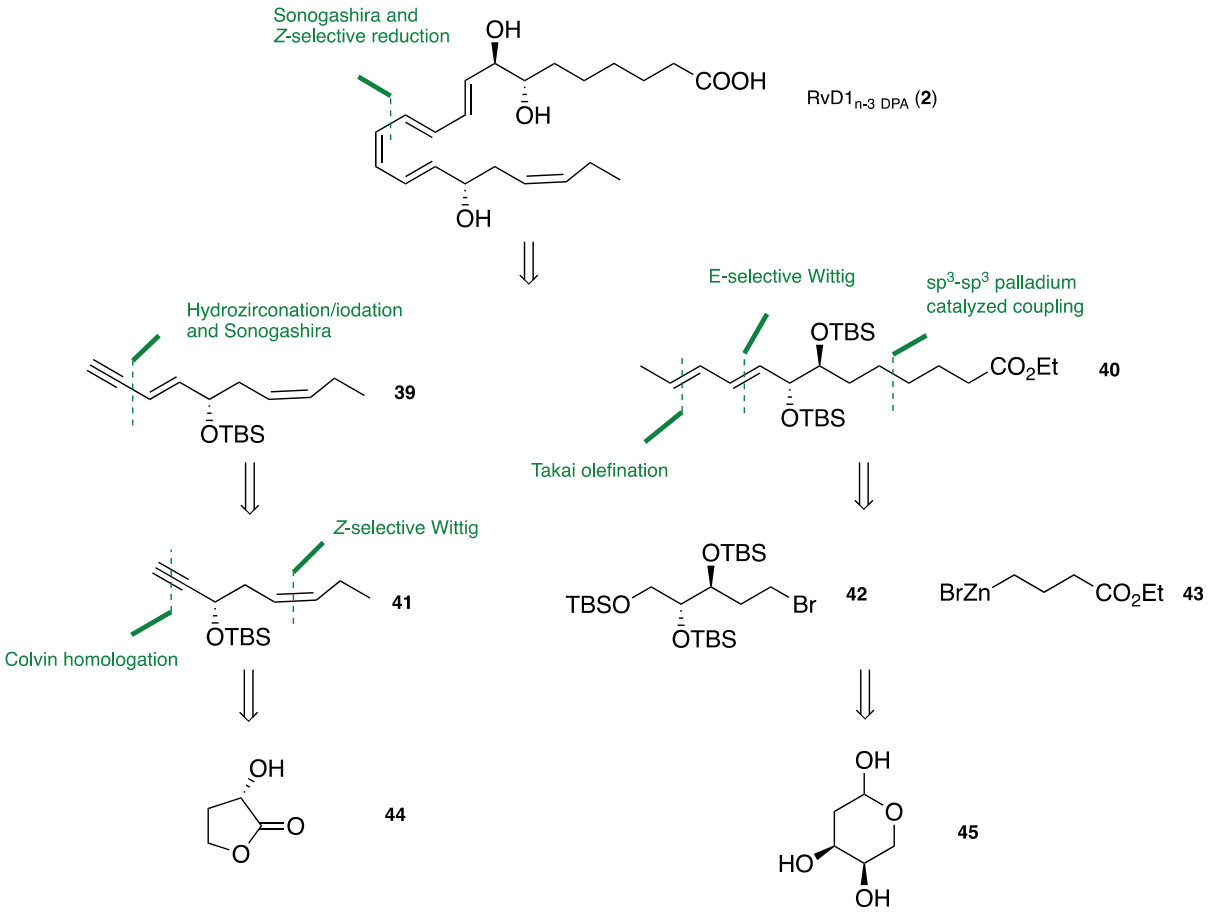

Figure 20: A retrosynthetic analysis of the total synthesis of $RvD1_{n\text{-}3\ DPA}$ reported by Tungen *et al.*[3] This figure is adapted from the master thesis of Reinertsen.[5]

1.7 Synthetic methods

Since the interactions of SPMs with their receptors are stereoselective, the stereoselectivity of the reactions used in total organic synthesis of SPMs are essential. In this section, four reactions used in the efforts towards making benzo-RvD1$_{n\text{-}3\ DPA}$ are highlighted. For the synthesis of the α-fragment, synthetic methods were performed in accordance to the published procedure of Tungen *et al.* and the master thesis of Reinertsen.[3, 5]

1.7.1 The Wittig olefination reaction

The Wittig reaction was used to convert the aldehyde to the *Z*-alkene, as shown in Figure 23. The Wittig reaction was discovered by Georg Wittig in 1954, for which he received the Nobel Prize in Chemistry in 1979.[146]

The Wittig olefination reaction is used to convert an aldehyde or a ketone to an alkene. This reaction can be either *Z* or *E* selective, depending on the ylide. If the ylide is stabilized, *i.e.* with substituents able to stabilize the negative charge, the reaction will be *E*-selective. If the ylide is not stabilized, the reaction will be *Z*-selective.[147] The phosphonium ylide in this reaction is an unstable ylide, in order to generate a *Z*-alkene as the main product. This alkene was reduced in the next step, so the diastereomeric purity of this product was not of importance.

An ylide is a compound that has a positive and a negative charge in the same molecule, on adjacent atoms. In a phosphonium ylide the phosphor atom has a much larger orbital than the carbon, so the orbitals do not sufficiently overlap.[148]

The phosphonium ylide is prepared by deprotonating a phosphonium salt with a strong base. The Wittig reaction begins with a nucleophilic attack on the carbonyl compound by the carbanion of the phosphonium ylide. The negatively charged oxygen atom attacks intramolecularly the phosphorus atom, which results in an intermediate, an oxaphosphetane. This is an unstable four-membered ring, so the ring breaks down to form two double bonds.

The product, the alkene, is formed along with phosphine oxide (P=O). The P=O bond is exceptionally strong and so the reaction is not reversible.[147]

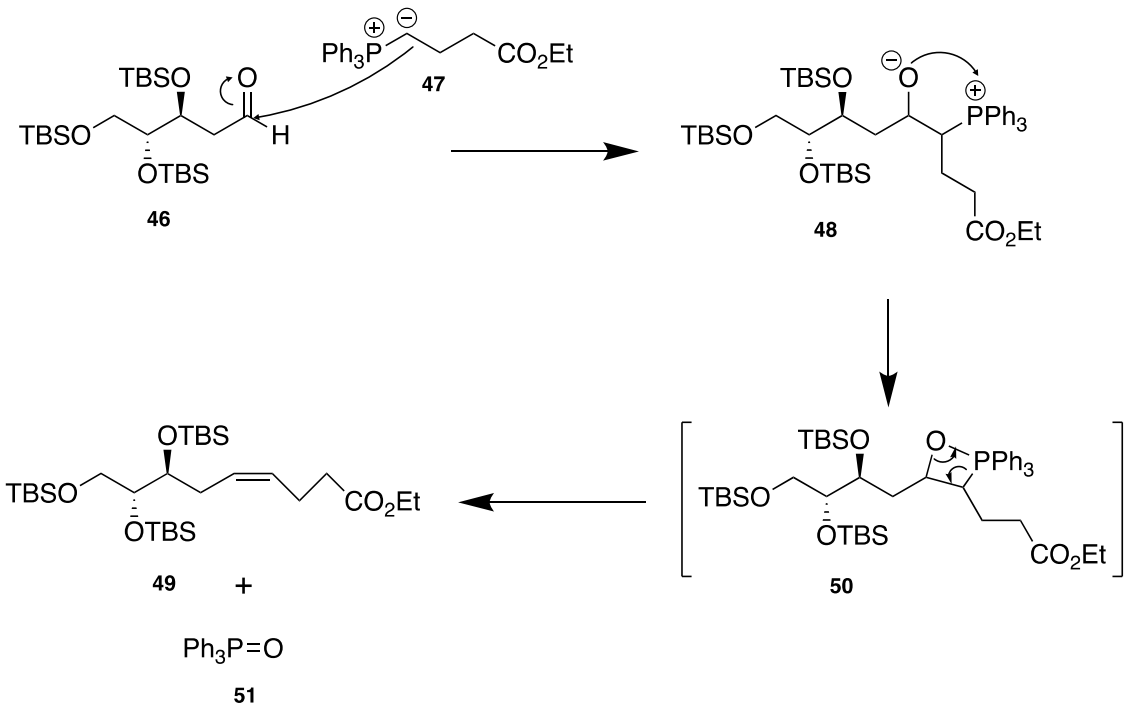

Scheme 3: An outline of the reaction mechanism of the Wittig olefination reaction.[147]

1.7.2 The Tebbe olefination reaction

For the reaction of the aldehyde to the terminal alkene, a Tebbe olefination reaction was performed. The Tebbe olefination gives better yields than a Wittig reaction, especially when encountering steric hindrance, such as the bulky TBS-groups. The Tebbe reaction can also be performed on sensitive substrates, as it does not require strong basic or acidic conditions, which can lead to racemization of the compound.[149, 150]

Dr. Fred N. Tebbe, an industrial chemist, reported the Tebbe reaction in 1978. The Tebbe reagent can react with carbonyl compounds such as aldehydes, ketones, esters and amides to afford an olefin.[151] The molecular formula for the Tebbe reagent is $(C_5H_5)_2TiCH_2ClAl(CH_3)_2$. The chemical structure elucidated by Thompson *et al.* in 2014 is presented in Figure 21.[152] The Tebbe reagent works both as a catalyst and as a methylation agent in the reaction.[151]

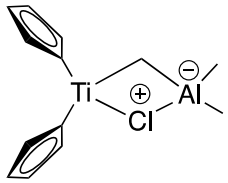

Tebbe reagent (**52**)

Figure 21: Structure of the Tebbe reagent **52** as elucidated by Thompson *et al.* in 2014.[152]

The Tebbe reagent has to be activated by a week Lewis base, such as pyridine, to generate a Shrock type carbene. After activation, the carbon atom of the Shrock type carbene attacks the carbonyl due to the nucleophilic character of the Shrock type carbene, leading to a negative charge on the oxygen atom. The oxygen atom attacks the oxophilic titanium atom, resulting in a four-membered ring called oxatitanacyclobutane, which quickly decomposes to an alkene and a stable titanium oxide. Since there are both an aldehyde and an ester present, only one equivalent of the Tebbe reagent was used to ensure regioselectivity. This reaction is driven by the stability of the titanium oxide formed, and is not reversible.[153] The reaction mechanism of the Tebbe reagent is presented in Scheme 4.

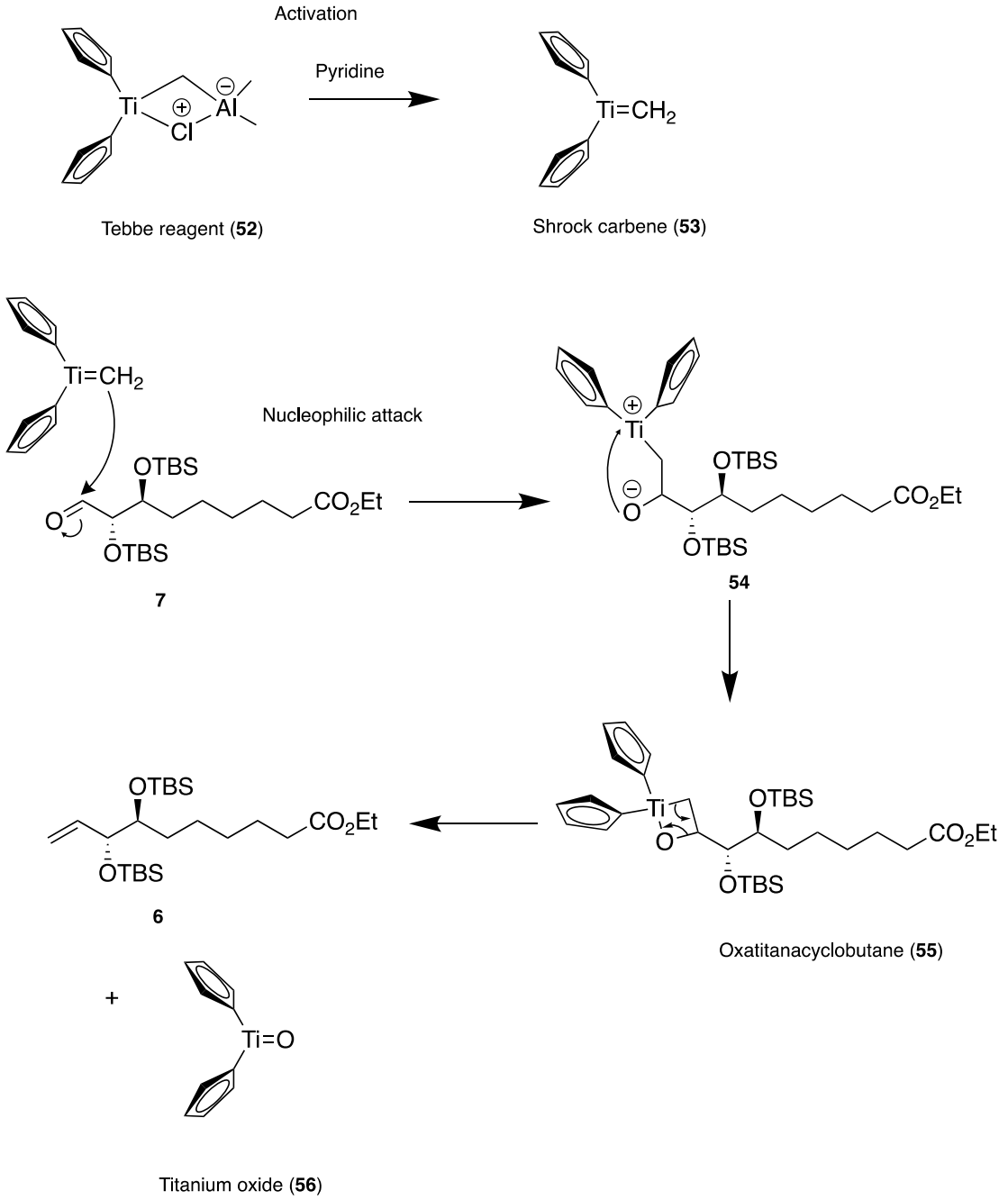

Scheme 4: An outline of the reaction mechanism of the Tebbe olefination. The first step is the activation of the Tebbe reagent to a Shrock type carbene. Further, there is a nucleophilic attack of the carbonyl and then an intramolecular nucleophilic attack of the titanium atom generating a oxatitanacyclobutane, which quickly decomposes to the corresponding alkene.[153]

1.7.3 The Heck-Mizoroki cross-coupling reaction

Dr. Richard F. Heck and Dr. Tsutomu Mizoroki discovered this cross-coupling reaction in the 1970s.[154, 155] Other palladium-catalyzed reactions have been developed, such as the Sonogashira-Hagihara and the Suzuki-Miyaura.[156] Dr. Richard F. Heck received the Nobel prize in Chemistry in 2010 for his work with cross coupling palladium-catalyzed reactions, together with Akira Suzuki and Ei-Ichi Negishi.[157]

The Heck reaction refers to a palladium-catalyzed addition of an aryl halide to an alkene in the presence of a base. Heck reactions are *trans* selective. Several different reagents and palladium-complexes can be used, and it is useful on a broad variety of compounds.[156]

The reaction mechanism of the Heck-Mizoroki reaction used in this thesis is presented in Scheme 5. The first step is an oxidative addition, where the palladium complex inserts itself between the aryl and the halide atom. Next, the palladium complex forms a π-complex with the alkene, and then the palladium-complex binds to the alkene through a carbometallation to form a Pd-σ intermediate. Further, there is a β-hydride elimination that forms a new π -complex. The Pd(0) is regenerated by adding a base such as triethylamine, which removes hydrogen halide from the complex. This is a catalytic cycle, the palladium (0) is ready to react with other molecules, so the amount of catalyst added is small.[158]

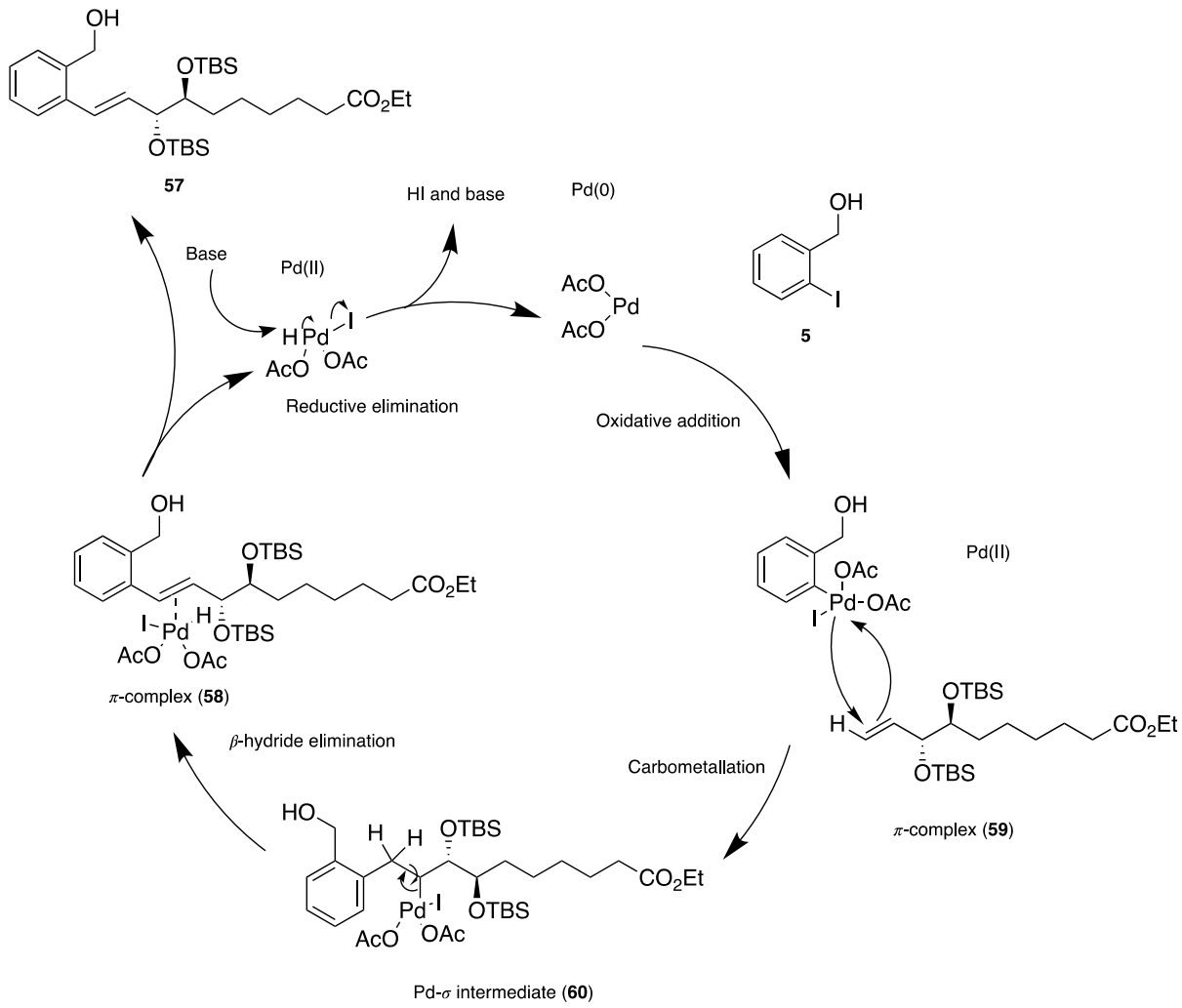

Scheme 5: An outline of the palladium-catalyzed Heck-Mizoroki reaction used in this thesis.[158]

1.7.4 The Barbier reaction

The Barbier reaction was reported by Barbier in 1899.[159] The reaction is similar to the Grignard reaction. The difference is the use of different metallic reagents, such as the use of Zn and In as well as Mg. A Barbier reagent is made *in situ*. The advantage of a Barbier reaction is the tolerance for moisture.[160] The reaction product is a primary, secondary or tertiary alcohol. The mechanism is not analogous to a Grignard reaction, as an organometallic species is not formed.[161]

In this thesis, a Barbier reaction was conducted under nitrogen atmosphere under anhydrous conditions to afford the product compound. The substrate used was an allylic bromide. The reaction utilizes zinc dust, an organic halide and a carbonyl group of an aldehyde or a ketone. The carbon connected to the halide atom attacks the carbon of the carbonyl, due to its nucleophilic character. The reaction mechanism is not clear, but is presumably by a radical mechanism.[161, 162] A general Barbier reaction procedure is presented in Scheme 6.

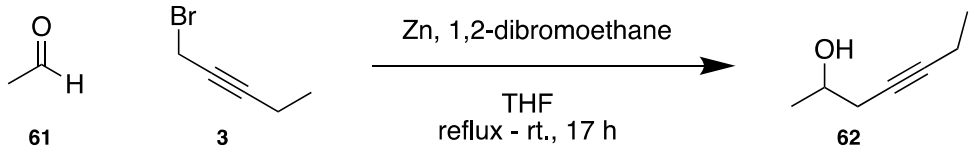

Scheme 6: Outline of a general Barbier reaction procedure.

2 Results and discussions

The first part of this study was to prepare the α-fragment **6** following the procedure of Dr. Jørn E. Tungen and the Master thesis of Reinertsen from the LIPCHEM group at the University of Oslo.[3, 5] A Tebbe olefination reaction was performed as the final step towards α-fragment **6**. α-fragment **6** was prepared in eight steps with an overall yield of 3% (7% based on recovered starting material (brsm)). Further reactions to insert the benzo-moiety and the ω-end were performed on the α-fragment to afford compound **63**. The synthesis from α-fragment **6** to compound **63** was performed over three steps with an overall yield of 23% (71% brsm). The total synthesis from 2-deoxy-D-ribose to compound **63** was performed over 11 steps in an overall yield of 1% (5% brsm). A retrosynthetic analysis is presented in Figure 22.

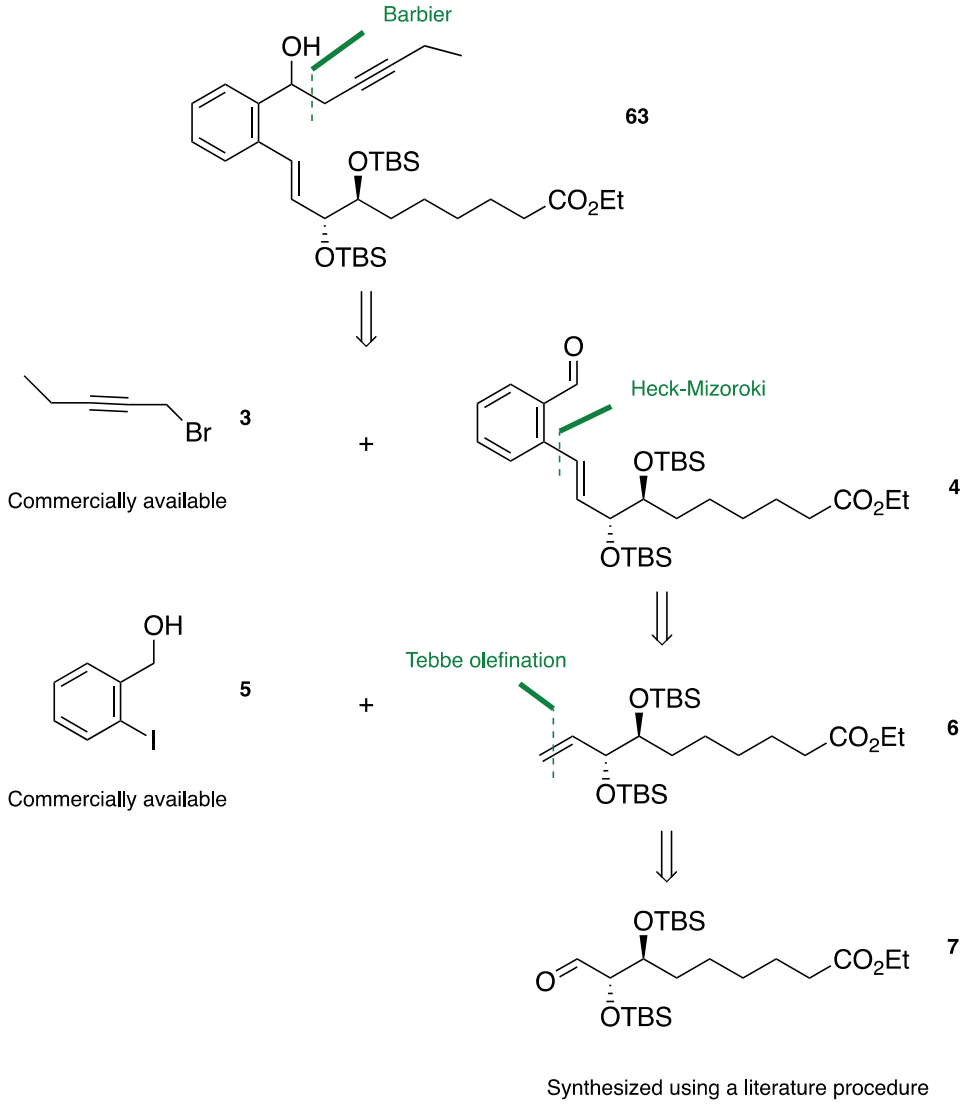

Figure 22: Retrosynthetic analysis of compound **63**.

2.1 Overview of the synthesis towards benzo-RvD1$_{n\text{-}3\ DPA}$

Scheme 7 presents an outline of the synthesis towards benzo-RvD1$_{n\text{-}3\ DPA}$. 2-Deoxy-D-ribose **45** was treated with ethanethiol in concentrated hydrochloric acid (HCl) to afford thioacetal **64**, which was further treated with an excess of 2,6-lutidine as base and *tert*-butyldimethylsilyl triflate (TBSOTf) to yield *tris*-TBS protected compound **65**. The next step afforded aldehyde **46** by oxidizing **65** with *N*-bromosuccinimide (NBS) with 2,6-lutidine as a base. Aldehyde **46** was treated with phosphonium ylide **47** and sodium *bis*(trimethylsilyl)amide (NAHMDS) in a *Z*-selective Wittig reaction to afford alkene **49**. Catalytic hydrogenation with palladium on carbon (Pd/C) afforded compound **66**. Selective deprotection of primary alcohol in compound **66** was performed using *p*-toluenesulfonic acid (PTSA) to yield compound **67**, which was further oxidized with Dess-Martin periodinane (DMP) to afford aldehyde **7**. The α-fragment **6**, was achieved using a Tebbe reagent in dry THF.

Further reactions were performed on the α-fragment **6** to afford compound **63**. The Tebbe product **6** was reacted in a Heck-Mizoroki cross-coupling reaction with 2-iodo-benzyl alcohol **5**, using palladium acetate (Pd(OAc)$_2$) as a catalyst and *o*(tolyl)$_3$P to insert the aromatic moiety in compound **57**. DMP was used to oxidize the primary alcohol in compound **57** to *ortho*-benzaldehyde **4**, which was finally reacted with zinc powder and 1-bromo-2-pentyne **3** in a Barbier reaction to afford compound **63**.

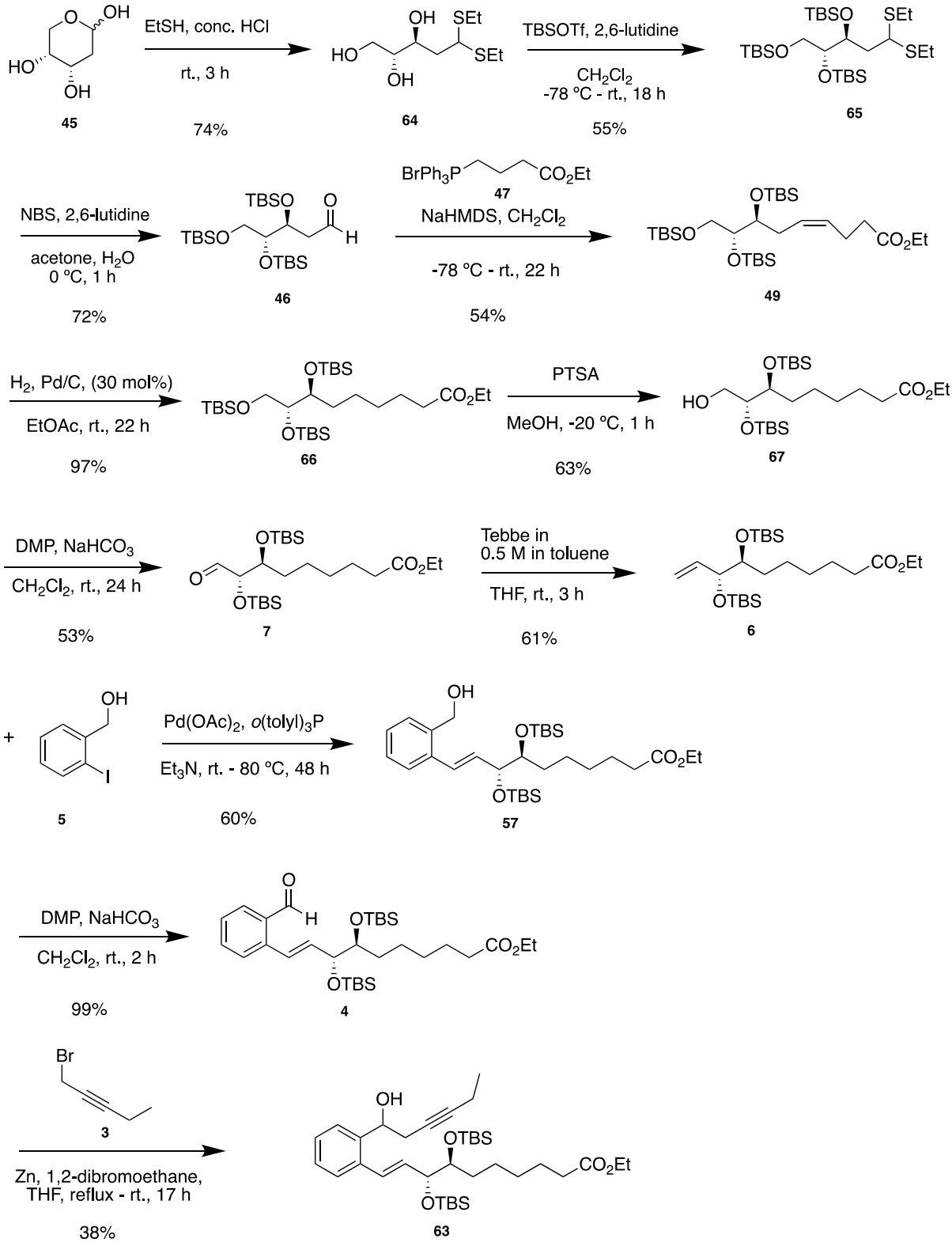

Scheme 7: Outline of the synthesis to afford compound **63**.

Further details on the synthetic methods are found in the experimental section. The obtained ^{1}H NMR and ^{13}C NMR data are found in the appendix, and are discussed in detail below.

2.2 Synthesis of thioacetal 64

2-Deoxy-D-ribose **45** exists as three isomers in aqueous conditions, that is a six-membered ring, an open chain and a five-membered ring,[163] as seen in Scheme 8. The six-membered ring is the dominating isomer in the equilibrium. 2-Deoxy-D-ribose is commercially available.

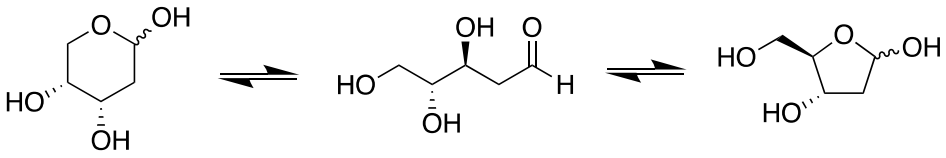

Scheme 8: The chemical equilibrium of 2-deoxy-D-ribose **45** in solution.[163]

To avoid ring cyclization of the open chain, the aldehyde was protected as a thioacetal, as illustrated in Scheme 9. This reaction procedure was performed in accordance with the published procedure of Tungen *et al.*[3] One equivalent of 2-deoxy-D-ribose **45** was dissolved in concentrated HCl and treated with two equivalents of ethanethiol. Concentrated HCl activated the carbonyl moiety for the nucleophilic attack by the ethanethiol. Thiols are weak nucleophiles. After aqueous workup, the crude product was purified by flash chromatography on silica gel to afford thioacetal **64** in 74% yield as a clear yellow oil. All spectral data correspond to the reported data.[3]

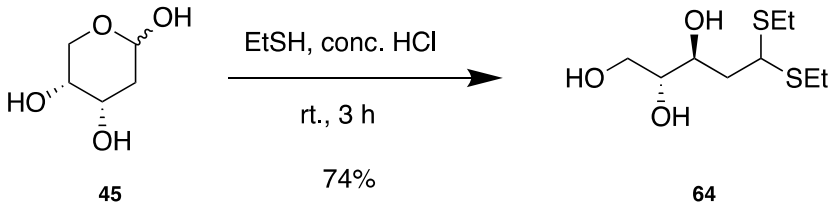

Scheme 9: Outline of the synthesis of thioacetal **64.**

2.3 Characterization of thioacetal 64

2.3.1.1 ^{1}H NMR chemical shifts

The hydrogen atoms of the hydroxy groups does not appear in the ^{1}H NMR spectrum, most likely due to exchange with deuterium. The most downfield signals at 4.12 ppm (dd, *J* = 11.2, 3.6 Hz, 1H) and 3.93-3.87 ppm (m, 1H) are characteristic for the carbinol hydrogen atoms, and have the highest chemical shift values due to the electron withdrawing effect of the oxygen atoms leaving the hydrogen atoms deshielded. Hence, the hydrogen atoms will absorb a higher frequency of radiation. The carbon atom connected to the primary alcohol is chiral, giving rise to two different signals of the methylene-hydrogen atoms due to different chemical environments; 3.73 ppm (dd, *J* = 11.3, 3.8 Hz, 1H) and 3.58 ppm (dd, *J* = 11.3, 6.6 Hz, 1H). There is also a roofing effect of the signals, which shows that the signals are splitting each other. The signal at 3.46 ppm (td, *J* = 6.7, 3.8 Hz, 1H) signals for the hydrogen atoms at the carbon atom vicinal to the thioacetal. The splitting is complex because the vicinal carbon atom is chiral, which gives two signals at 2.10 ppm (ddd, *J* = 13.9, 11.2, 2.4 Hz, 1H) and 1.88 ppm (ddd, *J* = 14.2, 10.2, 3.7 Hz, 1H). The ethyl groups of the thioacetal give two signals at 2.69 ppm (m, 4H) for the methylene groups, and 1.27 ppm (td, *J* = 7.4, 3.8 Hz, 6H) for the methyl groups. It is expected that the methylene groups and the methyl groups of the thioacetal show up as a quartet and a triplet, respectively. These signals are a strong indication for å successful conversion to thioacetal **64**. The ethyl groups of the thioacetal give different chemical shift values. This could be due to spatial arrangement, and so the hydrogen atoms are not chemically equivalent because one moiety is more shielded. This gives two overlapping signals that appear more complex in the spectrum. In total, there are seventeen hydrogen atoms in the spectrum combined with the three hydroxy hydrogen atoms not showing. This is in accordance with the twenty hydrogen atoms of the molecule, giving rise to nine signals due to symmetry.

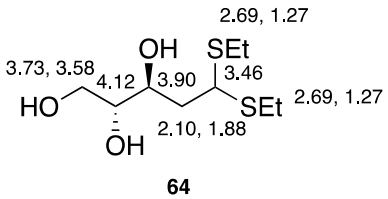

64

Figure 23: Assignment of ^{1}H NMR chemical shifts for compound **64**.

2.3.1.2 ^{13}C NMR chemical shifts

The most downfield signals at 76.4 ppm, 70.8 ppm and 64.7 ppm, are characteristic for the carbinol atoms due to deshielding effects. The signal at 49.1 ppm, in the middle of the MeOH-*d*$_4$ signal, is from the carbon atom bound to the thioacetal. The carbon atom vicinal to the hydroxy groups in the center of the molecule gives a signal at 40.9 ppm. The four upfield signals at 25.2 ppm, 24.2 ppm, 14.9 ppm and 14.8 ppm are signaling for the carbon atoms of the ethyl groups of the thioacetal. It was expected that the carbon atoms of the ethyl groups would give rise to two signals both integrating for two carbon atoms. The spatial arrangement could lead to different chemical shift values due to proximity to the electron withdrawing groups in the molecule, such as the hydroxy groups. The spectrum shows signals accounting for nine carbon atoms, which is in accordance with the total number of carbon atoms in the molecule.

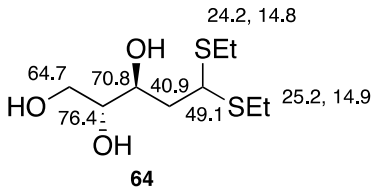

Figure 24: Assignment of ^{13}C NMR chemical shifts for compound **64**.

2.3.1.3 Specific optical rotation

The specific optical rotation measured was -19.2 (c = 2.5, MeOH), which is identical to the earlier reported value of -19.2 (c = 1.0, MeOH) for compound **64**.[3] This is a strong indication of a successful conversion of **45** to the product compound **64**.

2.4 Synthesis of *tris*-silylated compound 65

The reaction was carried out in order to protect the three hydroxy groups in **64**, and was done according to the published procedure of Tungen *et al.*[3] TBSOTf was used herein, as it can silylate both primary, secondary and tertiary alcohols. The oxygen attacks the silicon and then the 2,6-lutidine removes the excess proton (Scheme 10).

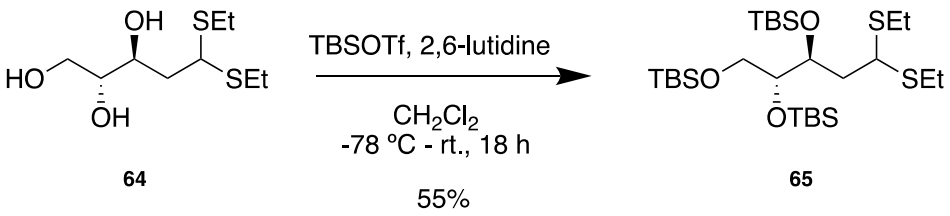

Scheme 10: Outline of the synthesis of compound **65**.

One equivalent of (2*R*,3*S*)-5,5-bis(ethylthio)pentane-1,2,3-triol was dissolved in CH_2Cl_2 and cooled to -78 °C. The solution was stirred for 10 minutes before the addition of an excess of 2,6-lutidine and TBSOTf. The reaction mixture was allowed to slowly reach room temperature in a dry ice/acetone bath for 18 hours. After aqueous workup, flash chromatography was performed on silica gel to afford the product in 55% yield as a clear, colorless oil. All spectral data correspond to the reported data.[3]

2.5 Characterization *tris*-silylated compound 65

2.5.1.1 ^{1}H NMR chemical shifts

The upfield signal at 0.91-0.88 (m, 27H) is characteristic for the hydrogen atoms of the *tert*-butyl substituents in the TBS-groups, and indicates a successful silylation of the hydroxy groups. They appear as singlets because equivalent hydrogen atoms do not split each other. The signal at 0.11-0.04 ppm (m, 18H) corresponds to the hydrogen atoms of the methyl groups bound to the silicon atoms of the TBS-groups, and are four overlapping singlets. The remaining signals correspond to the signals reported from the starting material. In total, there are ten signals integrating for 62 protons in the spectrum, which correspond to the total number of hydrogen atoms in the molecule.

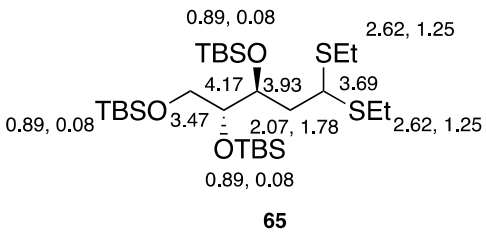

Figure 25: Assignment of ^{1}H NMR chemical shifts for compound **65**.

2.5.1.2 ^{13}C NMR chemical shifts

The signals at 26.2 ppm (3C), 26.1 ppm (3C) and 26.1 ppm (3C) correspond to the carbon atoms of the *tert*-butyl substituents in the TBS-groups. The signals at 18.4 ppm and 18.3 ppm correspond to the fully substituted carbon atoms in the TBS-groups. The upfield signals at -2.8 ppm, -3.5 ppm, -4.4 ppm, -4.7 ppm, -5.3 ppm and -5.3 ppm correspond to the methyl groups connected to the silicon atoms of the TBS-groups. The remaining signals correspond to the signals reported from the starting material. In total, there are 27 carbon atoms in the spectrum, which correspond to the total number of carbon atoms in the molecule.

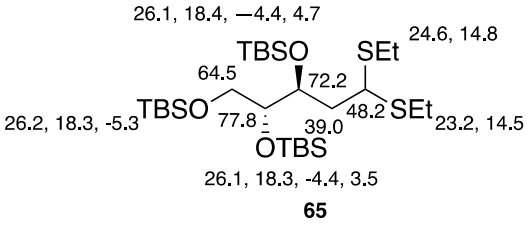

65

Figure 26: Assignment of ^{13}C NMR chemical shifts for compound **65**.

2.5.1.3 Specific optical rotation

The measured value for the specific optical rotation was -7.0 (c = 2.3, MeOH), which is not far from the earlier reported value of -8.9 (c = 1.0, MeOH).[3] This discrepancy may be due to minor errors in weighing the product compound or the solvent.

2.6 Synthesis of aldehyde 46

The next step was to deprotect the aldehyde by removing the thioacetal, as illustrated in Scheme 11. This reaction procedure was done in accordance with the published procedure of Tungen *et al.*[3] The base 2,6-lutidine was added to deprotonate the water molecules. The sulfur atoms reacts with the bromine in NBS, affording a good leaving group when the hydroxide attacks the carbon

of the thioacetal. This happens twice in a consecutive manner, affording the corresponding aldehyde **46**.

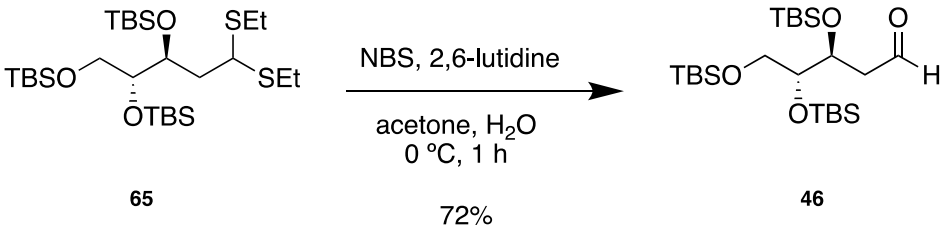

65 72% **46**

Scheme 11: Outline of the synthesis of aldehyde **46**.

One equivalent of **65** was dissolved in a mixture of acetone and water, and cooled to 0 °C. 2,6-Lutidine and *N*-bromosuccinimide was added in excess, and the resulting reaction mixture was allowed to stir for one hour at ambient temperature. After aqueous workup, the crude product was purified by flash chromatography on silica gel to afford aldehyde **46** in 72% yield as a clear, colorless oil. All spectral data correspond to the reported data.[3]

2.7 Characterization of aldehyde 46

2.7.1.1 ^{1}H NMR chemical shifts

The hydrogen atom of the aldehyde has a characteristic chemical shift value of 9.85 ppm (dd, *J* = 3.4, 1.7 Hz, 1H) indicating a successful conversion from *tris*-silylated compound **65** to aldehyde **46**. The splitting indicates two vicinal hydrogen atoms with different chemical shift values, which is in line with the signal at 2.63-2.43 ppm (m, 2H) signaling for the hydrogen atoms vicinal to the carbonyl. The signal shows complex splitting due to the chiral character of the carbon atom, giving rise to two different chemical shift values for the hydrogen atoms, due to the different chemical environments of their vicinal hydrogen atoms (the aldehyde hydrogen atom and the carbinol hydrogen atom). The remaining signals correspond to the signals reported from the starting material. In total, there are seven signals in the spectrum integrating for 52 hydrogen atoms, which correspond to the number of hydrogen atoms in the molecule.

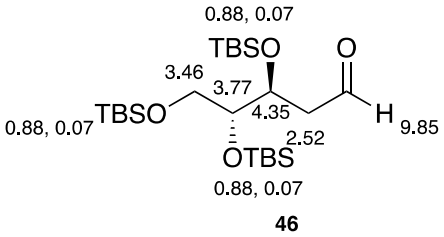

Figure 27: Assignment of ^{1}H NMR chemical shifts for compound **46**.

2.7.1.2 ^{13}C NMR chemical shifts

The downfield signal at 202.8 ppm is characteristic for the carbon atom of the aldehyde group. The signal at 45.8 ppm is the carbon atom vicinal to the carbonyl. The remaining signals correspond to the signals reported from the starting material. In total, there are twenty-three carbon atoms showing in the spectrum, which correspond to the total number of carbon atoms in the molecule.

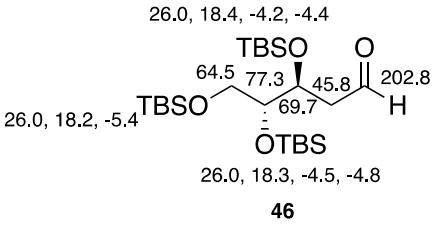

Figure 28: Assignment of ^{13}C NMR chemical shifts for aldehyde **46**.

2.7.1.3 Specific optical rotation

The measured value for the specific optical rotation was -4.9 (c = 1.2, MeOH), which is not far from the earlier reported value of -5.9 (c = 1.0, MeOH).[3] This discrepancy may be due to minor errors in weighing of the product compound or the solvent.

2.8 Synthesis of *Z*-alkene 49

Aldehyde **46** was reacted with a phosphonium salt **47** in a Wittig reaction (Scheme 12). Deprotonation of **47** with NaHMDS generated the corresponding phosphonium ylide. Phosphonium ylide **47** is an unstabilized ylide, favoring the formation of the *Z*-isomer. The reaction was performed at -78 C to afford a higher degree of selectivity towards the *Z*-alkene. This reaction procedure is in accordance with the Master thesis of Reinertsen.[5]

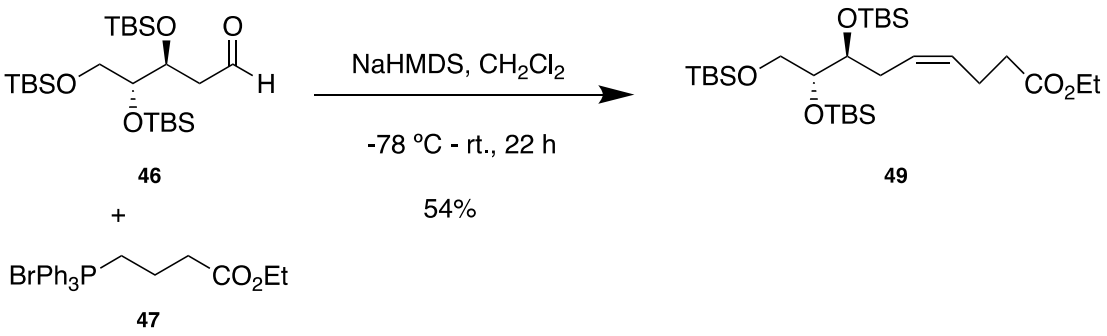

Scheme 12: Outline of the synthesis of *Z*-alkene **49**.

An excess of the Wittig salt was dissolved in CH_2Cl_2, and the reaction mixture was cooled to -78 °C. NaHMDS was added dropwise to afford a yellow solution. One equivalent of **46** was dissolved in dry CH_2Cl_2, and added to the mixture. The resulting solution was stirred for 22 hours while slowly reaching room temperature. After aqueous workup, the crude product was purified by flash chromatography on silica gel to afford *Z*-alkene **49** in 54% yield as a clear colorless oil. All spectral data correspond to the reported data.[5]

2.9 Characterization of *Z*-alkene 49

2.9.1.1 ^{1}H NMR chemical shifts

There is no downfield signal characteristic for an aldehyde proton, indicating a successful conversion from the starting material. The signal at 5.52-5.36 ppm (m, 2H) is the signal for the olefinic hydrogen atoms of the *Z*-double bond, with complex splitting because of the different chemical environments of the vicinal hydrogen atoms. The signal at 4.12 ppm (q, J = 7.1 Hz, 2H) and 1.24 ppm (t, J = 7.2 Hz, 3H) is characteristic for the ethyl moiety of the ester. The signal at 2.39-2.31 ppm (m, 3H) is due to the methylene groups closest and second closest to the carbonyl, and is overlapping with the signal at 2.31-2.22 ppm (m, 2H) that corresponds to the methylene group connected to the carbinol and the double bond. The remaining signals correspond to the signals reported from the starting material. There are eleven signals in the spectrum integrating for 62 hydrogen atoms, which correspond to the total number of hydrogen atoms in the molecule.

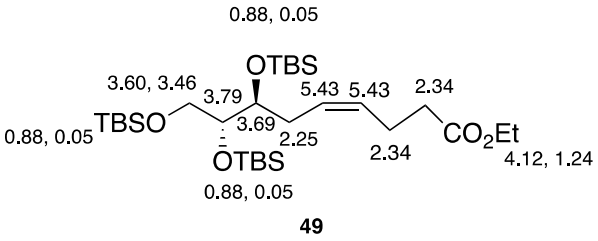

49

Figure 29: Assignment of ^{1}H NMR chemical shifts for *Z*-alkene **49**.

2.9.1.2 ^{13}C NMR chemical shifts

The downfield signals at 128.9 ppm and 128.6 ppm are characteristic for the olefin carbon atoms of the alkene. The signals at 60.4 and 14.4 ppm are signaling for the carbon atoms of the ester moiety. The signals at 34.4 ppm, 30.6 ppm and 23.2 ppm are signaling for the methylene groups. The remaining signals correspond to the signals reported from the starting material. There are 29 carbon atoms showing in the spectrum, which correspond to the total number of carbon atoms in the molecule.

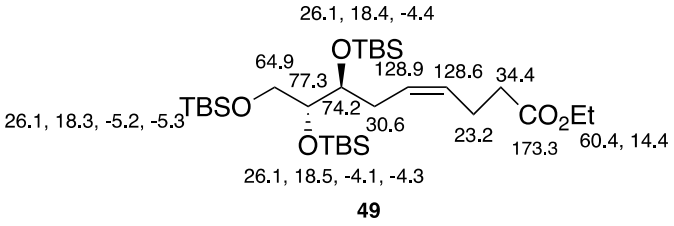

Figure 30: Assignment of ^{13}C NMR chemical shifts for *Z*-alkene **49**.

2.9.1.3 Specific optical rotation

The measured value for the specific optical rotation was -4.1 (c = 1.5, MeOH), which is close to the earlier reported value of -5.0 (c = 1.0, $CHCl_3$).[5] This indicates a successful conversion to the product compound.

2.10 Synthesis of ethyl ester 66

A catalytic hydrogenation reaction was performed to saturate the alkene, as illustrated in Scheme 13. This reaction procedure was done in accordance with the master thesis of Reinertsen.[5]

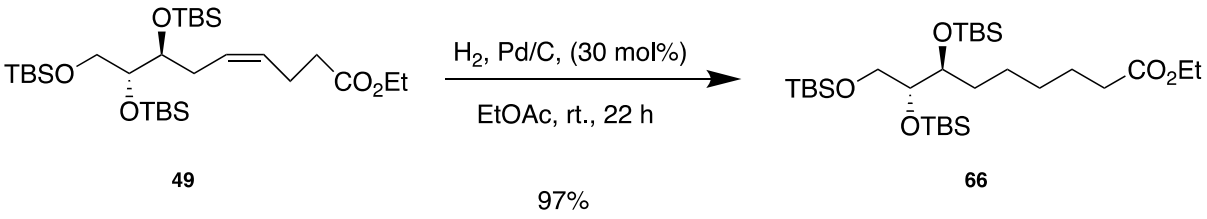

Scheme 13: Outline of the synthesis of ethyl ester **66**.

One equivalent of *Z*-alkene **49** was dissolved in EtOAc, followed by the addition of Pd/C to afford a black reaction mixture. The suspension was stirred for 22 hours at room temperature. The crude product was purified by filtration through a plug of celite to afford ethyl ester **66** in 97% yield as a clear, colorless oil. All spectral data correspond to the reported data.[3]

2.11 Characterization of ethyl ester 66

2.11.1.1 ^{1}H NMR chemical shifts

There are no signals characteristic for olefinic protons, which indicate a successful conversion from *Z*-alkene **49** to ethyl ester **66**. The signals at 2.28 ppm (t, *J* = 7.6 Hz, 2H), 1.62 ppm (p, *J* = 15.0, 7.5 Hz, 2H), 1.45-1.38 ppm (m, 2H) and 1.35-1.27 ppm (m, 4H) corresponds to the methylene groups. The triplet at 2.28 ppm (t, *J* = 7.6 Hz, 2H), which is the most downfield signal of the methylenes, is presumably due to the methylene adjacent to the carbonyl, which has two vicinal hydrogen atoms with the same chemical environment. The remaining signals correspond to the signals reported from the starting material. In total, there are eleven signals in the spectrum integrating for 64 protons, which correspond to the total number of hydrogen atoms in the molecule.

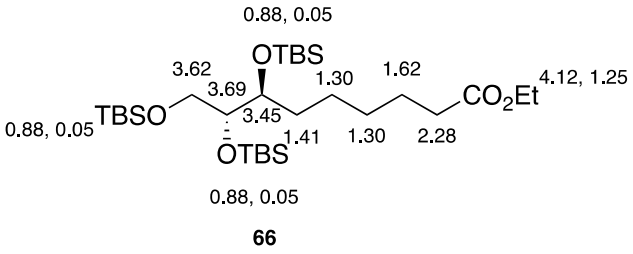

Figure 31: Assignment of ^{1}H NMR chemical shifts for ethyl ester **66**.

2.11.1.2 ^{13}C NMR chemical shifts

The carbon atoms of the methylene groups give rise to signals at 34.6 ppm, 32.5 ppm, 29.7 ppm, 25.3 ppm and 25.2 ppm. The most and second most downfield signal is presumably the carbon atom adjacent to the carbonyl and the carbon atom adjacent to the carbinol in the center of the molecule, respectively. The remaining signals correspond to the signals reported from the starting material. The total number of signals accounts for 29 carbon atoms, which correspond to the total number of carbon atoms in the molecule.

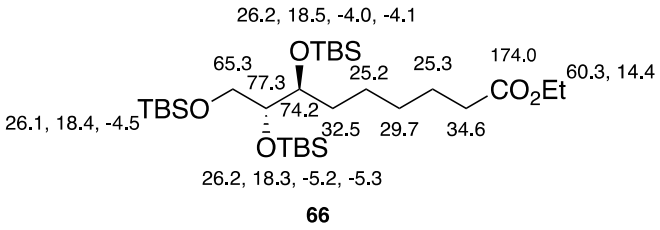

Figure 32: Assignment of ^{13}C NMR chemical shifts for ethyl ester **66**.

2.11.1.3 Specific optical rotation

The measured value for the specific optical rotation was -5.1 (c = 1.7, MeOH), which is further from the earlier reported values of -11.0 (c = 0.5, MeOH)[3] and -8.2 (c = 0.5, MeOH).[5] This discrepancy may be due to small impurities, or small errors in weighing the product compound or the solvents. The specific optical rotation is quite sensitive to small changes in concentration. All of the values are negative, and in the same magnitude. Based on the NMR data, this indicates a successful conversion to the product compound.

2.12 Synthesis of primary alcohol 67

The selective deprotection of the primary alcohol was performed using PTSA (Scheme 14). PTSA protonates the oxygen of the primary TBS group, making TBSOH a good leaving group. The oxygen atom of methanol reacts with a nucleophilic attack on the carbon atom.

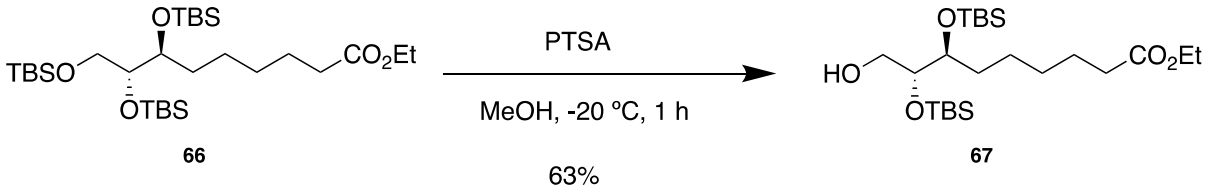

Scheme 14: Outline of the synthesis of primary alcohol **67**.

This reaction procedure is in accordance with the published procedure of Tungen *et al.*[3] One equivalent of ethyl ester **66** was dissolved in methanol and cooled to -20 °C, followed by the addition of one equivalent of PTSA. The reaction mixture was stirred for one hour, regardless

of any starting material left. This was to ensure that further deprotection of the other hydroxy groups were limited to a minimum. After aqueous workup, the crude product was purified by flash chromatography on silica gel, where the remaining starting material was recovered, to afford primary alcohol **67** in 63% yield (81% brsm) as a clear, colorless oil. All spectral data correspond to the reported data.[3]

2.13 Characterization of primary alcohol 67

2.13.1.1 ^{1}H NMR chemical shifts

The broad signal at 2.03 ppm (s, 1H) is characteristic for the hydrogen atom of the hydroxy group, and is an indication of a successful deprotection to primary alcohol **67**. The signals at 0.90 ppm (s, 9H) and 0.88 ppm (s, 9H) are the hydrogen atoms of the *tert*-butyl substituents in the remaining TBS-groups. The multiplet and singlet at 0.10-0.08 ppm (9H) and 0.06 ppm (3H), respectively, are the hydrogens of the methyl groups of the remaining TBS-groups. The remaining signals correspond to the signals reported from the starting material. There are 13 signals in the spectrum, which integrate for 50 protons. This is in line with the total number of hydrogen atoms in the molecule.

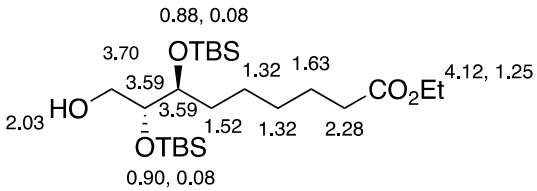

Figure 33: Assignment of ^{1}H NMR chemical shifts for primary alcohol **67**.

2.13.1.2 ^{13}C NMR chemical shifts

The signals correspond to the signals reported from the starting material, only three signals less because of the removed TBS-group. The total number of signals account for 23 carbon atoms, which correspond to the total number of carbon atoms in the molecule.

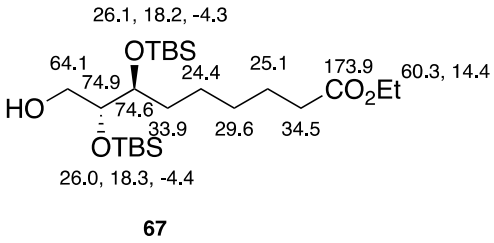

67

Figure 34: Assignment of ^{13}C NMR chemical shifts for primary alcohol **67**.

2.13.1.3 Specific optical rotation

The measured value for the specific optical rotation was -1.6 (c = 2.2, MeOH), which is close to the earlier reported value of -1.9 (c = 1.0, MeOH).[3] This indicates a successful conversion to the product compound.

2.14 Synthesis of aldehyde 7

Primary alcohol **67** was oxidized to the corresponding aldehyde **7** using Dess-Martin Periodinane (DMP), as illustrated in Scheme 15. DMP readily converts primary alcohols to aldehydes, and do not further oxidize the aldehydes to carboxylic acids. Since the bulky TBS-groups sterically hindered the primary alcohol, the reaction performed over a longer period than expected.

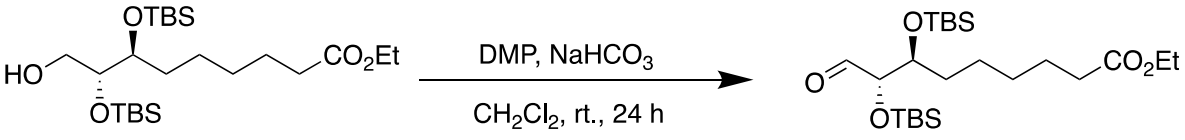

67 53% **7**

Scheme 15: Outline of the synthesis of aldehyde **7**.

This reaction procedure is in accordance with the procedure reported in the Master thesis of Reinertsen.[5] One equivalent of the primary alcohol was dissolved in CH_2Cl_2. An excess of $NaHCO_3$ was added to the solution, followed by the addition of at least two equivalents of Dess-Martin periodinane. The mixture was stirred for 24 hours over night. After aqueous workup,

the crude product was purified by flash chromatography on silica gel to afford aldehyde **7** in 53% yield as a clear, colorless oil. All spectral data correspond to the reported data.[5]

2.15 Characterization of aldehyde 7

2.15.1.1 ^{1}H NMR chemical shifts

The characteristic signal at 9.59 ppm (d, J = 1.7 Hz, 1H) is the hydrogen atom of the aldehyde, indicating a successful transformation to aldehyde **7** from the starting material. The remaining signals correspond to the signals reported from the starting material. The 11 signals in the spectrum integrate for 48 protons, which correspond to the total number of hydrogen atoms in the molecule.

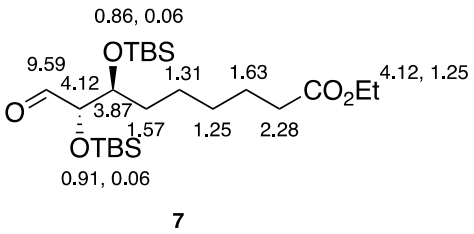

Figure 35: Assignment of ^{1}H NMR chemical shifts for aldehyde **7**.

2.15.1.2 ^{13}C NMR chemical shifts

The signal at 203.9 ppm is the characteristic carbon atom of the aldehyde. The remaining signals correspond to the signals reported from the starting material. The signals in the spectrum account for 23 carbon atoms, which correspond to the total number of carbon atoms in the molecule.

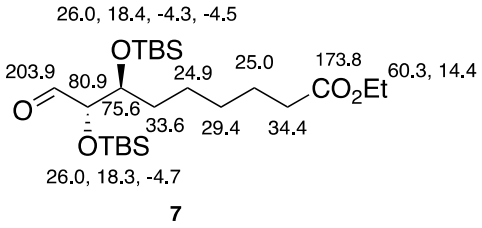

Figure 36: Assignment of ^{13}C NMR chemical shifts for aldehyde **7**.

2.15.1.3 Specific optical rotation

The measured value for the specific optical rotation was +7.6 (c = 2.3, MeOH), which is not far from the earlier reported value of +12.7 (c = 0.5, MeOH).[3] This could be due to slight errors in weighing the product compound or the solvents. The values are both positive and in the same magnitude. Based on the NMR data, this indicates a successful conversion to the product compound.

2.16 Synthesis of terminal alkene 6

For the reaction of aldehyde **7** to terminal alkene **6**, the Tebbe olefination reaction was performed (Scheme 16). This could have been done using the Wittig reaction, but because of the steric hindrance encountered by the bulky TBS-groups, the Tebbe reagent was considered a better option, as Wittig reactions are not as efficient with steric hindered carbonyls. Because the potential reactivity with the ester group, one equivalent of the Tebbe reagent was used to ensure the regioselectivity of the reaction.

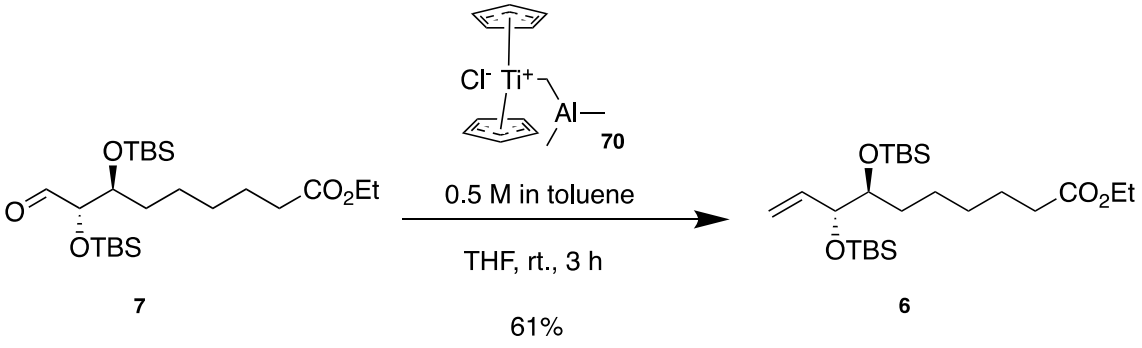

Scheme 16: Outline of the synthesis of terminal alkene **6**.

This reaction procedure is in accordance with the published procedure of Xuequan *et al.*[164] One equivalent of the aldehyde was dissolved in dry THF and added dropwise over 20 minutes to the Tebbe reagent, which was diluted in toluene. The reaction was allowed to stir for two hours. After aqueous workup, the crude product was purified by flash chromatography on silica gel to afford terminal alkene **6** in 61% yield (99% brsm) as a clear, colorless oil. All spectral data correspond with what is expected from this compound.

2.17 Characterization of terminal alkene 6

2.17.1.1 ^{1}H NMR chemical shifts

There are no signals downfield in the spectrum, and the signal at 5.87-5.75 ppm (m, 1H) and 5.17-5.07 ppm (m, 2H) are characteristic for the aliphatic hydrogen atoms. This indicates a successful conversion from aldehyde **7** into terminal alkene **6**. The two terminal hydrogen atoms at 5.17-5.07 ppm should have been a doublet, but this signal appears more complex in the spectrum. The remaining signals correspond to the signals reported from the starting material. The fourteen signals in the spectrum integrate for 50 protons, which correspond to the total number of hydrogen atoms in the molecule.

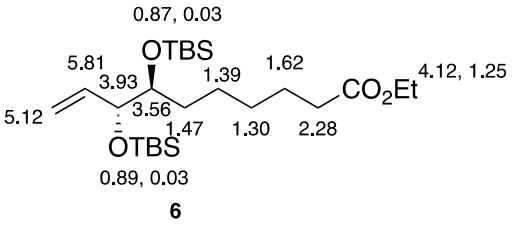

Figure 37: Assignment of ^{1}H NMR chemical shifts for terminal alkene **6**.

2.17.1.2 ^{13}C NMR chemical shifts

The signals at 139.3 ppm and 116.0 ppm are the aliphatic carbon atoms. The remaining signals correspond to the signals reported from the starting material. The signals in the spectrum account for 24 carbon atoms, which correspond to the total number of carbon atoms in the molecule.

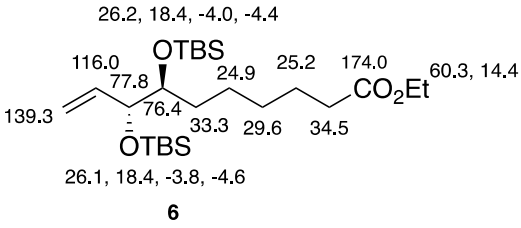

Figure 38: Assignment of ^{13}C NMR chemical shifts for terminal alkene **6**.

2.17.1.3 MS- and HRMS-characterization

The reported molecular weight and the peak at 481.3140 *m/z* is in correspondence with the exact mass of the sodium adduct. This indicates a successful conversion to the product compound.

2.17.1.4 Specific optical rotation

The calculated value for the specific optical rotation was +0.4 (c = 1.8, MeOH).

2.18 Synthesis of *ortho*-benzyl alcohol 57

The Heck cross-coupling reaction was performed to introduce the benzo-moiety, as illustrated in Scheme 17. Tri(*o*-tolyl)phosphine reduce the palladium from Pd(II) to Pd(0), and ensures that the Pd(0) is regenerated. 2-Iodobenzyl alcohol **5** and terminal alkene **6** reacted in the presence of a palladium catalyst and a base to give a *ortho*-benzyl alcohol **57**.

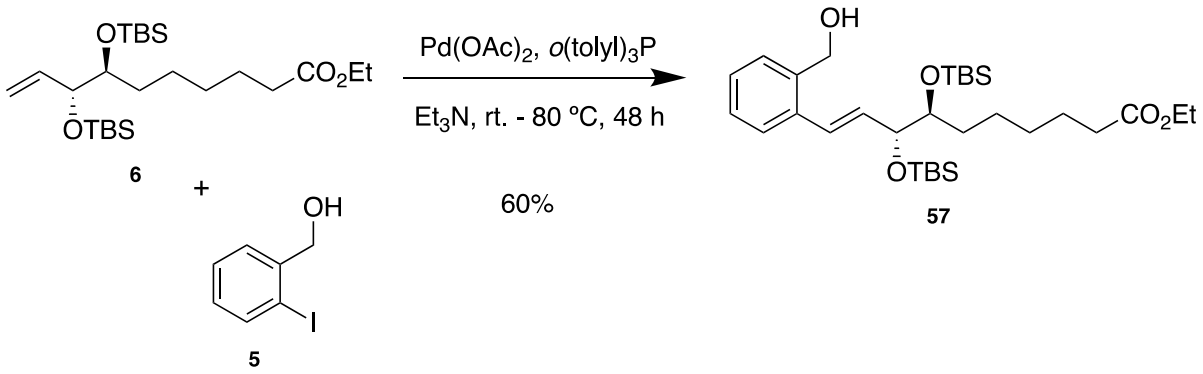

Scheme 17: Outline of the synthesis of *ortho*-benzyl alcohol **57**.

This reaction procedure is in accordance with the published procedure of Colm *et al.*[165] Just below one equivalent of 2-iodobenzyl alcohol **5** was dissolved in Et_3N and added to one equivalent of **6.** $Pd(OAc)_2$ and *o*$(tolyl)_3P$ was added, and the resulting reaction mixture was heated to 80 °C and stirred for 48 hours. After aqueous workup, the crude product was purified by flash chromatography on silica gel, where the remaining starting material was recovered, to afford *ortho*-benzyl alcohol **57** in 60% yield (86% brsm) as a clear, pale yellow oil. All spectral data correspond with what is expected from this compound.

2.19 Characterization of *ortho*-benzyl alcohol 57

2.19.1.1 ^{1}H NMR chemical shifts

There is no signal for the hydrogen atom in the hydroxy group, most likely due to exchange with deuterium. The signals at 7.47 ppm (dd, J = 7.2, 1.8 Hz, 1H), 7.38 ppm (dd, J = 7.0, 2.0 Hz, 1H) and 7.31 – 7.22 ppm (m, 2H) are characteristic for the aromatic moiety, and indicates a successful conversion from terminal alkene **6** to *ortho*-benzyl alcohol **57**.The signals at 6.79 ppm (d, J = 15.8 Hz, 1H) and 6.13 ppm (dd, J = 15.8, 7.0 Hz, 1H) are due to the aliphatic hydrogen atoms, and the coupling constant indicates that the alkene is in the *E*-configuration. The methylene hydrogen atoms adjacent to the hydroxy group give rise to a signal at 4.75 ppm (s, 2H). The remaining signals correspond to the signals reported from the starting material. The 18 signals in the spectrum integrate for 55 protons in addition to the hydroxy proton, which does not appear in the spectrum. This correspond to the total number of hydrogen atoms in the molecule.

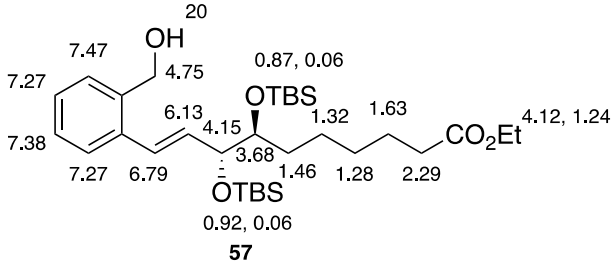

Figure 39: Assignment of ^{1}H NMR chemical shifts for *ortho*-benzyl alcohol **57**.

2.19.1.2 ^{13}C NMR chemical shifts

The aromatic carbon atoms give rise to characteristic signals at 133.4 ppm, 128.3 ppm, 128.2 ppm, 127.7 ppm, 127.6 ppm and 126.4 ppm. The aliphatic carbon atoms give the signals at 133.4 and 128.3 ppm. The carbon atom adjacent to the hydroxy group gives the signal at 63.5 ppm. The remaining signals correspond to the signals reported from the starting material. The signals in the spectrum account for 31 carbon atoms, which correspond to the total number of carbon atoms in the molecule.

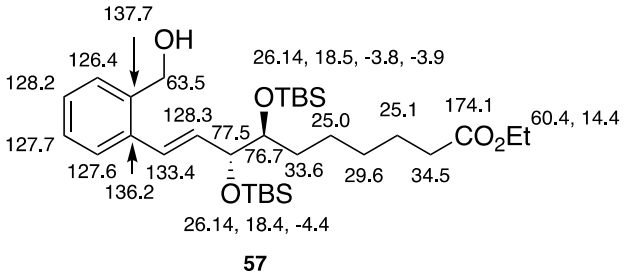

57

Figure 40: Assignment of ^{13}C NMR chemical shifts for *ortho*-benzyl alcohol **57**.

2.19.1.3 MS- and HRMS-characterization

The reported molecular weight and the peak at 587.3558 *m/z* is in correspondence with the exact mass of the sodium adduct. This indicates a successful conversion to the product compound.

2.19.1.4 Specific optical rotation

The calculated value for the specific optical rotation was -0.2 (c = 1.4, MeOH).

2.20 Synthesis of *ortho*-benzaldehyde 4

Dess-Martin periodinane was used to oxidize *ortho*-benzyl alcohol **57** into *ortho*-benzaldehyde **4** using the same conditions as reported earlier for the synthesis of compound **7**. The starting material was converted readily into *ortho*-benzaldehyde **4** (Scheme 18).

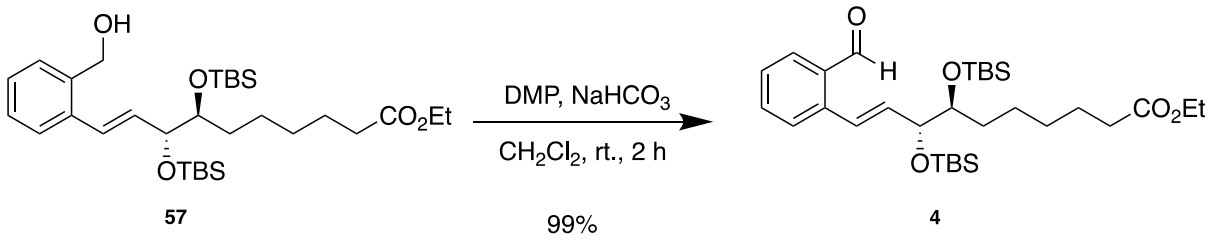

Scheme 18: Outline of the synthesis of *ortho*-benzaldehyde **4**.

This reaction procedure is in accordance with the procedure in the Master thesis of Reinertsen.[5] One equivalent of *ortho*-benzyl alcohol **57** was dissolved in CH_2Cl_2. An excess of $NaHCO_3$ was added to the solution, followed by the addition of over two equivalents of DMP. The reaction was stirred for 2 hours. After aqueous workup, the crude product was purified by flash chromatography on silica gel to afford *ortho*-benzaldehyde **4** in 99% yield as a clear, colorless oil. All spectral data correspond to what is expected from this compound.

2.21 Characterization of *ortho*-benzaldehyde 4

2.21.1.1 ^{1}H NMR chemical shifts

The hydrogen atom of the aldehyde gives a characteristic signal at 10.31 ppm (s, 1H), indicating a successful transformation from *ortho*-benzyl alcohol **57** to *ortho*-benzaldehyde **4**. The remaining signals correspond to the signals reported from the starting material. The 17 signals in the spectrum integrate for 54 protons, which correspond to the total number of hydrogen atoms in the molecule.

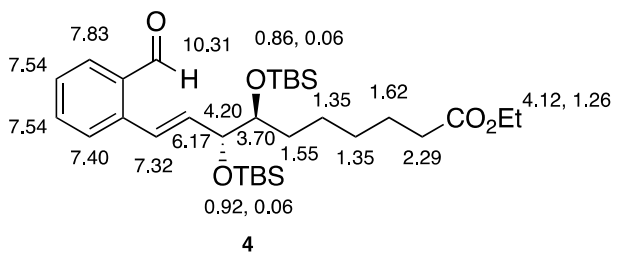

Figure 41: Assignment of ^{1}H NMR chemical shifts for *ortho*-benzaldehyde **4**.

2.21.1.2 ^{13}C NMR chemical shifts

The carbon atom of the aldehyde gives a characteristic signal at 192.2 ppm. The remaining signals correspond to the signals reported from the starting material. The signals in the spectrum account for 31 carbon atoms, which correspond to the total number of carbon atoms in the molecule.

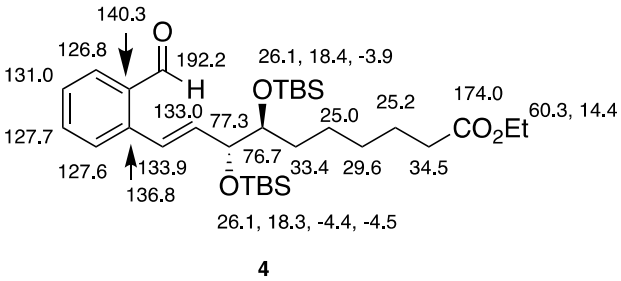

4

Figure 42: Assignment of ^{13}C NMR chemical shifts for *ortho*-benzaldehyde **4**.

2.21.1.3 MS- and HRMS-characterization

The reported molecular weight and the peak at 585.3401 *m/z* is in correspondence with the exact mass of the sodium adduct, only differing with 0.0001, which is within the requirements of the 10 ppm error criteria for HRMS. This indicates a successful conversion to *ortho*-benzaldehyde **4**.

2.21.1.4 Specific optical rotation

The calculated value for the specific optical rotation was -2.4 (c = 0.63, MeOH).

2.22 Synthesis of alkyne 63

The alkyne moiety was introduced by a Barbier reaction, as presented in Scheme 19. The modest yield achieved herein may be due to the steric hindrance of the bulky TBS-groups. This reaction procedure is in accordance with the published procedure of Yanagisawa *et al.*[166]

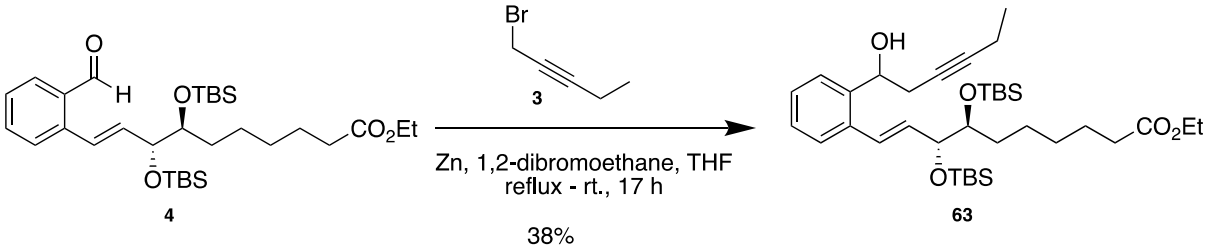

Scheme 19: Outline of the synthesis of alkyne **63**.

An excess of Zinc powder was dissolved in dry THF, and 1,2-dibromoethane was added. The reaction mixture was heated to reflux, stirred for 5 minutes and cooled to 0 °C. Two equivalents of 1-bromo-2-pentyne was dissolved in dry THF and added to the reaction mixture. The reaction mixture was stirred for one hour at 0 °C. One equivalent of *ortho*-benzaldehyde **4** was dissolved in dry THF and added to the reaction mixture at 0 °C. The reaction was heated to reflux and was allowed to stir for 17 hours. After aqueous workup, the crude product was purified by flash chromatography on silica gel, where the remaining starting material was recovered, to afford alkyne **63** in 38% yield (83% brsm) as a clear, colorless oil. All spectral data correspond to what is expected from this compound, but optimal ^{13}C NMR spectra were not obtained due to the Covid-19 situation. The ^{1}H NMR, MS and HRMS analysis performed confirm the successful conversion to the desired product compound. There are some impurities in the ^{1}H NMR spectrum, which indicates that the reaction gave some undesired by-products. Therefore the specific optical rotation measured is not for the pure compound. Unfortunately, there was no time to purify the product compound or analyze these possible by-products.

2.23 Characterization of alkyne 63

2.23.1.1 ^{1}H NMR chemical shifts

There are no signals downfield in the spectrum, which indicates a successful conversion from the starting material. The signal at 4.95 (t, J = 3.7 Hz, 1H) is characteristic for the benzylic carbinol hydrogen atom. The multiplet at 2.21 – 2.17 (2H) signals for the propargylic methylene hydrogens vicinal to the benzylic hydroxy group. The complexity of this signal is due to the different chemical environments of the two hydrogen atoms. The signal at 1.67 – 1.59 (m, 4H) is integrating for hydrogen atoms of the methylene group on C_3 and the propargylic hydrogen

atoms on C_{21}, which are overlapping each other. The triplet at 1.12 (t, J = 7.6, 0.9 Hz, 3H) accounts for the hydrogen atoms of the methyl group at the ω-end. The remaining signals correspond to the signals reported from the starting material. The signals in the spectrum account for 61 protons in addition to the hydroxy proton which does not appear in the spectrum. This correspond to the total number of hydrogen atoms in the molecule.

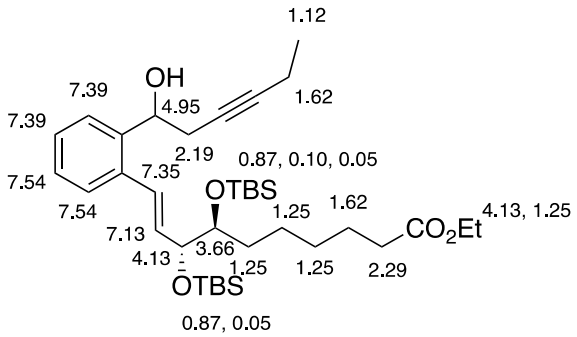

63

Figure 43: Assignment of ^{1}H NMR chemical shifts for alkyne **63**.

2.23.1.2 MS- and HRMS-characterization

The reported molecular weight and the peak at 653.4028 *m/z* is in correspondence with the exact mass of the sodium adduct. This indicates a successful conversion to alkyne **63**.

2.23.1.3 Specific optical rotation

The calculated value for the specific optical rotation was +423.2 (c = 0.41, CH_2Cl_2). This high value may be due to the evaporation of CH_2Cl_2, which gives a higher concentration of the product compound. A higher concentration equals a higher number of molecules that possess chiral qualities, which results in a higher specific optical rotation value.

2.24 Summary and future studies

2.24.1 Summary

This study has attempted to develop a total organic synthesis of a benzo-analog of RvD1$_{n\text{-}3\ DPA}$. The α-fragment **7** was successfully synthesized using the same synthetic methods reported by Tungen *et al.*[3] and in the Master thesis of Reinertsen.[5] A Tebbe olefination reaction was performed to yield terminal alkene **6**. Furthermore, a Heck-Mizoroki cross-coupling reaction was performed to insert the benzo-group and the 17-hydroxy group in compound **57**. The 17-hydroxy group was oxidized by DMP to afford *ortho*-benzaldehyde **4**, which was further subjected to a Barbier reaction to afford a triple bond in the C_{19}-C_{20} position, compound **63**.

The total synthesis from 2-deoxy-D-ribose to compound **63** was performed over 11 steps in an overall yield of 1% (5% brsm). All reactions have been successful, although some of the yields have been low. Due to the limited timeframe of this study and the Covid-19 situation, the total synthesis was not accomplished. What remains is the deprotection of the C_7 and C_8 hydroxy groups, a reduction of the triple bond and the hydrolysis of the ester to afford benzo-RvD1$_{n\text{-}3\ DPA}$.

2.24.2 Completion of the total synthesis

The 17-hydroxy group is a mixture of the *R*/*S* configuration. Since 17*S*-RvD1 and 17*R*-RvD1 (AT-derived) have demonstrated similar potencies and effects,[1] a mixture of the two epimers of benzo-RvD1$_{n\text{-}3\ DPA}$ could be tested in *in vitro* and *in vivo* assays. If it is desirable to isolate the two epimers, an oxidation to the ketone, and then further enantioselective ruthenium-catalyzed reduction could be performed. Alternatively, the diastereomers may be separated by high-performance liquid chromatography (HPLC). Since the 17*R*-RvD1 epimer has shown to resist enzymatic inactivation,[1] it could be interesting to synthesize the 17*R*-benzo-RvD1$_{n\text{-}3\ DPA}$. Deprotection of the hydroxy groups with TBAF in THF at 0 °C yields the C_7 and C_8 alcohols. Modified Lindlar conditions with Lindlar`s catalyst, 1-octene in EtOAc and pyridine under hydrogen atmosphere reduce the triple bond to a *Z*-alkene. The triple bond may be useful, as it is less prone to isomerization than the *Z*-double bond.[140] A basic hydrolysis of the ester with aqueous LiOH in methanol yields benzo-RvD1$_{n\text{-}3\ DPA}$. These conditions were used in the last steps of the total organic synthesis of PD1$_{n\text{-}3\ DPA}$ reported by Aursnes *et al.*[134] An outline of this synthetic strategy is presented in scheme 22.

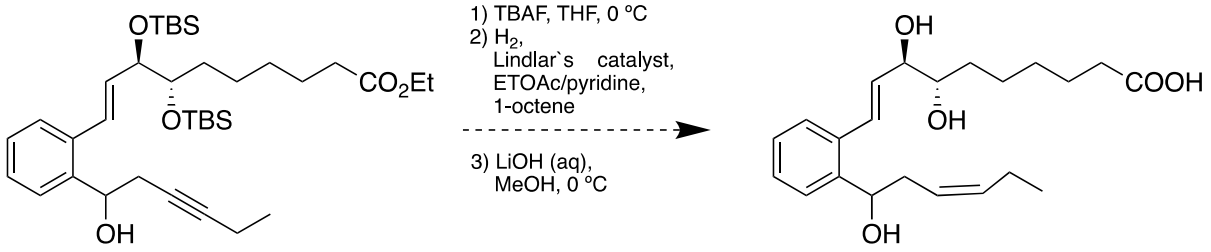

63 **1**

Scheme 20: Outline of the further synthetic strategies to afford benzo-RvD1$_{n\text{-}3\ DPA}$, as reported by Aursnes *et al*. in the last steps of the total organic synthesis of PD1$_{n\text{-}3\ DPA}$.[134]

2.24.3 Synthetic strategy I

Preparation of carbon tetrabromide, and then further synthesis using a Cory-Fuchs reaction to afford a triple bond, as seen in Scheme 23. This gives both isomers of the *R/S* configuration of the 17-hydroxy group, which could be oxidized and reduced using the same procedure as

mentioned above, with further deprotection of the TBS-protected alcohols, reduction of the triple bond and hydrolysis of the ester to afford a benzo-analog of $RvD1_{n\text{-}3\ DPA}$ with one less carbon in the ω-fragment.

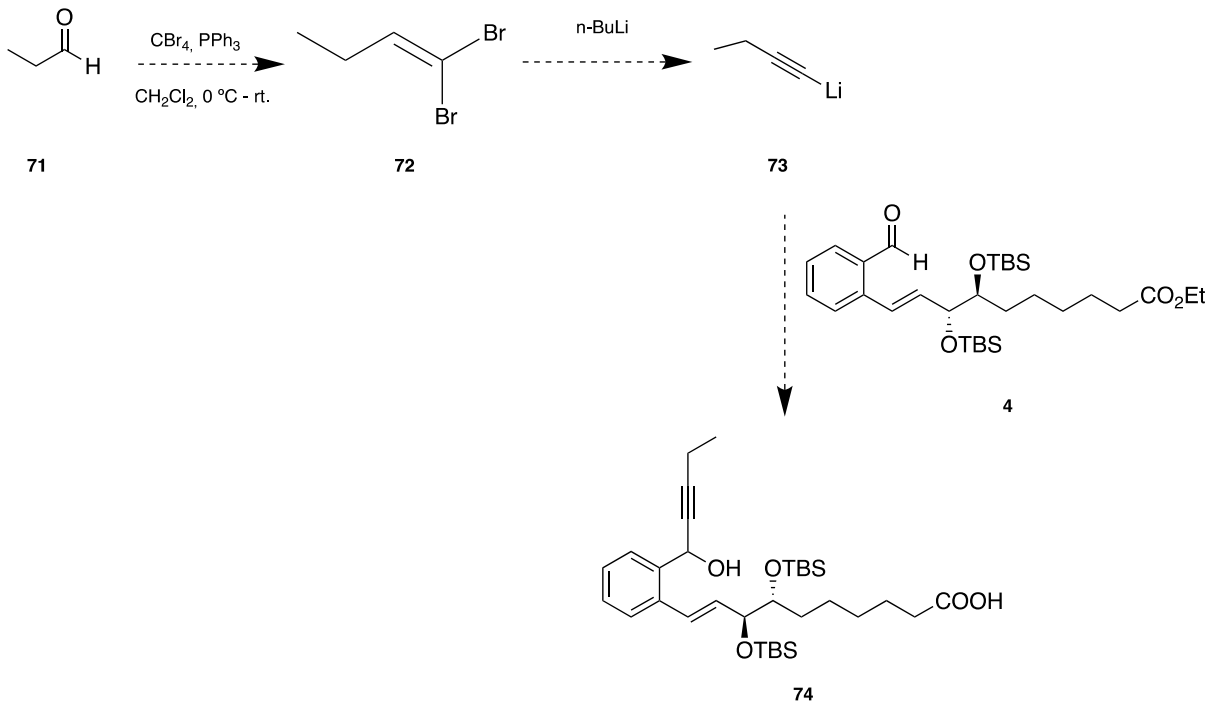

Scheme 21: Outline of the Corey-Fuchs reaction. The first step affords 1,1-dibromobutene **72**, while the second affords 1-lithium-2-butyn, which further reacts with *ortho*-benzaldehyde **4** to afford alkyne **74**.

2.24.4 Synthetic strategy II

Another approach using the same reactions and reagents in this study, but changing the order of events, could be useful. Preparation of the ω-end using the Barbier reaction with the propargylic bromide, followed by the Heck reaction with the alkene. An outline of this strategy is presented in Scheme 22. The last steps suggested under "Completetion of the total synthesis" yields benzo-RvD1$_{n\text{-}3\ DPA}$. This approach has been tried by Reinertsen, only with the aryl bromide, not the aryl iodide, where she reported that it could be due to a lack of reactivity of the aryl bromide, because aryl iodide usually reacts faster in cross-coupling reactions.[5, 167]

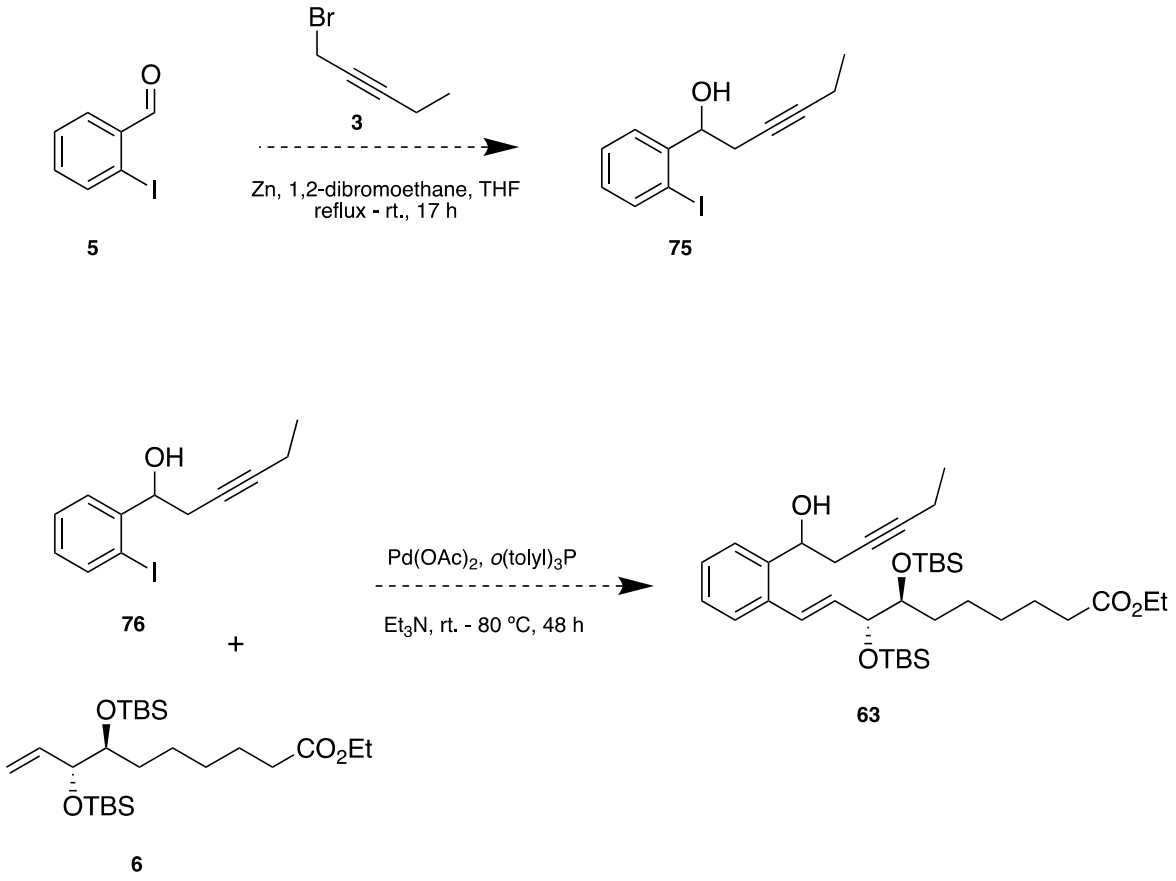

Scheme 22: Outline of the synthetic strategy to afford the product compound **63,** by changing the order of events.

2.24.5 Synthetic strategy III

Various versions of Barbier- or Grignard-type reactions may be useful to afford the ω-end. An allyl bromide can couple with the *ortho*-benzaldehyde **4** to afford allylic alcohol **78**. This type of reaction with lead in aqueous media has shown to give good yields.[168] Furthermore, a *Z*-selective ruthenium catalysis may afford the *tris*-silylated benzo-RvD1$_{n\text{-}3\ DPA}$ **79**. An outline of this reaction is presented in Scheme 23. Deprotection of the hydroxy groups in **79** yields benzo-RvD1$_{n\text{-}3\ DPA}$ **1**. A Barbier reaction with indium in place of zinc, analogous to the one used in this study, may be tried, although it has demonstrated to give a higher yield of allenic alcohols instead of propargylic alcohols.[162]

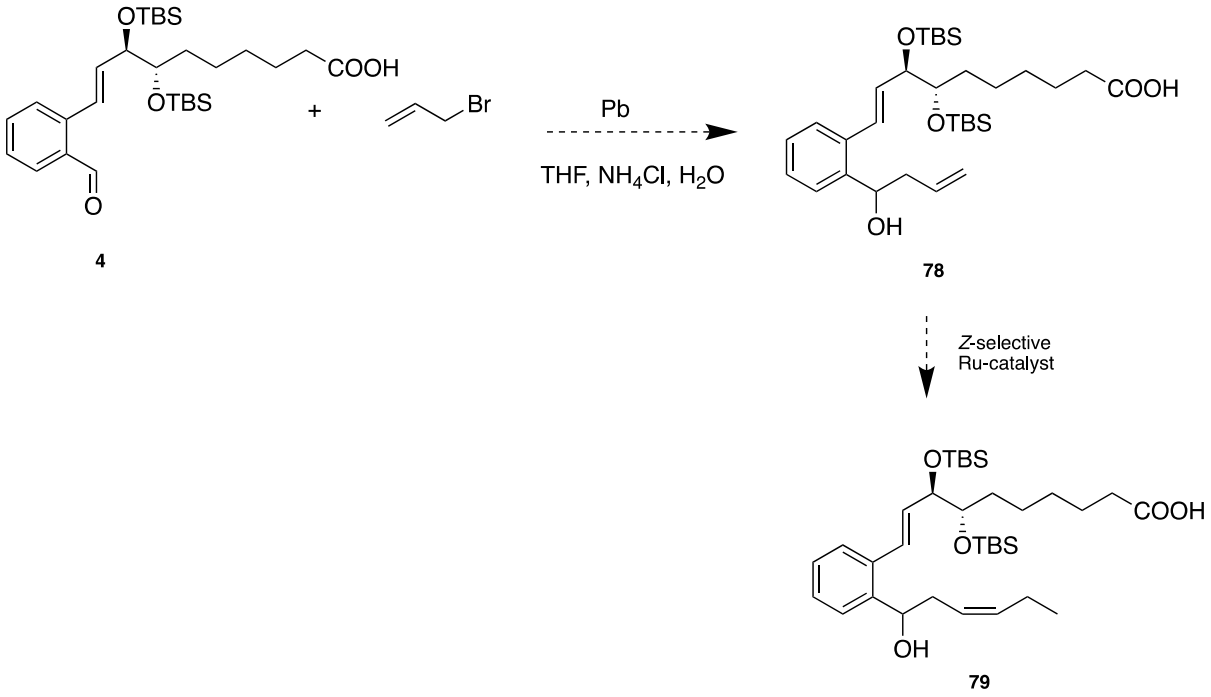

Scheme 23: Outline of the Barbier reaction using lead in aqueous media and a *Z*-selective Ru-catalyst to afford *tris*-silylated benzo-RvD1$_{n\text{-}3\ DPA}$ **79**.

3 Conclusion

This thesis reports different synthetic strategies taken towards a total asymmetric synthesis of benzo-RvD1$_{n\text{-}3\ DPA}$. Benzo-RvD1$_{n\text{-}3\ DPA}$ will hopefully exert the same pro-resolving properties as the structurally similar SPM RvD1$_{n\text{-}3\ DPA}$, and be more chemically stable due to the benzo-group that may mimic the *E,Z,E*-moiety of the labile tetraene system in RvD1$_{n\text{-}3\ DPA}$ **2**. The synthesis of SPMs and their analogs may lead to new therapeutics for the treatment of several inflammatory diseases.

The synthesis of alkyne **63** was performed over 11 steps, with an overall yield of 1% (5% brsm). The synthetic methods towards the α-fragment **7** of benzo-RvD1$_{n\text{-}3\ DPA}$ are based on previously published work performed by the LIPCHEM group. Further reactions include a Tebbe olefination reaction to yield a terminal alkene, a Heck-Mizoroki reaction to insert the benzo-group, and a Barbier reaction, to afford compound **63**.

Unfortunately, the limited time frame for this study, and the Covid-19 situation did not allow the performance of the last synthetic steps to afford benzo-RvD1$_{n\text{-}3\ DPA}$. The work reported in this thesis, may be the fundament for further studies on specialized pro-resolving mediators.

4 Experimental

4.1 Material and apparatus

Unless stated otherwise, all commercially available reagents and solvents were used in the form they were supplied without any further purification. The stated yields are based on isolated material. Thin layer chromatography was performed on silica gel 60 F254 aluminum-backed plates fabricated by Merck (Darmstadt, Germany). Various visualizing agents were used, depending on the reagents and products involved, including UV light, potassium permanganate ($KMnO_4$) and cerium-ammonium-molybdate (CAM).

Flash column chromatography was performed on silica gel 60 (40-63 µm) produced by Merck (Darmstadt, Germany), and was the primary method of purification.

NMR spectra were recorded on a Bruker AVII400 or a Bruker AVIII HD 400 spectrometer at 400 MHz for ^{1}H NMR, and at 100 MHz for ^{13}C NMR. Coupling constants (J) are reported in hertz, and chemical shift values are reported in part per million (δ) relative to the central residual protium solvent resonance in ^{1}H NMR ($CDCl_3$ δ_H = 7.26 and methanol-d_4 δ_H = 3.31) and the central carbon solvent resonance in ^{13}C NMR ($CDCl_3$ δ_C = 77.00 and methanol-d_4 δ_C = 49.00).

Mass spectra were recorded at 70 eV on a Waters Prospec Q using ESI as the method of ionization. High-resolution mass spectra were recorded at the Department of Chemistry, University of Oslo, on a Waters Prospec Q, using ESI as the method of ionization.

Optical rotations were measured using a 0.7 mL cell with a 1.0 dm path length on an Anton Paar MCP 100 polarimeter using the stated solvents.

4.2 Experimental procedures

4.2.1 Synthesis of (2*R*,3*S*)-5,5-bis(ethylthio)pentane-1,2,3-triol 64

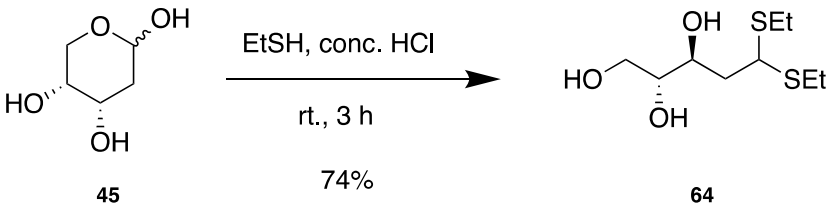

45 64

Scheme 24: Outline of the synthesis of thioacetal **64**.

This reaction procedure is in accordance with the published procedure of Tungen *et al.*[3] 2-Deoxy-D-ribose **45** (5.01 g, 37.4 mmol, 1.00 equiv.) was dissolved in concentrated HCl (6.5 mL), followed by the dropwise addition of ethanethiol (6.7 mL, 90 mmol, 2.4 equiv.). After completion, the reaction was quenched by addition of a saturated aqueous solution of K_2CO_3 (38 mL). The phases were separated ,and the aqueous phase was extracted with CH_2Cl_2 (3 x 50 mL). The organic phases were combined, dried over $MgSO_4$, and the solvent was removed *in vacuo*. The crude product was purified by flash chromatography on silica gel (CH_2Cl_2/MeOH 95:5) to afford product **64** as a clear, yellow oil. **Yield:** 6.64 g (74%), **TLC** (CH_2Cl_2/MeOH 1:9, with $KMnO_4$ stain) R_f = 0.41, $[\boldsymbol{\alpha}]_{\boldsymbol{D}}^{\boldsymbol{20}}$ -19.2 (c = 2.5, MeOH). **^{1}H NMR** (400 MHz, MeOH-d_4) δ 4.12 (dd, *J* = 11.2, 3.6 Hz, 1H), 3.93 – 3.87 (m, 1H), 3.73 (dd, *J* = 11.3, 3.8 Hz, 1H), 3.58 (dd, *J* = 11.3, 6.6 Hz, 1H), 3.46 (td, *J* = 6.7, 3.8 Hz, 1H), 2.78 – 2.57 (m, 4H), 2.10 (ddd, *J* = 13.9, 11.2, 2.4 Hz, 1H), 1.88 (ddd, 1H), 1.27 (td, *J* = 7.4, 3.8 Hz, 6H). **^{13}C NMR** (101 MHz, MeOH-d_4) δ 76.4, 70.8, 64.7, 49.1, 40.9, 25.2, 24.2, 14.9, 14.8.

4.2.2 Synthesis of (5*S*,6*R*)-5-(2,2-bis(ethylthio)ethyl)-6-((*tert*-butyldimethylsilyl)oxy)-2,2,3,3,9,9,10,10-octamethyl-4,8-dioxa-3,9-disilaundecane 65

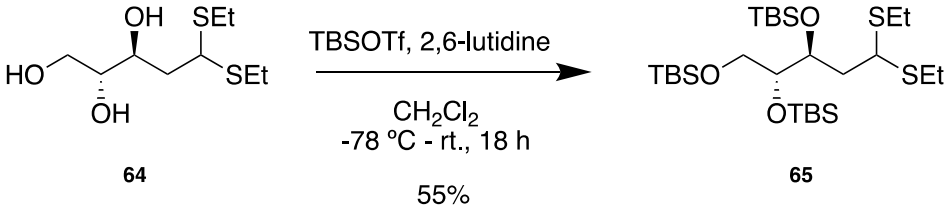

64 65

Scheme 25: Outline of the total synthesis of compound **65**.

This reaction procedure is in accordance with the published procedure of Tungen *et al.*[3] **64** (6.64 g, 21.2 mmol, 1.00 equiv.) was dissolved in CH_2Cl_2 (125 mL) and cooled to -78 °C. The solution was stirred for 10 minutes at this temperature before addition of 2,6-lutidine (25.5 mL, 169 mmol, 8.00 equiv.) and TBSOTf (25.2 mL, 0.0953 mmol, 4.00 equiv.), successively. The reaction mixture was slowly warmed to room temperature in a dry ice/acetone bath for 18 hours, then quenched with aqueous saturated NH_4Cl (86 mL). The phases were separated, and the aqueous phase was extracted with CH_2Cl_2 (3 x 50 mL). The organic phases were combined, washed with brine (40 mL), dried over $MgSO_4$ and the solvent was removed *in vacuo*. Flash chromatography was performed on silica gel (EtOAc/hexane 2:98) to afford product **65** as a clear, colorless oil. **Yield:** 8.89 g (55%), **TLC** (EtOAc/hexane 2:98 with $KMnO_4$ stain) R_f = 0.89, $[\boldsymbol{\alpha}]_{\boldsymbol{D}}^{\boldsymbol{20}}$: -7.0 (c = 2.3, MeOH). **^{1}H NMR** (400 MHz, $CDCl_3$) δ 4.17 (dd, 1H), 3.93 (dd, *J* = 11.0, 3.7 Hz, 1H), 3.69 (td, *J* = 7.1, 5.7, 1.4 Hz, 1H), 2.72 – 2.52 (m, 4H), 2.11 – 2.03 (m, 1H), 1.82 – 1.74 (m, 1H), 1.25 (q, *J* = 7.5, 6.2 Hz, 6H), 0.91 – 0.88 (m, 27H), 0.11 – 0.04 (m, 18H). **^{13}C NMR** (101 MHz, $CDCl_3$) δ 77.8, 72.2, 64.5, 48.2, 39.0, 26.2 (3C), 26.1 (3C), 26.1 (3C), 24.6, 23.2, 18.4, 18.4, 18.3, 14.8, 14.5, -2.8, -3.5, -4.4, -4.7, -5.3, -5.3.

4.2.3 Synthesis of (3S,4R)-3,4,5-tris((tert-butyldimethylsilyl)oxy)pentanal 46

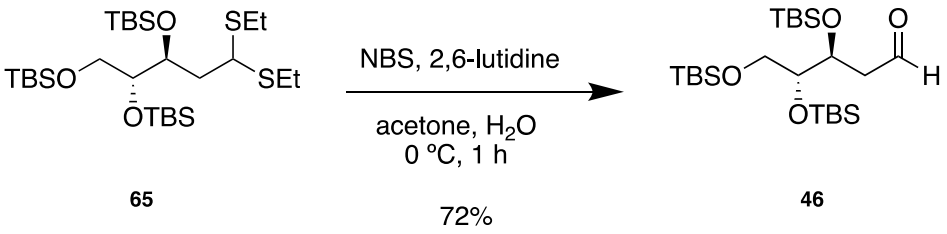

65 72% **46**

Scheme 26: Outline of the total synthesis of compound **46**.

This reaction procedure is in accordance with the published procedure of Tungen *et al.*[3] **65** (4.00 g, 6.90 mmol, 1.00 equiv.) was dissolved in a mixture of acetone (64 mL) and water (22 mL) and cooled to 0 °C, followed by the addition of 2,6-lutidine (6.4 mL, 55 mmol, 8.0 equiv.) and N-Bromosuccinimide (NBS) (9.80 g, 55.1 mmol, 8.00 equiv.). The reaction mixture was allowed to stir for one hour at ambient temperature, before it was quenched with saturated aqueous $Na_2S_2O_3$ (37 mL) and diluted with Et_2O (37 mL). The phases were separated and the aqueous phase was extracted with Et_2O (3 x 40 mL). The organic phases were combined, washed with HCl 1,0 M (15 mL) and $NaHCO_3$ (15 mL), dried over $MgSO_4$ and the solvent was removed *in vacuo*. The crude product was purified by flash chromatography (EtOAc/hexane 2:98) to afford product **46** as a clear, colourless oil. **Yield:** 2.34 g (72%), **TLC** (EtOAc/hexane 2:98 with CAM stain) R_f = 0.19, , $[\boldsymbol{\alpha}]_{\boldsymbol{D}}^{\boldsymbol{20}}$: -4.9 (c = 1.2, MeOH). **^{1}H NMR** (400 MHz, $CDCl_3$) δ 9.85 (dd, *J* = 3.4, 1.7 Hz, 1H), 4.35 (td, *J* = 5.2, 2.3 Hz, 1H), 3.80 – 3.74 (m, 1H), 3.52 – 3.38 (m, 2H), 2.63 – 2.43 (dq, 2H), 0.90 – 0.86 (m, 27H), 0.10 – 0.04 (m, 18H). **^{13}C NMR** (101 MHz, $CDCl_3$) δ 202.8, 77.3, 69.7, 64.5, 45.8, 26.0 (6C), 26.0 (3C), 18.4, 18.3, 18.2, -4.2, -4.4, -4.5, -4.8, -5.3, -5.4.

4.2.4 Synthesis of ethyl (7*S*,8*R*,*Z*)-7,8,9-tris((*tert*-butyldimethylsilyl)oxy)non-4-enoate 49

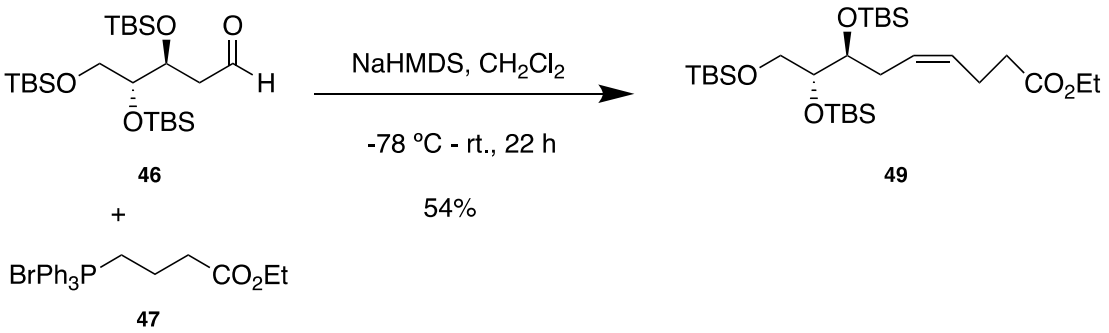

Scheme 27: Outline of the total synthesis of compound **49**.

This reaction procedure is in accordance with the Master thesis of Reinertsen.[5] The Wittig salt **47** (2.65 g, 4.80 mmol, 1.20 equiv.) was dissolved in CH_2Cl_2 (35 mL), and the reaction mixture was cooled to -78 °C. NaHMDS (9.5 mL, 0.6 M in toluene, 1.20 equiv.) was added dropwise to afford a yellow solution. **46** (2.3 g, 4.8 mmol, 1.0 equiv.) was dissolved in dry CH_2Cl_2 (1.5 mL) and added to the mixture. The resulting solution was stirred for 22 hours while slowly reaching room temperature. The reaction was quenched with a phosphate buffer (pH ≈7,33 mL) and diluted with Et_2O (46 mL). The phases were separated, and the aqueous phase was extracted with Et_2O (3 x 30 mL), dried over $MgSO_4$, and the solvent was removed *in vacuo*. The crude product was purified by flash chromatography (silica gel, EtOAc/hexane 2.5:97.5) to afford product **49** as a clear colorless oil. **Yield:** 1.50 g (54%), **TLC** (EtOAc/hexane 2.5:98.5 with CAM stain) R_f = 0.29, , $[\boldsymbol{\alpha}]_{\boldsymbol{D}}^{\boldsymbol{20}}$: -4.1 (c = 1.5, MeOH). **^{1}H NMR** (400 MHz, $CDCl_3$) δ 5.52 – 5.36 (m, 2H), 4.12 (q, *J* = 7.1 Hz, 2H), 3.79 (td, *J* = 6.9, 5.5, 2.3 Hz, 1H), 3.69 (td, *J* = 6.1, 2.3 Hz, 1H), 3.60 (dd, *J* = 10.2, 6.4 Hz, 1H), 3.46 (dd, *J* = 10.1, 5.9 Hz, 1H), 2.39 – 2.31 (m, 4H), 2.31 – 2.22 (m, 2H), 1.24 (t, *J* = 7.2 Hz, 3H), 0.93 – 0.86 (m, 27H), 0.10 – 0.02 (m, 18H). **^{13}C NMR** (101 MHz, $CDCl_3$) δ 173.3, 128.9, 128.6, 77.3, 74.2, 64.9, 60.4, 34.4, 30.6, 26.1 (9C), 23.2, 18.5, 18.4, 18.3, 14.4, -4.1, -4.3, -4.4, -4.4, -5.2, -5.3.

4.2.5 Synthesis of ethyl (7*S*,8*R*)-7,8,9-tris((*tert*-butyldimethylsilyl)oxy)nonanoate 66

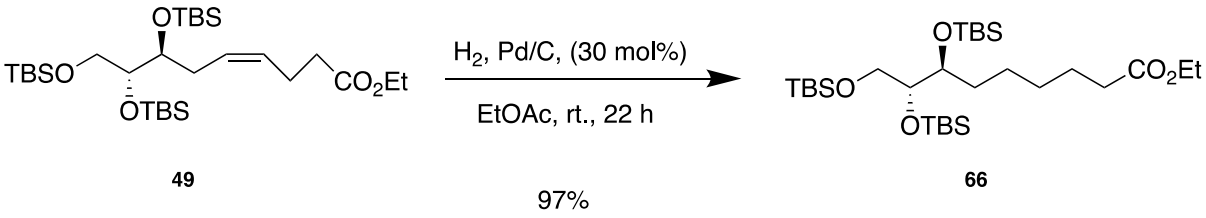

49 97% **66**

Scheme 28: Outline of the total synthesis of compound **66**.

This reaction procedure is in accordance with the Master thesis of Reinertsen.[5] **49** (1.45 g, 1.74 mmol, 1.00 equiv.) was dissolved in EtOAc (35 mL), followed by the addition of Pd/C (10 wt%, 0.85 g, 30 mol%) to afford a black reaction mixture. The suspension was stirred for 22 hours at room temperature, and purified by filtration through a plug of celite (EtOAc). The solvent was removed *in vacuo* to afford product **66** as a clear, colorless oil. **Yield:** 1.50 g (97%), **TLC** (EtOAc/hexane 2.5:97.5 with CAM stain) R_f = 0.50, , $[\boldsymbol{\alpha}]_{\boldsymbol{D}}^{\boldsymbol{20}}$: -5.1 (c = 1.7, MeOH). **^{1}H NMR** (400 MHz, $CDCl_3$) δ 4.12 (q, *J* = 7.2 Hz, 2H), 3.71 – 3.67 (m, 1H), 3.66 – 3.58 (m, 2H), 3.45 (dt, *J* = 9.2, 5.0 Hz, 1H), 2.28 (t, *J* = 7.6 Hz, 2H), 1.62 (q, *J* = 15.0, 7.5 Hz, 2H), 1.45 – 1.38 (m, 2H), 1.35 – 1.27 (m, 4H), 1.25 (t, *J* = 7.1 Hz, 3H), 0.91 – 0.85 (m, 27H), 0.08 – 0.02 (m, 18H). **^{13}C NMR** (101 MHz, $CDCl_3$) δ 174.0, 77.3, 74.2, 65.3, 60.3, 34.5, 32.5, 29.7, 26.2 (3C), 26.2 (3C), 26.1 (3C), 25.3, 25.2, 18.5, 18.4, 18.3, 14.4, -4.0, -4.1, -4.5, -5.2, -5.3.

4.2.6 Synthesis of ethyl (7*S*,8*R*)-7,8-*bis*((*tert*-butyldimethylsilyl)oxy)-9-hydroxynonanoate 67

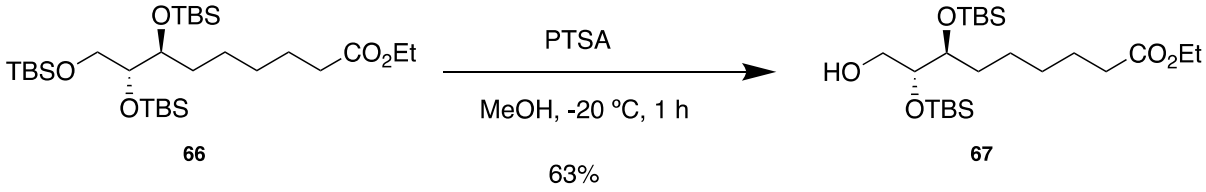

66 63% **67**

Scheme 29: Outline of the total synthesis of compound **67**.

This reaction procedure is in accordance with the published procedure of Tungen *et al.*[3] **66** (1.46 g, 3.15 mmol, 1.00 equiv.) was dissolved in MeOH (30 mL) and cooled to -20 °C, followed by the addition of PTSA (0.48 g, 2.78 mmol, 1.00 equiv.). The reaction mixture was stirred for one hour, and quenched with saturated aqueous $NaHCO_3$ (50 mL). The mixture was diluted with EtOAc (30 mL), the phases were separated, and the aqueous phase was extracted with EtOAc (3 x 30 mL). The combined organic phases were washed with brine (25 mL), dried over $MgSO_4$ and the solvent removed *in vacuo*. The crude product was purified with flash chromatography (silica gel, EtOAc/hexane 1:9) to afford product **67** as a clear, colorless oil. **Yield:** 0.103 g (63%, 81% brsm), **TLC** (EtOAc/hexane 1:9 with CAM stain) R_f = 0.38, $[\boldsymbol{\alpha}]_{\boldsymbol{D}}^{\boldsymbol{20}}$: -1.6 (c = 2.2, MeOH). **^{1}H NMR** (400 MHz, $CDCl_3$) δ 4.12 (p, *J* = 7.2 Hz, 2H), 3.75 – 3.66 (m, 2H), 3.63 – 3.56 (m, 2H), 2.28 (t, *J* = 7.5 Hz, 2H), 2.03 (s, 1H), 1.63 (q, *J* = 7.4 Hz, 2H), 1.57 – 1.46 (m, 2H), 1.41 – 1.27 (m, 4H), 1.25 (t, *J* = 7.2 Hz, 3H), 0.90 (s, 9H), 0.88 (s, 9H), 0.10 – 0.08 (m, 9H), 0.06 (s, 3H). **^{13}C NMR** (101 MHz, $CDCl_3$) δ 173.9, 74.9, 74.6, 64.1, 60.3, 34.5, 33.9, 29.6, 26.1 (3C), 26.0 (3C), 25.1, 24.4, 18.3, 18.3, 14.4, -4.3, -4.3, -4.4.

4.2.7 Synthesis of ethyl (7*S*,8*S*)-7,8-bis((*tert*-butyldimethylsilyl)oxy)-9-oxononanoate 7

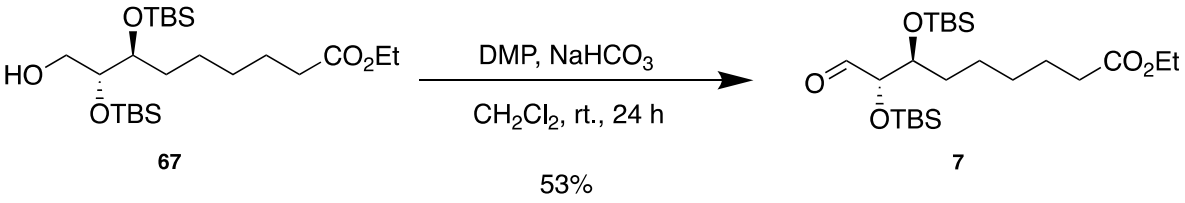

Scheme 30: Outline of the total synthesis of compound **7**.

This reaction procedure is in accordance with the procedure reported in the Master thesis of Reinertsen.[5] **67** (0.709 g, 1.53 mmol, 1.00 equiv.) was dissolved in CH_2Cl_2 (40 mL). $NaHCO_3$ (0.727 g, 8.65 mmol, 5.60 equiv.) was added to the solution, followed by the addition of Dess-Martin periodinane (DMP) (1.41 g, 3.33 mmol, 2.20 equiv.). The mixture was stirred for 24 hours over night, and quenched with a saturated, aqueous solution of $Na_2S_2O_3$ (25 mL). The phases were separated, and the aqueous phase was extracted with CH_2Cl_2 (3 x 25 mL). The organic phases were combined, washed with brine (25 mL), dried over $MgSO_4$ and the solvent

was removed *in vacuo*. The crude product was purified by flash chromatography (silica gel, EtOAc/hexane 5:95) to afford product **7** as a clear, colorless oil. **Yield:** 0.372 g (53%,), **TLC** (EtOAc/hexane 1:9 with CAM stain) R_f = 0.30, $[\boldsymbol{\alpha}]_{\boldsymbol{D}}^{\boldsymbol{20}}$: 7.6 (c = 2.3, MeOH). **^{1}H NMR** (400 MHz, $CDCl_3$) δ 9.59 (d, *J* = 1.7 Hz, 1H), 4.16 – 4.09 (m, 3H), 3.89 – 3.84 (m, 1H), 2.28 (t, *J* = 7.5 Hz, 2H), 1.67 – 1.62 (m, 2H), 1.58 – 1.52 (m, 2H), 1.33 – 1.29 (m, 4H), 1.27 – 1.22 (m, 5H), 0.91 (s, 9H), 0.86 (s, 9H), 0.08 – 0.05 (m, 12H). **^{13}C NMR** (101 MHz, $CDCl_3$) δ 203.9, 173.8, 80.9, 75.6, 60.3, 34.4, 33.6, 29.4, 26.0 (3C), 25.9 (3C), 25.0, 24.9, 18.4, 18.2, 14.4, -4.3, -4.5, -4.7.

4.2.8 Synthesis of ethyl (7*S*,8*R*)-7,8-bis((*tert*-butyldimethylsilyl)oxy)dec-9-enoate 6

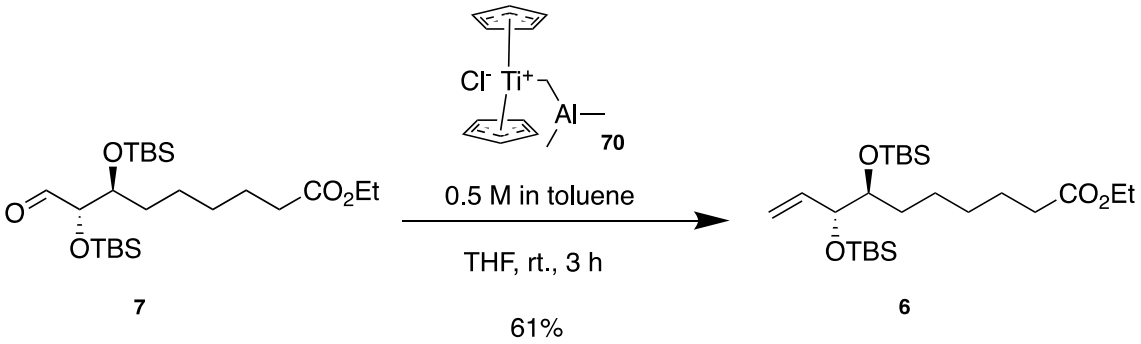

Scheme 31: Outline of the total synthesis of compound **6**.

This reaction procedure is in accordance with the published procedure of Xuequan *et al.*[164] Tebbe reagent **70** (1.2 mL, 0.5 M in toluene) was diluted with dry toluene (15 mL). **7** (0.25 g, 0.54 mmol, 1.0 equiv.) dissolved in dry THF (15 mL), was added dropwise over 20 minutes. After stirring for two hours, the reaction was quenched with aqueous NaOH (1.0 M,30 mL). The phases were separated, and the aqueous phase was extracted with Et_2O (3 x 10 mL). The organic phases were combined, dried over Na_2SO_4 and the solvent was removed *in vacuo*. Purification by flash chromatography (silica gel, EtOAc/hexane 5:95) afforded product **6** as a clear, colorless oil. **Yield:** 0.15 g (61%, 99% brsm), **TLC** (EtOAc/hexane 5:95 with CAM stain) R_f = 0.49, $[\boldsymbol{\alpha}]_{\boldsymbol{D}}^{\boldsymbol{20}}$: 0.4 (c = 1.8, MeOH). **^{1}H NMR** (400 MHz, $CDCl_3$) δ 5.87 – 5.75 (m, 1H), 5.17 – 5.07 (m, 2H), 4.12 (q, *J* = 7.1, 1.7 Hz, 2H), 3.96 – 3.90 (m, 1H), 3.59 – 3.53 (m,

1H), 2.28 (t, *J* = 7.6 Hz, 2H), 1.62 (p, 2H), 1.54 – 1.42 (m, 2H), 1.41 – 1.33 (m, 2H), 1.31 – 1.28 (m, 2H), 1.25 (t, *J* = 7.2 Hz, 3H), 0.89 (s, 9H), 0.87 (s, 9H), 0.05 – -0.00 (m, 12H). **^{13}C NMR** (101 MHz, $CDCl_3$) δ 174.0, 139.3, 116.0, 77.8, 76.4, 60.3, 34.5, 33.3, 29.6, 26.2 (3C), 26.1 (3C), 25.2, 24.9, 18.4, 18.4, 14.4, -3.8, -4.0, -4.4, -4.6.

4.2.9 Synthesis of ethyl (7*S*,8*R*,*E*)-7,8-bis((*tert*-butyldimethylsilyl)oxy)-10-(2-(hydroxymethyl)phenyl)dec-9-enoate 57

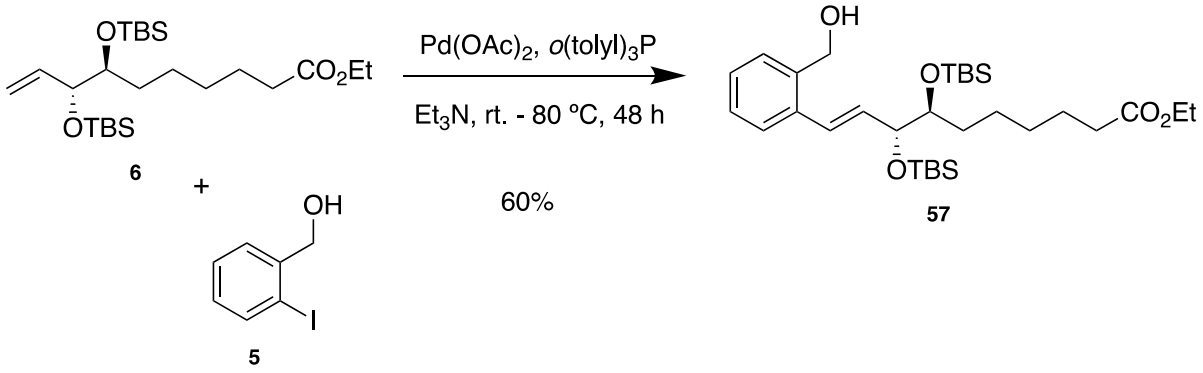

Scheme 32: Outline of the total synthesis of compound **57**.

This reaction procedure is in accordance with the published procedure of Colm *et al.*[165] 2-Iodo-benzyl alcohol **5** (23,5 mg, 0.096 mmol, 0.70 equiv.) was dissolved in Et_3N (0.2 mL) and added to **6** (60 mg, 0.13 mmol, 1.0 equiv.). $Pd(OAc)_2$ (1.2 mg, 0.0053 mmol, 5 mol%) and *o*(tolyl)$_3$P (2.7 mg, 0.0089 mmol, 9 mol%) was added, and the resulting reaction mixture was heated to 80 °C and stirred for 48 hours. The reaction mixture was quenched by aqueous NaOH (0.25 M, 4 mL) and diluted with Et_2O (3 ml) The phases were separated and the aqueous phase was extracted with Et_2O (3 x 10 mL). The organic phases were combined and washed with brine (1 mL), dried over $MgSO_4$ and the solvent was removed *in vacuo*. The crude product was purified by flash chromatography (silica gel, EtOAc/hexane 1:4) to afford product **57** as a clear, pale yellow oil. **Yield:** 44.0 mg (60%, 86% brsm), **TLC** (EtOAc/hexane 1:4 with CAM stain) R_f = 0.44, $[\boldsymbol{\alpha}]_{\boldsymbol{D}}^{\boldsymbol{20}}$: -0.2 (c = 1.4, MeOH). **^{1}H NMR** (400 MHz, $CDCl_3$) δ 7.47 (dd, *J* = 7.2, 1.8 Hz, 1H), 7.38 (dd, *J* = 7.0, 2.0 Hz, 1H), 7.31 – 7.22 (m, 2H), 6.79 (d, *J* = 15.8 Hz, 1H), 6.13 (dd, *J* = 15.8, 7.0 Hz, 1H), 4.75 (s, 2H), 4.18 – 4.14 (m, 1H), 4.12 (q, *J* = 7.1 Hz, 2H), 3.71 – 3.65 (m, 1H), 2.29 (t, *J* = 7.6 Hz, 2H), 1.63 (q, *J* = 7.5 Hz, 2H), 1.52 – 1.42 (m, 2H), 1.34 – 1.31 (m,

2H), 1.30 – 1.26 (m, 2H), 1.24 (t, *J* = 7.1 Hz, 3H), 0.92 (s, 9H), 0.87 (s, 9H), 0.13 – 0.02 (m, 12H). **^{13}C NMR** (101 MHz, $CDCl_3$) δ 174.1, 137.7, 136.2, 133.4, 128.3, 128.2, 127.7, 127.6, 126.4, 76.7, 63.5, 60.4, 34.5, 33.6, 29.6, 26.1 (3C), 25.1 (3C), 25.0, 18.5, 18.4, 14.4, -3.8, -3.9, -4.4. **HRMS (APCI):** Exact mass calculated for $C_{31}H_{56}O_5Si_2Na$ [M+Na]+: 587.3558, found: 587.3558.

4.2.10 Synthesis of ethyl (7*S*,8*R*,*E*)-7,8-bis((*tert*-butyldimethylsilyl)oxy)-10-(2-formylphenyl)dec-9-enoate 4

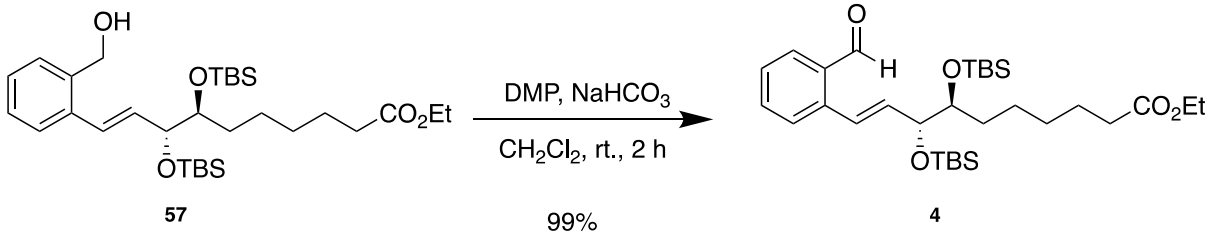

Scheme 33: Outline of the total synthesis of compound **4**.

This reaction procedure is in accordance with the procedure in the Master thesis of Reinertsen.[5] **57** (57.0 mg, 0.101 mmol, 1.00 equiv.) was dissolved in CH_2Cl_2 (3.2 mL). $NaHCO_3$ (48 mg, 0.57 mmol, 5.6 equiv.) was added to the solution, followed by the addition of DMP (0.10 g, 0.22 mmol, 2.2 equiv.). The reaction was stirred for 2 hours, then quenched with saturated, aqueous $Na_2S_2O_3$ (2 mL). The phases were separated, and the aqueous phase was extracted with CH_2Cl_2 (3 x 10 mL). The organic phases were combined, washed with brine (2 mL), dried over $MgSO_4$ and the solvent was removed *in vacuo*. The crude product was purified by flash chromatography (silica gel, EtOAc/hexane 1:4) to afford product **4** as a clear, colorless oil. **Yield:** 56.0 mg (99%), **TLC** (EtOAc/hexane 1:9) visualized by UV, R_f = 0.23, $[\boldsymbol{\alpha}]_{\boldsymbol{D}}^{\boldsymbol{20}}$: -2.4 (c = 0.63, MeOH). **^{1}H NMR** (400 MHz, $CDCl_3$) δ 10.31 (s, 1H), 7.83 (dd, *J* = 7.5, 1.2 Hz, 1H), 7.58 – 7.51 (m, 2H), 7.42 – 7.37 (m, 1H), 7.32 (d, *J* = 16.9 Hz, 1H), 6.17 (dd, *J* = 15.8, 6.9 Hz, 1H), 4.22 – 4.18 (m, 1H), 4.12 (q, *J* = 7.1 Hz, 2H), 3.72 – 3.67 (m, 1H), 2.29 (t, *J* = 7.5 Hz, 2H), 1.69 – 1.59 (m, 2H), 1.57 – 1.51 (m, 2H), 1.43 – 1.28 (m, 4H), 1.26 (t, *J* = 7.1 Hz, 3H), 0.92 (s, 9H), 0.86 (s, 9H), 0.11 – 0.02 (m, 12H). **^{13}C NMR** (101 MHz, $CDCl_3$) δ 192.2, 174.0, 140.3, 136.8, 133.9, 133.0, 131.0, 127.7, 127.6, 126.8, 77.3, 76.7, 60.3, 34.5, 33.8, 29.6, 26.1 (3C), 26.1 (3C),

25.2, 25.0, 18.5, 18.3, 14.4, -3.9, -3.9, -4.4, -4.5. **HRMS (APCI):** Exact mass calculated for $C_{31}H_{54}O_5Si_2Na$ $[M+Na]^+$: 585.3402, found: 585.3401.

4.2.11 Synthesis of ethyl (7*S*,8*R*,*E*)-7,8-bis((*tert*-butyldimethylsilyl)oxy)-10-(2-(1-hydroxyhex-3-yn-1-yl)phenyl)dec-9-enoate 63

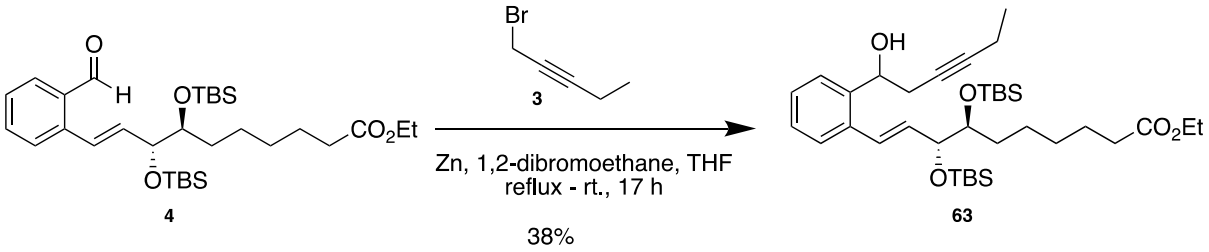

Scheme 34: Outline of the total synthesis of compound **63**.

This reaction procedure is in accordance with the published procedure of Yanagisawa *et al.*[166] Zinc powder (20.5 mg, 3.14 mmol, 40.0 equiv.) was dissolved in dry THF (0.2 mL), and 1,2-dibromoethane (0.01 mg, 0.02 mmol, 0.2 equiv.) was added. The reaction mixture was heated to reflux, stirred for 5 minutes and cooled to 0 °C. 1-Bromo-2-pentyne **3** (23.1 mg, 0.157 mmol, 2.00 equiv.), dissolved in dry THF (0.1 mL), was added, and the reaction mixture was stirred for one hour at 0 °C. **4** (44 mg, 0.078 mmol, 1.0 equiv.) was dissolved in dry THF (0.2 mL), and added to the reaction mixture at 0 °C. The reaction was allowed to slowly warm up to ambient temperature for 17 hours and then quenched by addition of a saturated, aqueous solution of NH_4Cl (0.8 mL). The phases were separated and the aqueous phase was extracted with diethyl ether (3 x 10 mL), dried over $MgSO_4$ and the solvent was removed *in vacuo*. The crude product was purified by flash chromatography (silica gel, gradient elution, EtOAc/hexane, 1:9 to 2:8) to afford product **63** as a clear colorless oil. **Yield:** 17 mg (38%, 83% brsm), **TLC** (EtOAc/hexane 1:9) visualized by UV R_f = 0.15, $[\boldsymbol{\alpha}]_{\boldsymbol{D}}^{\boldsymbol{20}}$: 423.2 (c = 0.41, CH_2Cl_2). **^{1}H NMR** (400 MHz, $CDCl_3$) δ 7.58 – 7.49 (m, 2H), 7.48 – 7.38 (m, 2H), 7.38 – 7.33 (m, 1H), 7.13 (dd, *J* = 8.6, 2.6 Hz, 1H), 4.95 (t, *J* = 3.7 Hz, 1H), 4.15 – 4.10 (m, 3H), 3.69 – 3.64 (m, 1H), 2.29 (t, *J* = 7.6 Hz, 2H), 2.21 – 2.17 (m, 2H), 1.67 – 1.59 (m, 4H), 1.27 – 1.24 (m, 11H), 1.12 (dd, *J* = 7.6, 0.9 Hz, 3H), 0.90 – 0.86 (m, 18H), 0.10 (s, 3H), 0.06 – 0.03 (m, 9H). **^{13}C NMR** data missing due to The University of Oslo closing down because of the Corona

virus. **HRMS (APCI):** Exact mass calculated for $C_{36}H_{62}O_5Si_2Na$ [M+Na]+: 653.4028, found: 653.4028.

5 References

1. Sun, Y., *et al., Resolvin D1 and Its Aspirin-Triggered 17R Epimer - Stereochemical Assignments, Anti-Inflammatory Properties, and Enzymatic Inactivation.* The Journal of Biological Chemistry, 2007. **282**(13): p. 9323-9334.
2. Petasis, N.A., *et al., Design and Synthesis of Benzo-Lipoxin A4 Analogs with Enhanced Stability and Potent Anti-Inflammatory Properties.* Bioorganic & Medicinal Chemistry Letters, 2008. **18**(4): p. 1382-1387.
3. Tungen, J.E., *et al., Resolving Inflammation: Synthesis, Configurational Assignment, and Biological Evaluations of RvD1n−3 DPA.* Chemistry – A European Journal, 2019. **25**(6): p. 1476-1480.
4. Dalli, J., Colas, R.A., and Serhan, C.N., *Novel N-3 Immunoresolvents: Structures and Actions.* Scientific Reports, 2013. **3**(1).
5. Reinertsen, A.F., *Synthetic Studies Towards an Analog of the Specialized Pro-Resolving Mediator RvD1n-3 DPA, Department of Pharmacy*. 2019, University of Oslo: Oslo.
6. Serhan, C.N., Yacoubian, S., and Yang, R., *Anti-Inflammatory and Proresolving Lipid Mediators.* Annual Review of Pathology: Mechanisms of Disease, 2008. **3**(1): p. 279-312.
7. Serhan, C.N., *Resolution Phase of Inflammation: Novel Endogenous Anti-Inflammatory and Proresolving Lipid Mediators and Pathways.* Annual Review of Immunology, 2007. **25**: p. 101-137.
8. Levy, B.D. and Serhan, C.N., *Resolution and Regulation of Inflammation*, in *Pathobiology of Human Disease*, McManus, L.M. and Mitchell, R.N. (Editors). 2014, Academic Press: San Diego. p. 332-348.
9. Serhan, C.N., Chiang, N., and Dyke, T.E.V., *Resolving Inflammation: Dual Anti-Inflammatory and Pro-Resolution Lipid Mediators.* Nature Reviews Immunology, 2008. **8**(5): p. 349-361.
10. Ward, P.A., *Acute and Chronic Inflammation*, in *Fundamentals of Inflammation*, Serhan, C.N., Ward, P.A., and Gilroy, D.W. (Editors). 2010, Cambridge University Press: New York, NY. p. 1-16.

11. Sutton, N.R., Baek, A., and Pinsky, D.J., *Endothelial Cells and Inflammation*, in *Encyclopedia of Medical Immunology: Autoimmune Diseases*, Mackay, I.R., *et al.* (Editors). 2014, Springer New York: New York, NY. p. 367-381.
12. Karp, C.L., *Links between Innate Immunity and Adaptive Immunity*, in *Fundamentals of Inflammation*, Serhan, C.N., Ward, P.A., and Gilroy, D.W. (Editors). 2010, Cambridge University Press: New York, NY. p. 28-37.
13. Smith, C.W., *et al.*, *Recognition of an Endothelial Determinant for CD18-Dependent Human Neutrophil Adherence and Transendothelial Migration.* The Journal of Clinical Investigation, 1988. **82**(5): p. 1746-1756.
14. Norling, L.V., *et al.*, *Cell Adhesion Molecules*, in *Fundamentals of Inflammation*, Serhan, C.N., Ward, P.A., and Gilroy, D.W. (Editors). 2010, Cambridge University Press: New York, NY. p. 208-216.
15. Filep, J.G. and Colgan, S.P., *Neutrophil-Endothelial Cell Interactions*, in *Fundamentals of Inflammation*, Serhan, C.N., Ward, P.A., and Gilroy, D.W. (Editors). 2010, Cambridge University Press: New York, NY. p. 141-151.
16. Gilroy, D.W., *Resolution of Inflammation and Woud Healing*, in *Fundamentals of Inflammation*, Serhan, C.N., Ward, P.A., and Gilroy, D.W. (Editors). 2010, Cambridge University Press: New York, NY. p. 17-27.
17. Varani, J. and Ward, P.A., *Mechanism of Neutrophil-Dependent and Neutrophil-Independent Endothelial Cell Injury.* Biological Signals, 1994. **3**(1): p. 1-14.
18. Serhan, C.N. and Petasis, N.A., *Resolvins and Protectins in Inflammation Resolution.* Chemical Reviews, 2011. **111**(10): p. 5922-5943.
19. Serhan, C.N. and Savill, J., *Resolution of Inflammation: The Beginning Programs the End.* Nature Immunology, 2005. **6**(12): p. 1191-1197.
20. Raza, K. and Gordon, C., *Rheumatoid Arthritis/SLE*, in *Fundamentals of Inflammation*, Serhan, C.N., Ward, P.A., and Gilroy, D.W. (Editors). 2010, Cambridge University Press: New York, NY. p. 267-281.
21. Rogerio, A.P., *et al.*, *Resolvin D1 and Aspirin-Triggered Resolvin D1 Promote Resolution of Allergic Airways Responses.* Journal of Immunology (Baltimore, Md. : 1950), 2012. **189**(4): p. 1983-1991.
22. Merched, A.J., *et al.*, *Atherosclerosis: Evidence for Impairment of Resolution of Vascular Inflammation Governed by Specific Lipid Mediators.* The FASEB Journal, 2008. **22**(10): p. 3595-3606.

23. Chiang, N. and Serhan, C.N., *Structural Elucidation and Physiologic Functions of Specialized Pro-Resolving Mediators and Their Receptors.* Molecular Aspects of Medicine, 2017. **58**: p. 114-129.
24. Lindell, D.M. and Lukacs, N.W., *Cytokines and Chemokines in Inflammation*, in *Fundamentals of Inflammation*, Serhan, C.N., Ward, P.A., and Gilroy, D.W. (Editors). 2010, Cambridge University Press, New York, NY. p. 175-185.
25. Tabas, I. and Glass, C.K., *Anti-Inflammatory Therapy in Chronic Disease: Challenges and Opportunities.* Science, 2013. **339**(6116): p. 166-172.
26. Serhan, C.N., *A Search for Endogenous Mechanisms of Anti-Inflammation Uncovers Novel Chemical Mediators: Missing Links to Resolution.* Histochemistry and Cell Biology, 2004. **122**(4): p. 305-321.
27. Levy, B.D., *et al.*, *Protectin D1 Is Generated in Asthma and Dampens Airway Inflammation and Hyperresponsiveness.* Journal of Immunology (Baltimore, Md. : 1950), 2007. **178**(1): p. 496-502.
28. Giera, M., *et al.*, *Lipid and Lipid Mediator Profiling of Human Synovial Fluid in Rheumatoid Arthritis Patients by Means of LC–MS/MS.* BBA - Molecular and Cell Biology of Lipids, 2012. **1821**(11): p. 1415-1424.
29. Zhu, M., *et al.*, *Can Inflammation Be Resolved in Alzheimer's Disease?* Therapeutic Advances in Neurological Disorders, 2018. **11**: p. 1-16.
30. Ayoub, S.S. and Flower, R., *Nonsteroidal Anti-Inflammatory Drugs*, in *Fundamentals of Inflammation*, Serhan, C.N., Ward, P.A., and Gilroy, D.W. (Editors). 2010, Cambridge University Press: New York, NY. p. 234-243.
31. Serhan, C.N. and Haeggström, J.Z., *Lipid Mediators in Acute Inflammation and Resolution: Eicosanoids, PAF, Resolvins, and Protectins*, in *Fundamentals of Inflammation*, Serhan, C.N., Ward, P.A., and Gilroy, D.W. (Editors). 2010, Cambridge University Press: New York, NY. p. 153-174.
32. Rhen, T. and Cidlowski, J.A., *Antiinflammatory Action of Glucocorticoids — New Mechanisms for Old Drugs.* The New England Journal of Medicine, 2005. **353**(16): p. 1711-1723.
33. Dinarello, C.A., *Anti-Inflammatory Agents: Present and Future.* Cell, 2010. **140**(6): p. 935-950.
34. Antoni, C. and Braun, J., *Side Effects of Anti-TNF Therapy: Current Knowledge.* Clinical and Experimental Rheumatology, 2002. **20**(6 Suppl 28): p. S152-S157.

35. Borgeat, P., Hamberg, M., and Samuelsson, B., *Transformation of Arachidonic Acid and Homo-Gamma-Linolenic Acid by Rabbit Polymorphonuclear Leukocytes. Monohydroxy Acids from Novel Lipoxygenases.* The Journal of Biological Chemistry, 1976. **251**(24): p. 7816-7820.
36. Ferdinandusse, S., *et al.*, *Identification of the Peroxisomal B-Oxidation Enzymes Involved in the Biosynthesis of Docosahexaenoic Acid.* The Journal of Lipid Research, 2001. **42**(12): p. 1987-1995.
37. Hussein, N., *et al.*, *Artificial Rearing of Infant Mice Leads to N-3 Fatty Acid Deficiency in Cardiac, Neural and Peripheral Tissues.* Lipids, 2009. **44**(8): p. 685-702.
38. EFSA Panel on Dietetic Products, Nutrition and Allergies, *Scientific Opinion on the Tolerable Upper Intake Level of Eicosapentaenoic Acid (EPA), Docosahexaenoic Acid (DHA) and Docosapentaenoic Acid (DPA).* EFSA journal, 2012. **10**(7): p. 2815.
39. Calder, P.C., *Immunomodulation by Omega-3 Fatty Acids.* Prostaglandins, Leukotrienes and Essential Fatty Acids, 2007. **77**(5): p. 327-335.
40. Marchioli, R., *et al.*, *Assessment of Absolute Risk of Death after Myocardial Infarction by Use of Multiple-Risk-Factor Assessment Equations: Gissi-Prevenzione Mortality Risk Chart.* European Heart Journal, 2001. **22**(22): p. 2085-2103.
41. Kremer, J.M., *et al.*, *Fish-Oil Fatty Acid Supplementation in Active Rheumatoid Arthritis. A Double-Blinded, Controlled, Crossover Study.* Annals of Internal Medicine, 1987. **106**(4): p. 497-503.
42. Kamido, H., Matsuzawa, Y., and Tarui, S., *Lipid Composition of Platelets from Patients with Atherosclerosis: Effect of Purified Eicosapentaenoic Acid Ethyl Ester Administration.* Lipids, 1988. **23**(10): p. 917-923.
43. Arm, J.P., *et al.*, *Effect of Dietary Supplementation with Fish Oil Lipids on Mild Asthma.* Thorax, 1988. **43**(2): p. 84-92.
44. Serhan, C.N., *et al.*, *Novel Functional Sets of Lipid-Derived Mediators with Antiinflammatory Actions Generated from Omega-3 Fatty Acids Via Cyclooxygenase 2 - Nonsteroidal Antiinflammatory Drugs and Transcellular Processing.* Journal of Experimental Medicine, 2000. **192**(8): p. 1197-1204.
45. Zhang, M.J. and Spite, M., *Resolvins: Anti-Inflammatory and Proresolving Mediators Derived from Omega-3 Polyunsaturated Fatty Acids.* Annual Review of Nutrition, 2012. **32**: p. 203-227.

46. Levy, B., *et al.*, *Lipid Mediator Class Switching During Acute Inflammation: Signals in Resolution.* Nature Immunology, 2001. **2**(7): p. 612-619.
47. Takano, T., *et al.*, *Neutrophil-Mediated Changes in Vascular Permeability Are Inhibited by Topical Application of Aspirin-Triggered 15-Epi-Lipoxin A4 and Novel Lipoxin B4 Stable Analogues.* The Journal of Clinical Investigation, 1998. **101**(4): p. 819-826.
48. Borgeat, P. and Naccache, P.H., *Biosynthesis and Biological Activity of Leukotriene B4.* Clinical Biochemistry, 1990. **23**(5): p. 459-468.
49. Hedqvist, P., *et al.*, *Biological Profile of Ieukotrienes C4 and D4.* Acta Physiologica Scandinavica, 1980. **110**(3): p. 331-333.
50. Drazen, J.M., *et al.*, *Comparative Airway and Vascular Activities of Leukotrienes C-1 and D in Vivo and in Vitro.* Proceedings of the National Academy of Sciences of the United States of America, 1980. **77**(7): p. 4354-4358.
51. Caliendo, G., *et al.*, *Synthesis and Biological Effects of Hydrogen Sulfide (H2S): Development of H2S-Releasing Drugs as Pharmaceuticals.* Journal of Medicinal Chemistry, 2010. **53**(17): p. 6275-6286.
52. Chiang, N., *et al.*, *Inhaled Carbon Monoxide Accelerates Resolution of Inflammation Via Unique Proresolving Mediator-Heme Oxygenase-1 Circuits.* Journal of Immunology (Baltimore, Md. : 1950), 2013. **190**(12): p. 6378-6388.
53. Ehrentraut, H., *et al.*, *CD73+ Regulatory T Cells Contribute to Adenosine-Mediated Resolution of Acute Lung Injury.* The FASEB Journal, 2013. **27**(6): p. 2207-2219.
54. Mirakaj, V., *et al.*, *Vagus Nerve Controls Resolution and Pro-Resolving Mediators of Inflammation.* Journal of Experimental Medicine, 2014. **211**(6): p. 1037-1048.
55. Pavlov, V.A. and Tracey, K.J., *The Vagus Nerve and the Inflammatory Reflex—Linking Immunity and Metabolism.* Nature Reviews Endocrinology, 2012. **8**(12): p. 743-754.
56. Norling, L.V. and Serhan, C.N., *Profiling in Resolving Inflammatory Exudates Identifies Novel Anti-Inflammatory and Pro-Resolving Mediators and Signals for Termination.* Journal of Internal Medicine, 2010. **268**(1): p. 15-24.
57. Dalli, J., *et al.*, *Proresolving and Tissue-Protective Actions of Annexin A1-Based Cleavage-Resistant Peptides Are Mediated by Formyl Peptide Receptor 2/Lipoxin A(4) Receptor.* Journal of Immunology (Baltimore, Md. : 1950), 2013. **190**(12): p. 6478-6487.

58. Serhan, C.N. and Chiang, N., *Resolution Phase Lipid Mediators of Inflammation: Agonists of Resolution.* Current Opinion in Pharmacology, 2013. **13**(4): p. 632 - 640.
59. Dalli, J., Chiang, N., and Serhan, C.N., *Elucidation of Novel 13-Series Resolvins That Increase with Atorvastatin and Clear Infections.* Nature Medicine, 2015. **21**(9): p. 1071-1075.
60. Vik, A., Dalli, J., and Hansen, T.V., *Recent Advances in the Chemistry and Biology of Anti-Inflammatory and Specialized Pro-Resolving Mediators Biosynthesized from N-3 Docosapentaenoic Acid.* Bioorganic & Medicinal Chemistry Letters, 2017. **27**(11): p. 2259-2266.
61. Chiang, N., *et al.*, *Infection Regulates Pro-Resolving Mediators That Lower Antibiotic Requirements.* Nature, 2012. **484**(7395): p. 524-528.
62. Serhan, C.N., *et al.*, *Macrophage Proresolving Mediator Maresin 1 Stimulates Tissue Regeneration and Controls Pain.* The FASEB Journal, 2012. **26**(4): p. 1755-1765.
63. Rodriguez, A.R. and Spur, B.W., *First Total Synthesis of Pro-Resolving and Tissue-Regenerative Maresin Sulfido-Conjugates.* Tetrahedron Letters, 2015. **56**(25): p. 3936-3940.
64. Dalli, J. and Serhan, C.N., *Identification and Structure Elucidation of the Pro-Resolving Mediators Provides Novel Leads for Resolution Pharmacology.* British Journal of Pharmacology, 2019. **176**(8): p. 1024-1037.
65. Qu, L. and Caterina, M.J., *Accelerating the Reversal of Inflammatory Pain with NPD1 and Its Receptor GPR37.* The Journal of Clinical Investigation, 2018. **128**(8): p. 3246-3249.
66. Flak, M.B., *et al.*, *GPR101 Mediates the Pro-Resolving Actions of RvD5n-3 DPA in Arthritis and Infections.* The Journal of Clinical Investigation, 2020. **130**(1): p. 359-373.
67. Chiang, N., *et al.*, *The Lipoxin Receptor ALX: Potent Ligand-Specific and Stereoselective Actions in Vivo.* Pharmacological Reviews, 2006. **58**(3): p. 463-487.
68. Recchiuti, A., *Resolvin D1 and Its GPCRs in Resolution Circuits of Inflammation.* Prostaglandins & Other Lipid Mediators, 2013. **107**: p. 64-76.
69. Mizwicki, M.T., *et al.*, *1α,25-Dihydroxyvitamin D3 and Resolvin D1 Retune the Balance between Amyloid-β Phagocytosis and Inflammation in Alzheimer's Disease Patients.* Journal of Alzheimer's Disease, 2013. **34**(1): p. 155-170.

70. Arita, M., *et al.*, *Stereochemical Assignment, Antiinflammatory Properties, and Receptor for the Omega-3 Lipid Mediator Resolvin E1.* Journal of Experimental Medicine, 2005. **201**(5): p. 713-722.
71. Chiang, N., *et al.*, *Identification of Resolvin D2 Receptor Mediating Resolution of Infections and Organ Protection.* Journal of Experimental Medicine, 2015. **212**(8): p. 1203-1217.
72. Serhan, C.N., *Lipoxins and Aspirin-Triggered 15-Epi-Lipoxin Biosynthesis: An Update and Role in Anti-Inflammation and Pro-Resolution.* Prostaglandins and Other Lipid Mediators, 2002. **68**: p. 433-455.
73. Morris, T., *et al.*, *Effects of Low-Dose Aspirin on Acute Inflammatory Responses in Humans.* Journal of Immunology (Baltimore, Md. : 1950), 2009. **183**(3): p. 2089-2096.
74. Chiang, N., *et al.*, *Aspirin Triggers Antiinflammatory 15-Epi-Lipoxin A4 and Inhibits Thromboxane in a Randomized Human Trial.* Proceedings of the National Academy of Sciences of the United States of America, 2004. **101**(42): p. 15178-15183.
75. Serhan, C.N., *et al.*, *Resolvins: A Family of Bioactive Products of Omega-3 Fatty Acid Transformation Circuits Initiated by Aspirin Treatment That Counter Proinflammation Signals.* Journal of Experimental Medicine, 2002. **196**(8): p. 1025-1037.
76. Claria, J. and Serhan, C.N., *Aspirin Triggers Previously Undescribed Bioactive Eicosanoids by Human Endothelial Cell-Leukocyte Interactions.* Proceedings of the National Academy of Sciences of the United States of America, 1995. **92**(21): p. 9475-9479.
77. Lee, T.H., *et al.*, *Identification of Lipoxin A4 and Its Relationship to the Sulfidopeptide Leukotrienes C4, D4, and E4 in the Bronchoalveolar Lavage Fluids Obtained from Patients with Selected Pulmonary Diseases.* The American Review of Respiratory Disease, 1990. **141**(6): p. 1453-1458.
78. Godson, C., *et al.*, *Cutting Edge: Lipoxins Rapidly Stimulate Nonphlogistic Phagocytosis of Apoptotic Neutrophils by Monocyte-Derived Macrophages.* Journal of Immunology (Baltimore, Md. : 1950), 2000. **164**(4): p. 1663-1667.
79. Wu, S.H., *et al.*, *Efficacy and Safety of 15(R/S)-Methyl-Lipoxin A4 in Topical Treatment of Infantile Eczema.* British Journal of Dermatology, 2013. **168**(1): p. 172-178.

80. Vong, L., *et al.*, *Up-Regulation of Annexin-A1 and Lipoxin A4 in Individuals with Ulcerative Colitis May Promote Mucosal Homeostasis.* PLoS ONE, 2012. **7**(6): p. e39244.
81. Walker, J., *et al.*, *Lipoxin A4 Increases Survival by Decreasing Systematic Inflammation and Bacterial Load in Sepsis.* Shock, 2011. **36**(4): p. 410-416.
82. Serhan, C.N., *et al.*, *Reduced Inflammation and Tissue Damage in Transgenic Rabbits Overexpressing 15-Lipoxygenase and Endogenous Anti-Inflammatory Lipid Mediators.* Journal of Immunology (Baltimore, Md. : 1950), 2003. **171**(12): p. 6856-6865.
83. Krönke, G., *et al.*, *The 12/15-Lipoxygenase Pathway Counteracts Fibroblast Activation and Experimental Fibrosis.* Annals of The Rheumatic Diseases, 2012. **71**(6): p. 1081-1087.
84. Serhan, C.N., Hamberg, M., and Samuelsson, B., *Trihydroxytetraenes: A Novel Series of Compounds Formed from Arachidonic Acid in Human Leukocytes.* Biochemical and Biophysical Research Communications, 1984. **118**(3): p. 943-949.
85. Arita, M., *et al.*, *Resolvin E1 Selectively Interacts with Leukotriene B4 Receptor BLT1 and ChemR23 to Regulate Inflammation.* Journal of Immunology (Baltimore, Md. : 1950), 2007. **178**(6): p. 3912-3917.
86. Qu, X., *et al.*, *Resolvins E1 and D1 Inhibit Interstitial Fibrosis in the Obstructed Kidney Via Inhibition of Local Fibroblast Proliferation.* The Journal of Pathology, 2012. **228**(4): p. 506-519.
87. Yu, S., *et al.*, *Resolvin E1 Attenuates Murine Psoriatic Dermatitis.* Scientific Reports, 2018. **8**(1): p. 1-9.
88. *Resolvyx Announces Positive Data from Phase 2 Clinical Trial of the Resolvin Rx-10045 in Patients with Dry Eye Syndrome.(Clinical Report).* in *Clinical Trials*. 2009. p. 33.
89. *Study Findings from Resolvyx Pharmaceuticals Provide New Insights into Inflammation (Inhibition of Corneal Inflammation by the Resolvin E1).* Life Science Weekly, 2015: p. 1360.
90. Hasturk, H., *et al.*, *RvE1 Protects from Local Inflammation and Osteoclast-mediated Bone Destruction in Periodontitis.* The FASEB Journal, 2006. **20**(2): p. 401-403.
91. Haworth, O., *et al.*, *Resolvin E1 Regulates Interleukin 23, Interferon-γ and Lipoxin A4 to Promote the Resolution of Allergic Airway Inflammation.* Nature Immunology, 2008. **9**(8): p. 873-879.

92. Rodriguez, A.R. and Spur, B.W., *First Total Synthesis of Pro-Resolving and Tissue-Regenerative Resolvin Sulfido-Conjugates.* Tetrahedron Letters, 2017. **58**(16): p. 1662-1668.
93. Huang, L., *et al.*, *Enduring Prevention and Transient Reduction of Postoperative Pain by Intrathecal Resolvin D1.* Pain, 2011. **152**(3): p. 557-565.
94. Zhen-Zhong, X., *et al.*, *Resolvins RvE1 and RvD1 Attenuate Inflammatory Pain Via Central and Peripheral Actions.* Nature Medicine, 2010. **16**(5): p. 592-597.
95. Hellmann, J., *et al.*, *Resolvin D1 Decreases Adipose Tissue Macrophage Accumulation and Improves Insulin Sensitivity in Obese-Diabetic Mice.* The FASEB Journal, 2011. **25**(7): p. 2399-2407.
96. Tang, Y., *et al.*, *Proresolution Therapy for the Treatment of Delayed Healing of Diabetic Wounds.* Diabetes, 2013. **62**(2): p. 618-627.
97. Odusanwo, O., *et al.*, *Resolvin D1 Prevents TNF-Alpha-Mediated Disruption of Salivary Epithelial Formation.* American Journal of Physiology-Cell Physiology, 2012. **302**(9): p. C1331-C1345.
98. Bento, A.F., *et al.*, *Omega-3 Fatty Acid-Derived Mediators 17(R)-Hydroxy Docosahexaenoic Acid, Aspirin-Triggered Resolvin D1 and Resolvin D2 Prevent Experimental Colitis in Mice.* Journal of Immunology (Baltimore, Md. : 1950), 2011. **187**(4): p. 1957-1969.
99. Benjamim, C., *et al.*, *Aspirin-Triggered Resolvin D1, Atrvd1, Reverts Chronic Pulmonary Fibrosis in a Murine Model.* American Journal of Respiratory and Critical Care Medicine, 2016. **193**.
100. Bang, S., *et al.*, *17(R)-Resolvin D1 Specifically Inhibits Transient Receptor Potential Ion Channel Vanilloid 3 Leading to Peripheral Antinociception.* British Journal of Pharmacology, 2012. **165**(3): p. 683-692.
101. Lima-Garcia, J., *et al.*, *The Precursor of Resolvin D Series and Aspirin-Triggered Resolvin D1 Display Anti-Hyperalgesic Properties in Adjuvant-Induced Arthritis in Rats.* British Journal of Pharmacology, 2011. **164**(2): p. 278-293.
102. Terrando, N., *et al.*, *Aspirin-Triggered Resolvin D1 Prevents Surgery-Induced Cognitive Decline.* The FASEB Journal, 2013. **27**(9): p. 3564-3571.
103. Clària, J., *et al.*, *Resolvin D1 and Resolvin D2 Govern Local Inflammatory Tone in Obese Fat.* Journal of Immunology (Baltimore, Md. : 1950), 2012. **189**(5): p. 2597-2605.

104. Spite, M., *et al.*, *Resolvin D2 Is a Potent Regulator of Leukocytes and Controls Microbial Sepsis.* Nature, 2009. **461**(7268): p. 1287-1291.
105. Bohr, S., *et al.*, *Resolvin D2 Prevents Secondary Thrombosis and Necrosis in a Mouse Burn Wound Model.* Wound Repair and Regeneration, 2013. **21**(1): p. 35-43.
106. Menon, R., Krzyszczyk, P., and Berthiaume, F., *Pro-Resolution Potency of Resolvins D1, D2 and E1 on Neutrophil Migration and in Dermal Wound Healing.* Nano Life, 2017. **7**(1): p. 1750002.
107. Arnardottir, H.H., *et al.*, *Resolvin D3 Is Dysregulated in Arthritis and Reduces Arthritic Inflammation.* Journal of Immunology (Baltimore, Md. : 1950), 2016. **197**(6): p. 2362-2368.
108. Rodriguez, A.R. and Spur, B.W., *Total Synthesis of Pro-Resolving and Tissue-Regenerative Protectin Sulfido-Conjugates.* Tetrahedron Letters, 2015. **56**(42): p. 5811-5815.
109. Schwab, J., M. , *et al.*, *Resolvin E1 and Protectin D1 Activate Inflammation-Resolution Programmes.* Nature, 2007. **447**(7146): p. 869-874.
110. Serhan, C.N., *et al.*, *Protectins and Maresins: New Pro-Resolving Families of Mediators in Acute Inflammation and Resolution Bioactive Metabolome.* BBA - Molecular and Cell Biology of Lipids, 2015. **1851**(4): p. 397-413.
111. Marcheselli, V.L., *et al.*, *Novel Docosanoids Inhibit Brain Ischemia-Reperfusion-Mediated Leukocyte Infiltration and Pro-Inflammatory Gene Expression.* The Journal of Biological Chemistry, 2003. **278**(44): p. 43807-43817.
112. Bazan, N.G., *et al.*, *Novel Aspirin-Triggered Neuroprotectin D1 Attenuates Cerebral Ischemic Injury after Experimental Stroke.* Experimental Neurology, 2012. **236**(1): p. 122-130.
113. Stark, D. and Bazan, N.G., *Neuroprotectin D1 Induces Neuronal Survival and Downregulation of Amyloidogenic Processing in Alzheimer's Disease Cellular Models.* Molecular Neurobiology, 2011. **43**(2): p. 131-138.
114. Mukherjee, P.K., *et al.*, *Neuroprotectin D1: A Docosahexaenoic Acid-Derived Docosatriene Protects Human Retinal Pigment Epithelial Cells from Oxidative Stress.* Proceedings of the National Academy of Sciences of the United States of America, 2004. **101**(22): p. 8491-8496.
115. Bazan, N.G., Calandria, J.M., and Serhan, C.N., *Rescue and Repair During Photoreceptor Cell Renewal Mediated by Docosahexaenoic Acid-Derived Neuroprotectin D1.* The Journal of Lipid Research, 2010. **51**(8): p. 2018-2031.

116. Yamada, T., *et al.*, *Eosinophils Promote Resolution of Acute Peritonitis by Producing Proresolving Mediators in Mice.* The FASEB Journal, 2011. **25**(2): p. 561-568.
117. Park, C.-K., *et al.*, *Resolving TRPV1- and TNF-α-Mediated Spinal Cord Synaptic Plasticity and Inflammatory Pain with Neuroprotectin D1.* The Journal of Neuroscience, 2011. **31**(42): p. 15072-15085.
118. Gronert, K., *et al.*, *A Role for the Mouse 12/15-Lipoxygenase Pathway in Promoting Epithelial Wound Healing and Host Defense.* The Journal of Biological Chemistry, 2005. **280**(15): p. 15267-15278.
119. Chen, P., *et al.*, *Full Characterization of PDX, a Neuroprotectin/Protectin D1 Isomer, Which Inhibits Blood Platelet Aggregation.* FEBS Letters, 2009. **583**(21): p. 3478-3484.
120. Serhan, C.N., *et al.*, *Maresins: Novel Macrophage Mediators with Potent Antiinflammatory and Proresolving Actions.* Journal of Experimental Medicine, 2009. **206**(1): p. 15-23.
121. Deng, B., *et al.*, *Maresin Biosynthesis and Identification of Maresin 2, a New Anti-Inflammatory and Pro-Resolving Mediator from Human Macrophages.* PLoS ONE, 2014. **9**(7): p. e102362.
122. Dalli, J., *et al.*, *Identification and Actions of a Novel Third Maresin Conjugate in Tissue Regeneration: MCTR3.* PLoS ONE, 2016. **11**(2): p. e0149319.
123. Marcon, R., *et al.*, *Maresin 1, a Proresolving Lipid Mediator Derived from Omega-3 Polyunsaturated Fatty Acids, Exerts Protective Actions in Murine Models of Colitis.* Journal of Immunology (Baltimore, Md. : 1950), 2013. **191**(8): p. 4288-4298.
124. Nordgren, T.M., *et al.*, *Maresin-1 Reduces the Pro-Inflammatory Response of Bronchial Epithelial Cells to Organic Dust.* Respiratory Research, 2013. **14**(51).
125. Dalli, J., *et al.*, *The Novel 13S,14S -Epoxy-Maresin Is Converted by Human Macrophages to Maresin 1 (MaR1), Inhibits Leukotriene A4 Hydrolase (LTA4H), and Shifts Macrophage Phenotype.* The FASEB Journal, 2013. **27**(7): p. 2573-2583.
126. Dalli, J., Chiang, N., and Serhan, C.N., *Identification of 14-Series Sulfido-Conjugated Mediators That Promote Resolution of Infection and Organ Protection.* Proceedings of the National Academy of Sciences of the United States of America, 2014. **111**(44): p. 4753-4761.
127. Ramon, S., *et al.*, *The Protectin PCTR1 Is Produced by Human M2 Macrophages and Enhances Resolution of Infectious Inflammation.* The American Journal of Pathology, 2016. **186**(4): p. 962-973.

128. Dalli, J., *et al.*, *Novel Proresolving and Tissue-Regenerative Resolvin and Protectin Sulfido-Conjugated Pathways.* The FASEB Journal, 2015. **29**(5): p. 2120-2136.
129. Dalli, J., *et al.*, *Maresin Conjugates in Tissue Regeneration Biosynthesis Enzymes in Human Macrophages.* Proceedings of the National Academy of Sciences of the United States of America, 2016. **113**(43): p. 12232-12237.
130. Samuelsson, B., *Role of Basic Science in the Development of New Medicines: Examples from the Eicosanoid Field.* The Journal of Biological Chemistry, 2012. **287**(13): p. 10070-10080.
131. Gils, J.M., Zwaginga, J.J., and Hordijk, P.L., *Molecular and Functional Interactions among Monocytes, Platelets, and Endothelial Cells and Their Relevance for Cardiovascular Diseases.* Journal of Leukocyte Biology, 2009. **85**: p. 195-204.
132. Skulas-Ray, A., *et al.*, *Red Blood Cell Docosapentaenoic Acid (DPA N-3) Is Inversely Associated with Triglycerides and C-Reactive Protein (CRP) in Healthy Adults and Dose-Dependently Increases Following N-3 Fatty Acid Supplementation.* Nutrients, 2015. **7**(8): p. 6390-6404.
133. Gobbetti, T., *et al.*, *Protectin D1n-3 DPA and Resolvin D5n-3 DPA Are Effectors of Intestinal Protection.* Proceedings of the National Academy of Sciences of the United States of America, 2017. **114**(15): p. 3963-3968.
134. Aursnes, M., *et al.*, *Total Synthesis of the Lipid Mediator PD1n-3 DPA: Configurational Assignments and Anti-Inflammatory and Pro-Resolving Actions.* Journal of Natural Products, 2014. **77**(4): p. 910-916.
135. Tungen, J.E., *et al.*, *Total Synthesis of the Anti-Inflammatory and Pro-Resolving Lipid Mediator MaR1n−3 DPA Utilizing an Sp 3 –Sp 3 Negishi Cross-Coupling Reaction.* Chemistry – A European Journal, 2014. **20**(45): p. 14575-14578.
136. Frigerio, F., *et al.*, *N-3 Docosapentaenoic Acid-Derived Protectin D1 Promotes Resolution of Neuroinflammation and Arrests Epileptogenesis.* Brain, 2018. **141**(11): p. 3130-3143.
137. Sriram, K., *et al.*, *Resolvin D1 Binds Human Phagocytes with Evidence for Proresolving Receptors.* Proceedings of the National Academy of Sciences of the United States of America, 2010. **107**(4): p. 1660-1665.
138. Dalli, J., Colas, R.A., and Serhan, C.N., *Corrigendum: Novel N-3 Immunoresolvents: Structures and Actions.* Scientific Reports, 2014. **4**: p. 6726.

139. Guilford, W.J., *et al., Novel 3-Oxa Lipoxin A4 Analogues with Enhanced Chemical and Metabolic Stability Have Anti-Inflammatory Activity in Vivo.* Journal of Medicinal Chemistry, 2004. **47**(8): p. 2157-2165.
140. Orr, S.K., *et al., Proresolving Actions of a New Resolvin D1 Analog Mimetic Qualifies as an Immunoresolvent.* American Journal of Physiology - Lung Cellular and Molecular Physiology, 2015. **308**(9): p. 904-911.
141. Sun, Y.-P., *et al., Anti-Inflammatory and Pro-Resolving Properties of Benzo-Lipoxin A4 Analogs.* Prostaglandins, Leukotrienes and Essential Fatty Acids, 2009. **81**(5-6): p. 357-366.
142. Rodríguez, A.R. and Spur, B.W., *First Total Synthesis of 7(S),17(S)-Resolvin D5, a Potent Anti-Inflammatory Docosanoid.* Tetrahedron Letters, 2005. **46**(21): p. 3623-3627.
143. Rodríguez, A.R. and Spur, B.W., *First Total Synthesis of 7(S),16(R),17(S)-Resolvin D2, a Potent Anti-Inflammatory Lipid Mediator.* Tetrahedron Letters, 2004. **45**(47): p. 8717-8720.
144. Rodriguez, A.R. and Spur, B.W., *First Total Synthesis of the Anti-Inflammatory Lipid Mediator Resolvin D6.* Tetrahedron Letters, 2012. **53**(1): p. 86-89.
145. Sønderskov, J., *et al., Stereoselective Synthesis of MaR2n-3 DPA.* Tetrahedron Letters, 2020. **61**(7): p. 151510.
146. *The Noble Prize in Chemistry 1979.* [Accessed 29.04.2020]; Available from: https://www.nobelprize.org/prizes/chemistry/1979/summary/.
147. Byrne, P.A. and Gilheany, D.G., *The Modern Interpretation of the Wittig Reaction Mechanism.* Chemical Society Reviews, 2013. **42**(16): p. 6670-6696.
148. Clayden, J., *et al., Controlling the Geometry of Double Bonds*, in *Organic Chemistry*. 2000, Oxford University Press: New York, NY. p. 803-822.
149. Pine, S.H., Shen, G.S., and Hoang, H., *Ketone Methylenation Using the Tebbe and Wittig Reagents - a Comparison.* Synthesis, 1991. 10.1055/s-1991-26406(2): p. 165-167.
150. Pine, S.H., *et al., Carbonyl Methylenation Using a Titanium-Aluminum (Tebbe) Complex.* The Journal of Organic Chemistry, 1985. **50**: p. 1212-1216.
151. Tebbe, F.N., Parshall, G.W., and Reddy, G.S., *Olefin Homologation with Titanium Methylene Compounds.* Journal of the American Chemical Society, 1978. **100**(11): p. 3611-3613.

152. Thompson, R., *et al.*, *Structural Elucidation of the Illustrious Tebbe Reagent.* Organometallics, 2014. **33**(1): p. 429-432.
153. Hartley, R.C., *et al.*, *Titanium Carbenoid Reagents for Converting Carbonyl Groups into Alkenes.* Tetrahedron, 2007. **63**(23): p. 4825-4864.
154. Heck, R.F., *Palladium-Catalyzed Reactions of Organic Halides with Olefins.* Accounts of Chemical Research, 1979. **12**(4): p. 146-151.
155. Mizoroki, T., Mori, K., and Ozaki, A., *Arylation of Olefin with Aryl Iodide Catalyzed by Palladium.* Bulletin of the Chemical Society of Japan, 1971. **44**(2): p. 581-581.
156. Song, K., *et al.*, *Dichloropalladium Complexes Ligated by 4,5-Bis(Arylimino)Pyrenylidenes: Synthesis, Characterization, and Catalytic Behavior Towards Heck-Reaction.* Journal of Organometallic Chemistry, 2014. **751**: p. 453-457.
157. *The Nobel Prize in Chemistry 2010*. [Accessed 29.04.2020]; Available from: https://www.nobelprize.org/prizes/chemistry/2010/summary/.
158. Clayden, J., *et al.*, *Organometallic Chemistry*, in *Organic Chemistry*. 2000, Oxford University Press: New York, NY. p. 1311-1345.
159. Hanusa, T.P., *Alkaline Earth Organometallics*, in *Reference Module in Chemistry, Molecular Sciences and Chemical Engineering*. 2014, Elsevier.
160. Sun, X.-L., *et al.*, *The Introduction of the Barbier Reaction into Polymer Chemistry.* Nature Communications, 2017. **8**(1): p. 1210-1210.
161. Molle, G. and Bauer, P., *The Barbier Synthesis: A One-Slip Grignard Reaction?* Journal of the American Chemical Society, 1982. **104**(12): p. 3481-3487.
162. Jõgi, A. and Mäeorg, U., *Zn Mediated Regioselective Barbier Reaction of Propargylic Bromides in THF/Aq. NH4Cl Solution.* Molecules: A Journal of Synthetic Chemistry and Natural Product Chemistry, 2001. **6**(12): p. 964-968.
163. Klein, D., *Carbohydrates*, in *Organic Chemistry*. 2012, John Wiley and Sons, Inc.: John Hopkins University. p. 1151-1192.
164. Lu, X., Arthur, G., and Bittman, R., *Synthesis of a Novel Ceramide Analogue Via Tebbe Methylenation and Evaluation of Its Antiproliferative Activity.* Organic letters, 2005. **7**(8): p. 1645-1648.
165. Duffy, C.D., *et al.*, *Synthesis and Biological Evaluation of Pyridine-Containing Lipoxin A4 Analogues.* ChemMedChem, 2010. **5**: p. 517-522.

166. Yanagisawa, A., Habaue, S., and Yamamoto, H., *Regioselective Allylation and Propargylation Using Acylsilanes: Facile Synthesis of PGE3 and Methyl Ester.* Tetrahedron, 1992. **46**(11): p. 1969-1980.
167. Chinchilla, R. and Nájera, C., *The Sonogashira Reaction: A Booming Methodology in Synthetic Organic Chemistry.* Chemical Reviews, 2007. **107**(3): p. 874-922.
168. Zhou, J.Y., *et al.*, *Barbier-Type Allylation of Aldehydes and Ketones: With Metallic Lead in Aqueous Media.* Synthetic Communications, 1997. **27**(11): p. 1899-1906.

6 Appendix

6.1 ^{1}H NMR and ^{13}C NMR spectra

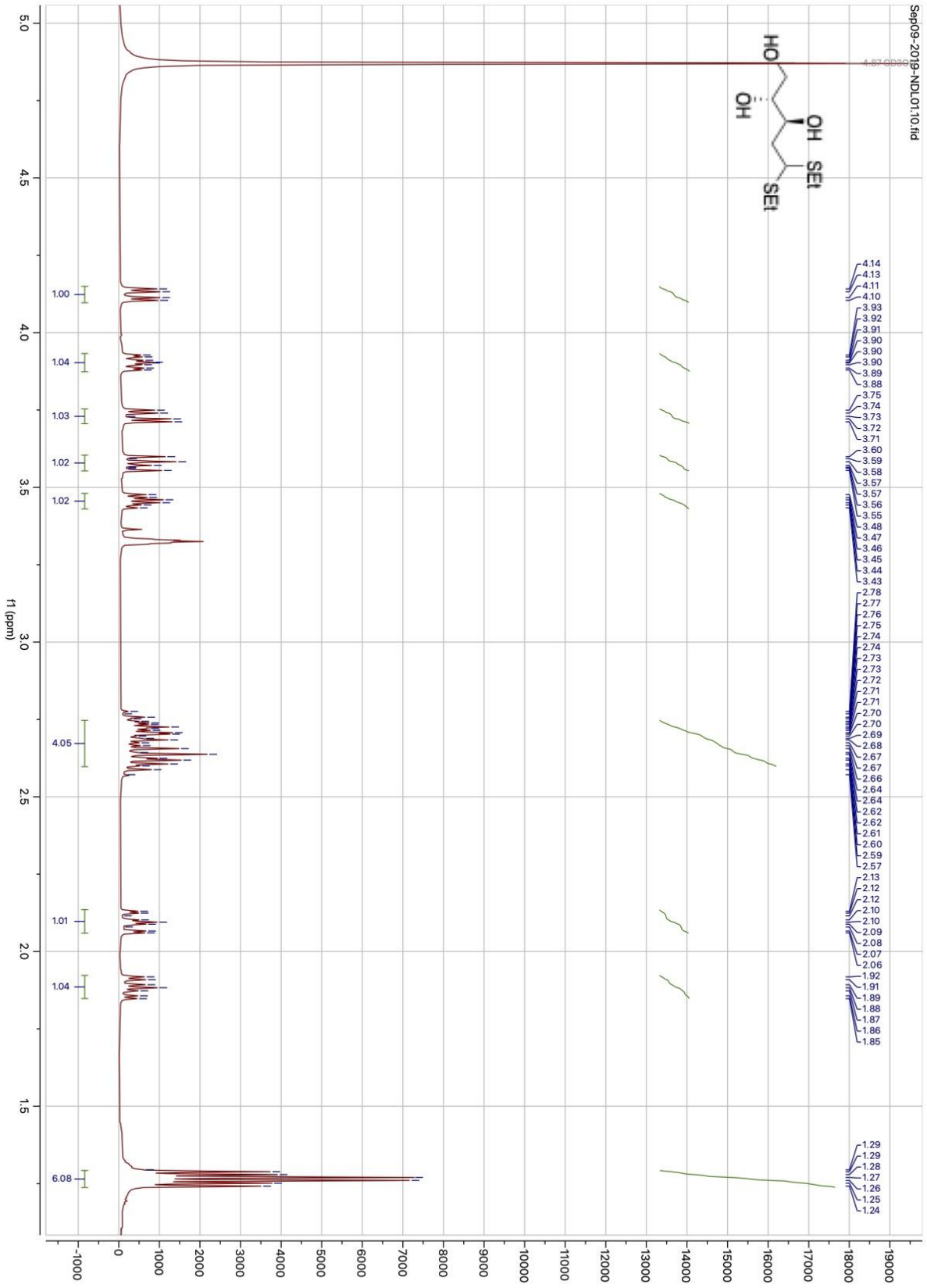

Figure 44: ^{1}H NMR spectrum of thioacetal **64**.

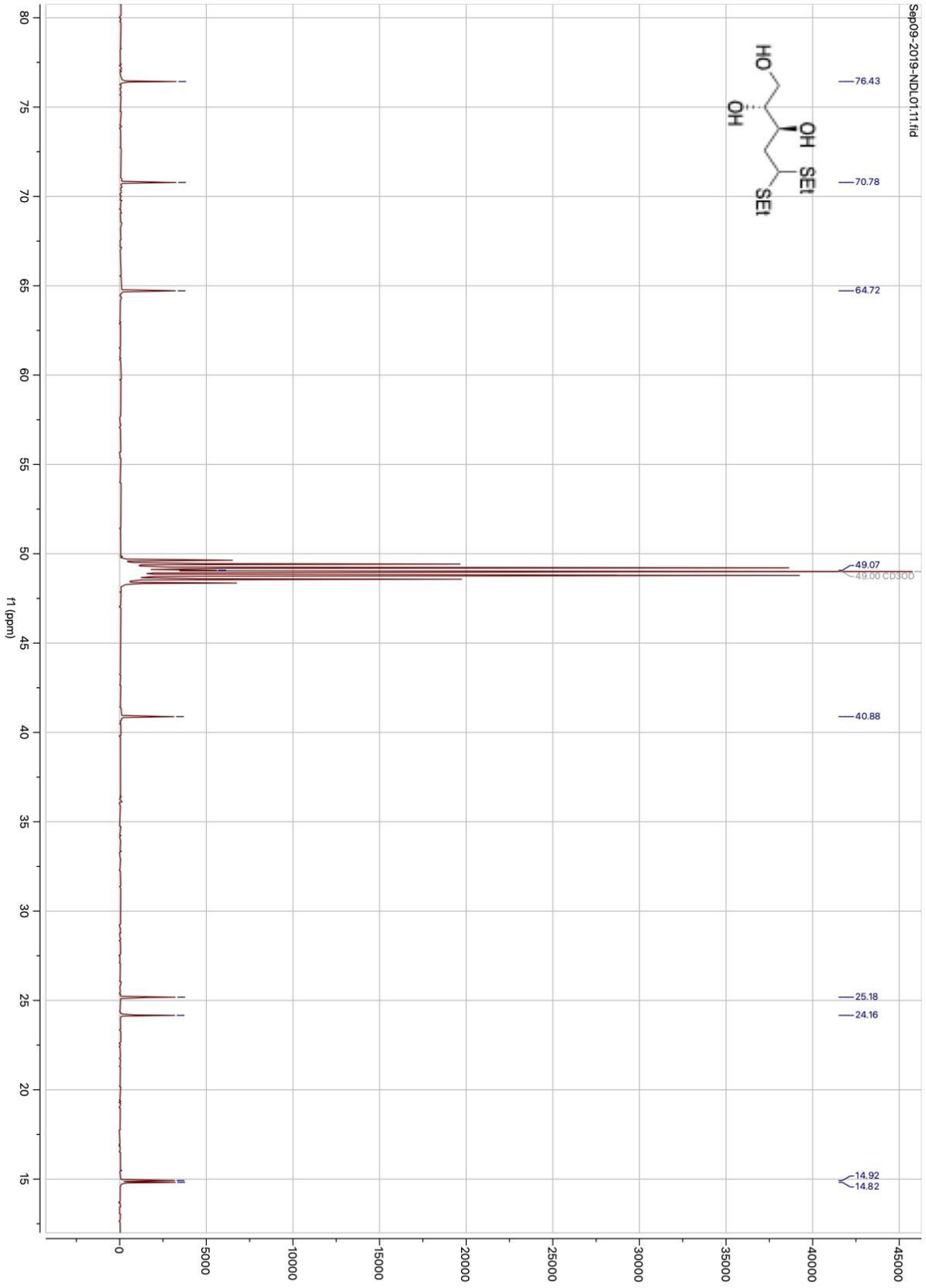

Figure 45: ^{13}C NMR spectrum of thioacetal **64**.

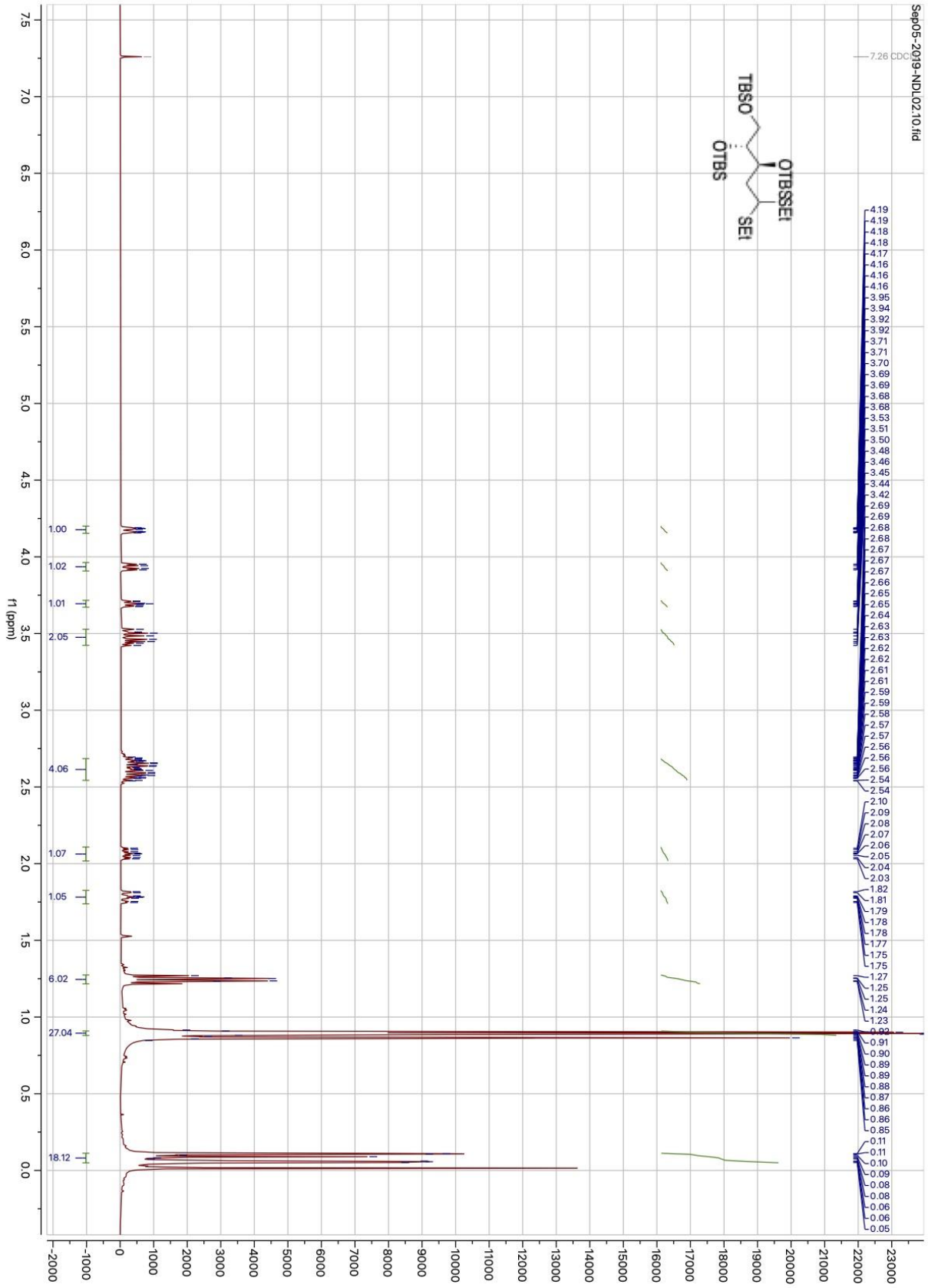

Figure 46: ^{1}H NMR spectrum of *tris*-silylated compound **65**.

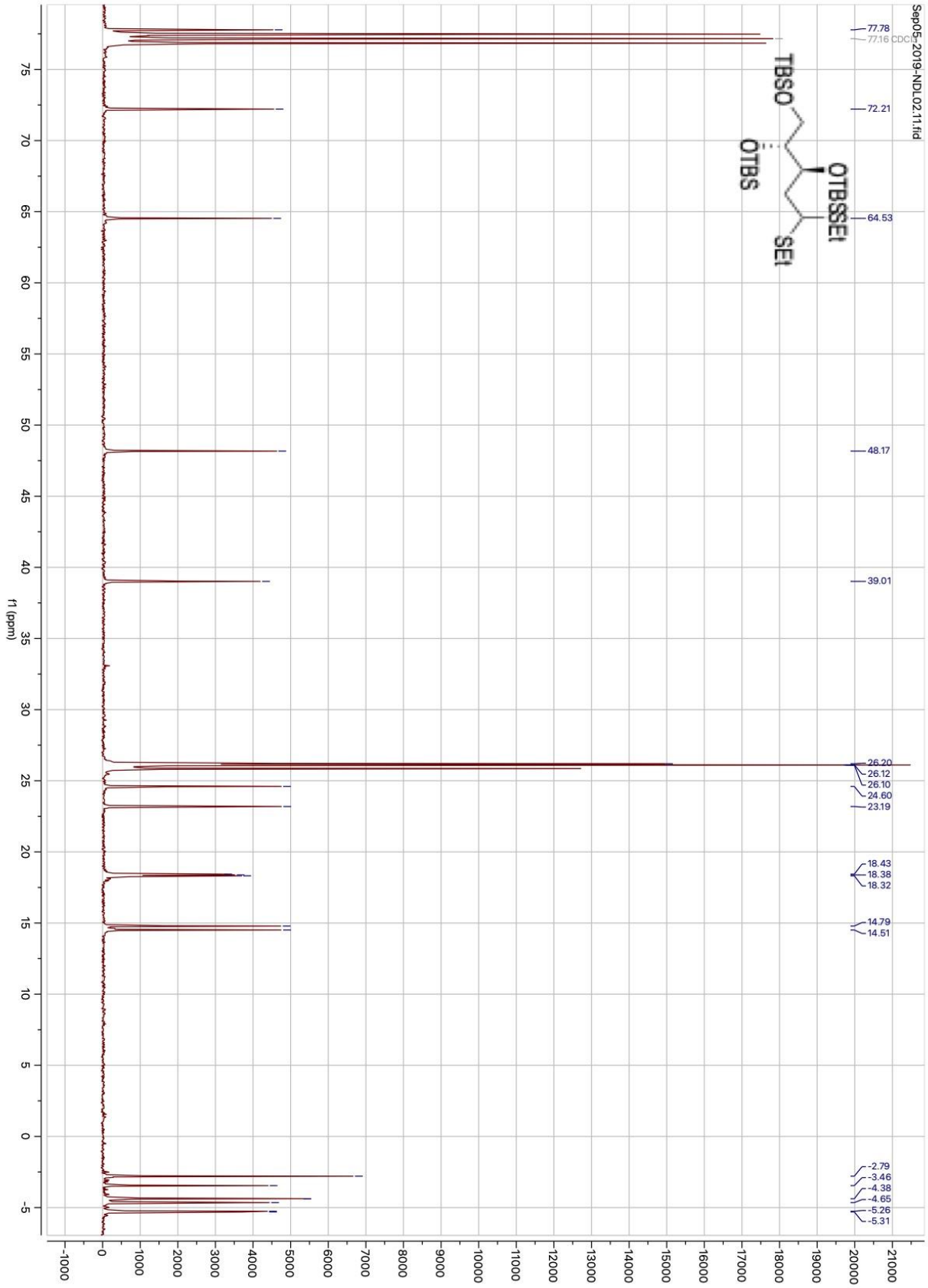

Figure 47: ^{13}C NMR spectrum of *tris*-silylated compound **65**.

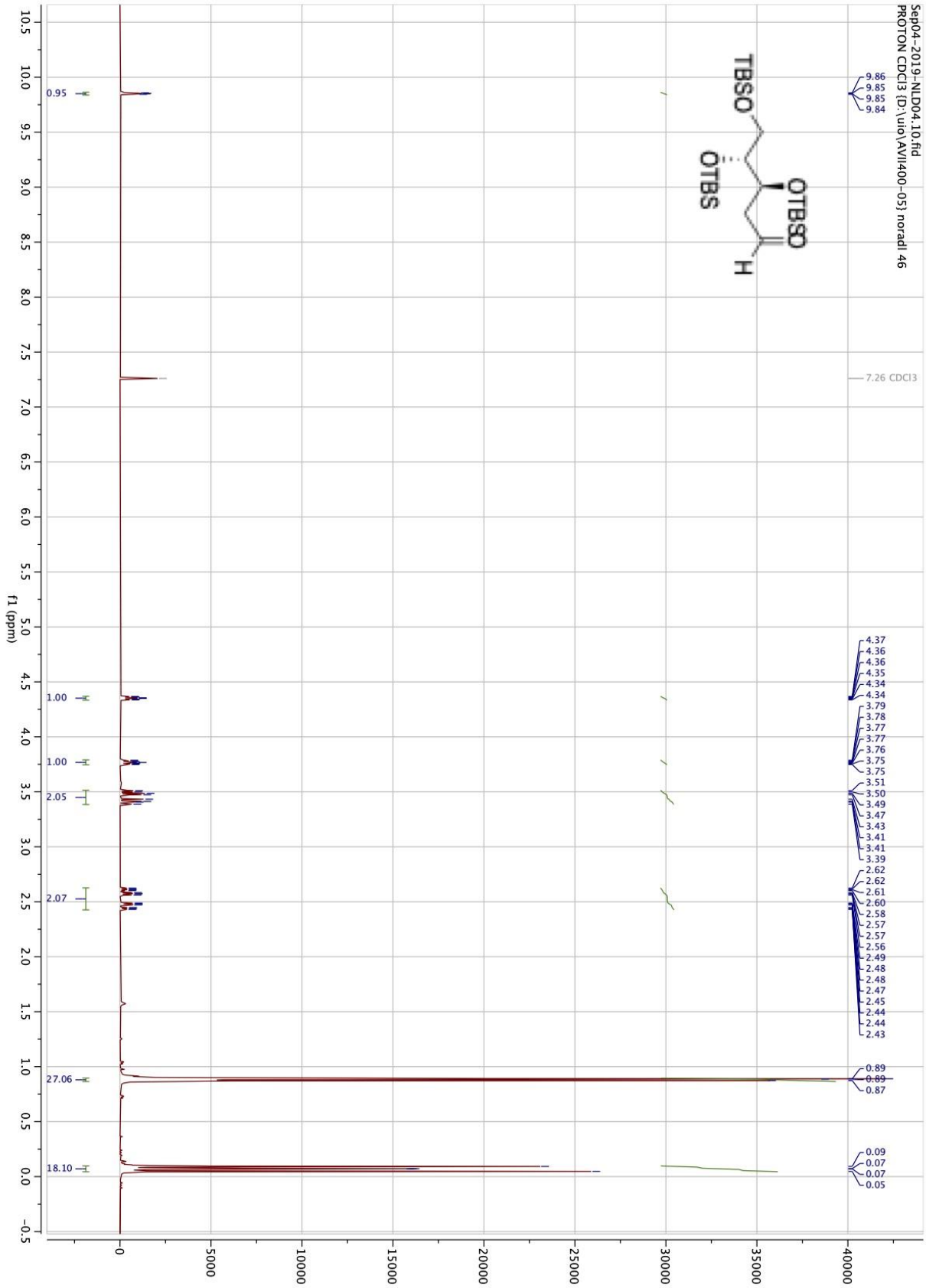

Figure 48: ^{1}H NMR spectrum of aldehyde **46**.

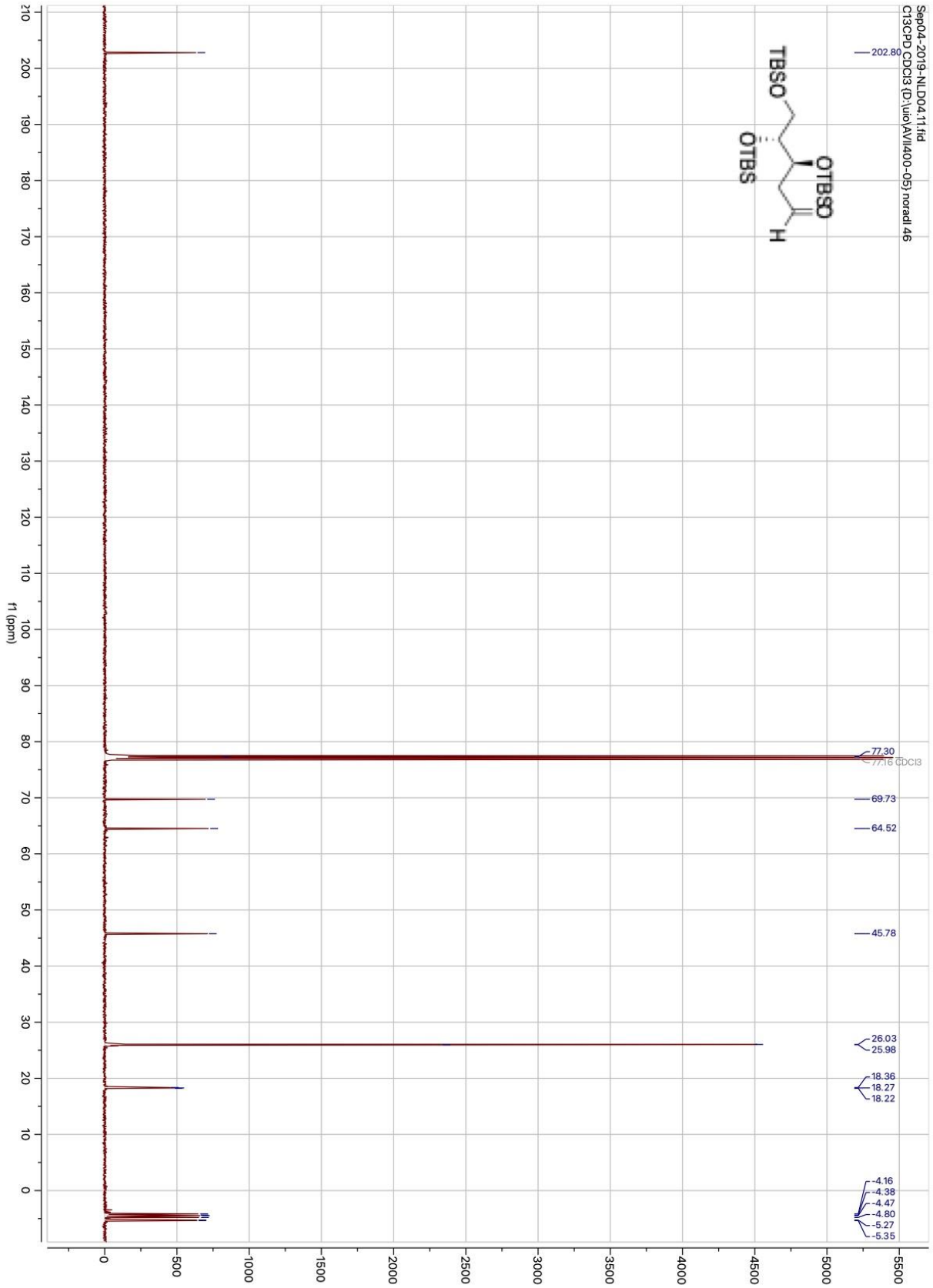

Figure 49: ^{13}C NMR spectrum of aldehyde **46**.

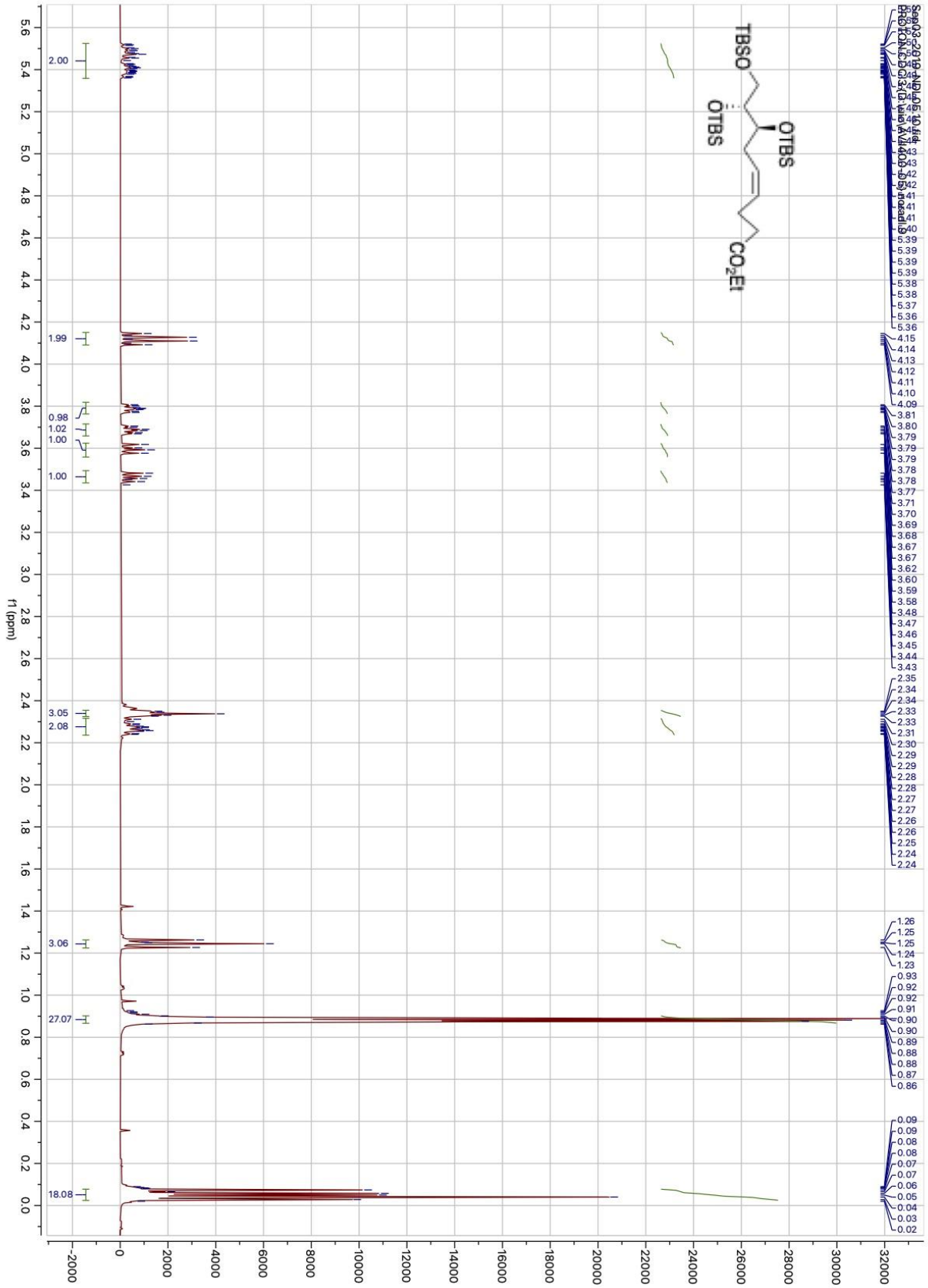

Figure 50: ^{1}H NMR spectrum of *Z*-alkene **49**.

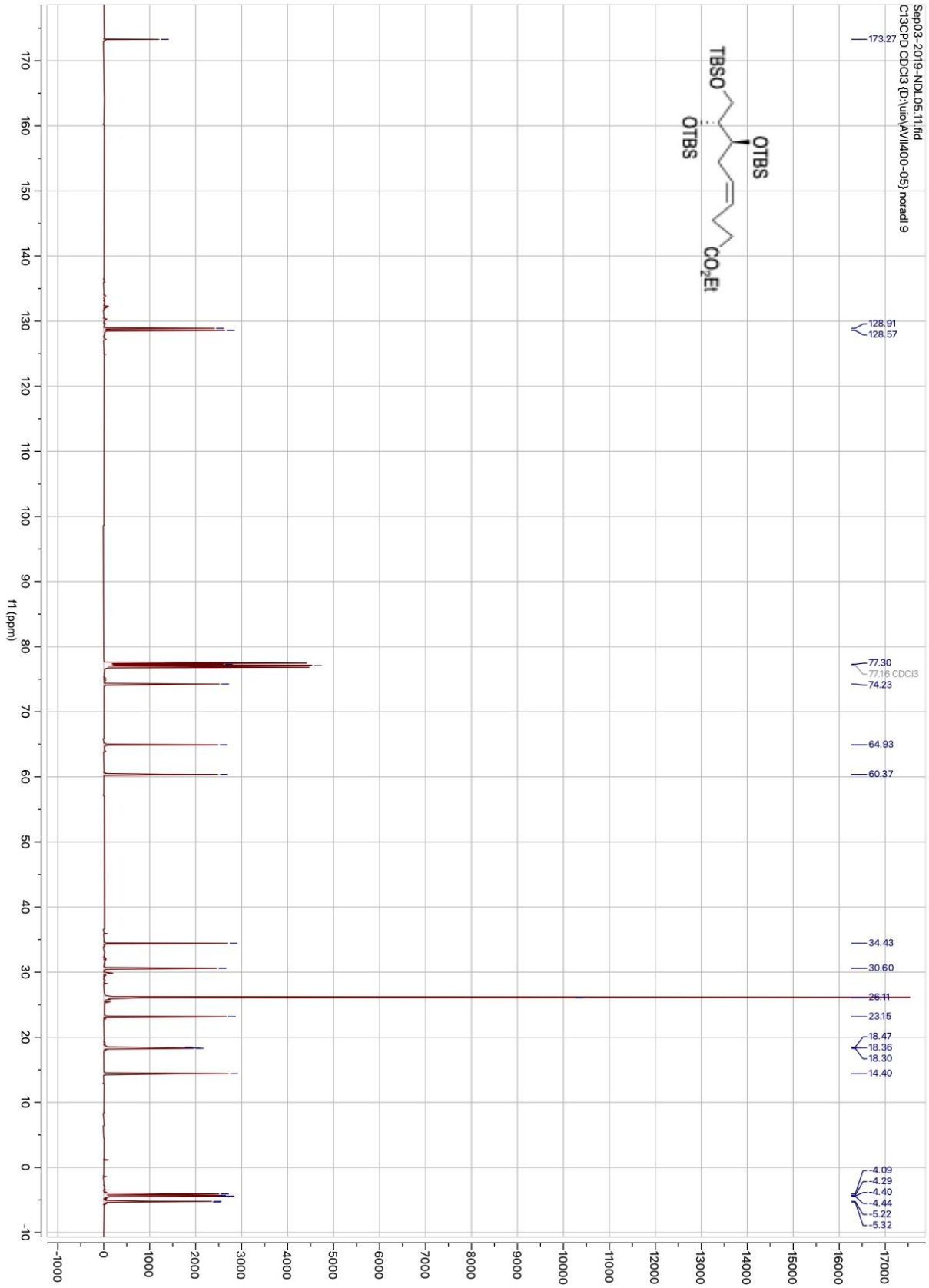

Figure 51: ^{13}C NMR spectrum of *Z*-alkene **49**.

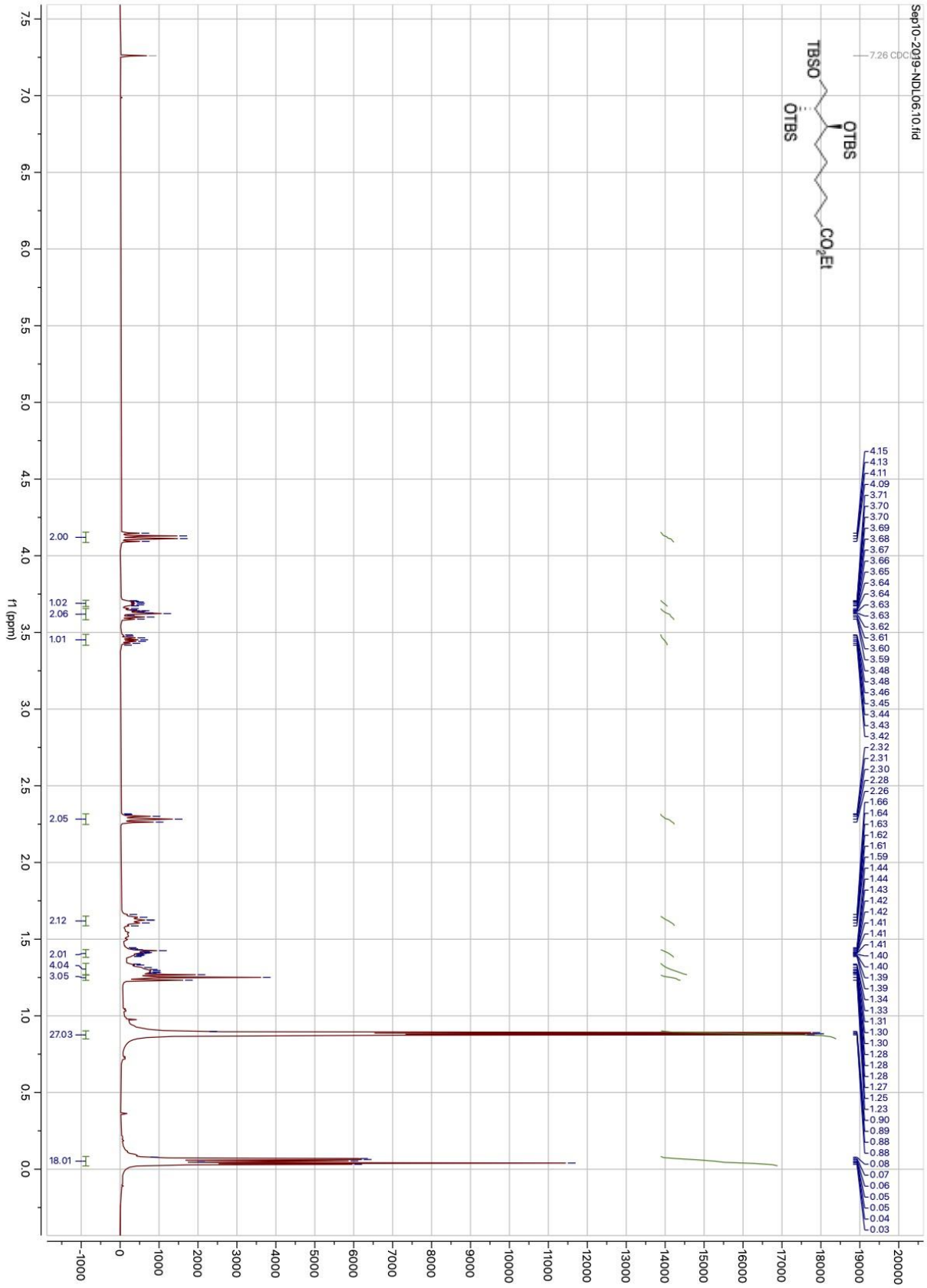

Figure 52: ^{1}H NMR spectrum of ethyl ester **66**.

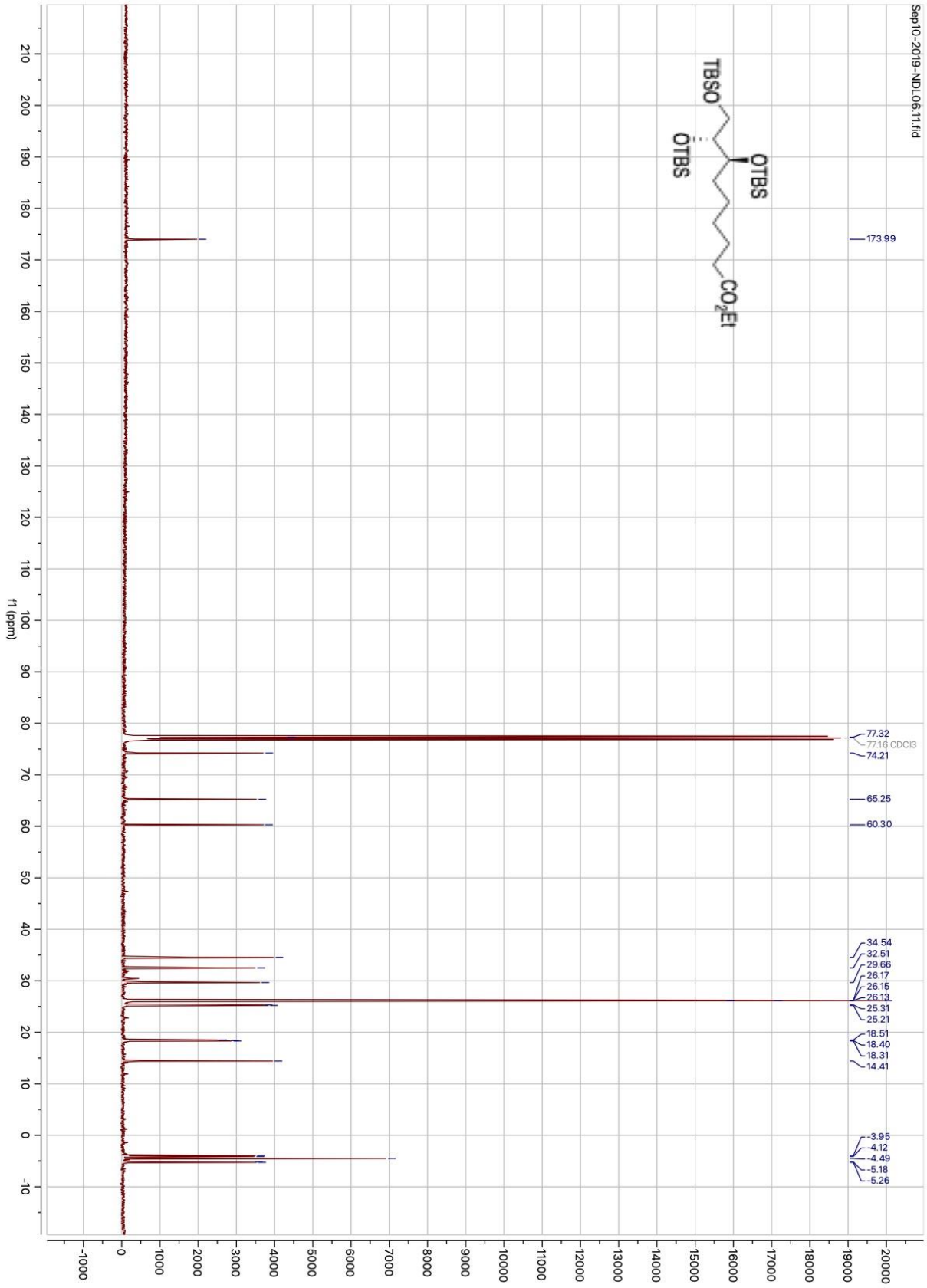

Figure 53: ^{13}C NMR spectrum of ethyl ester **66**.

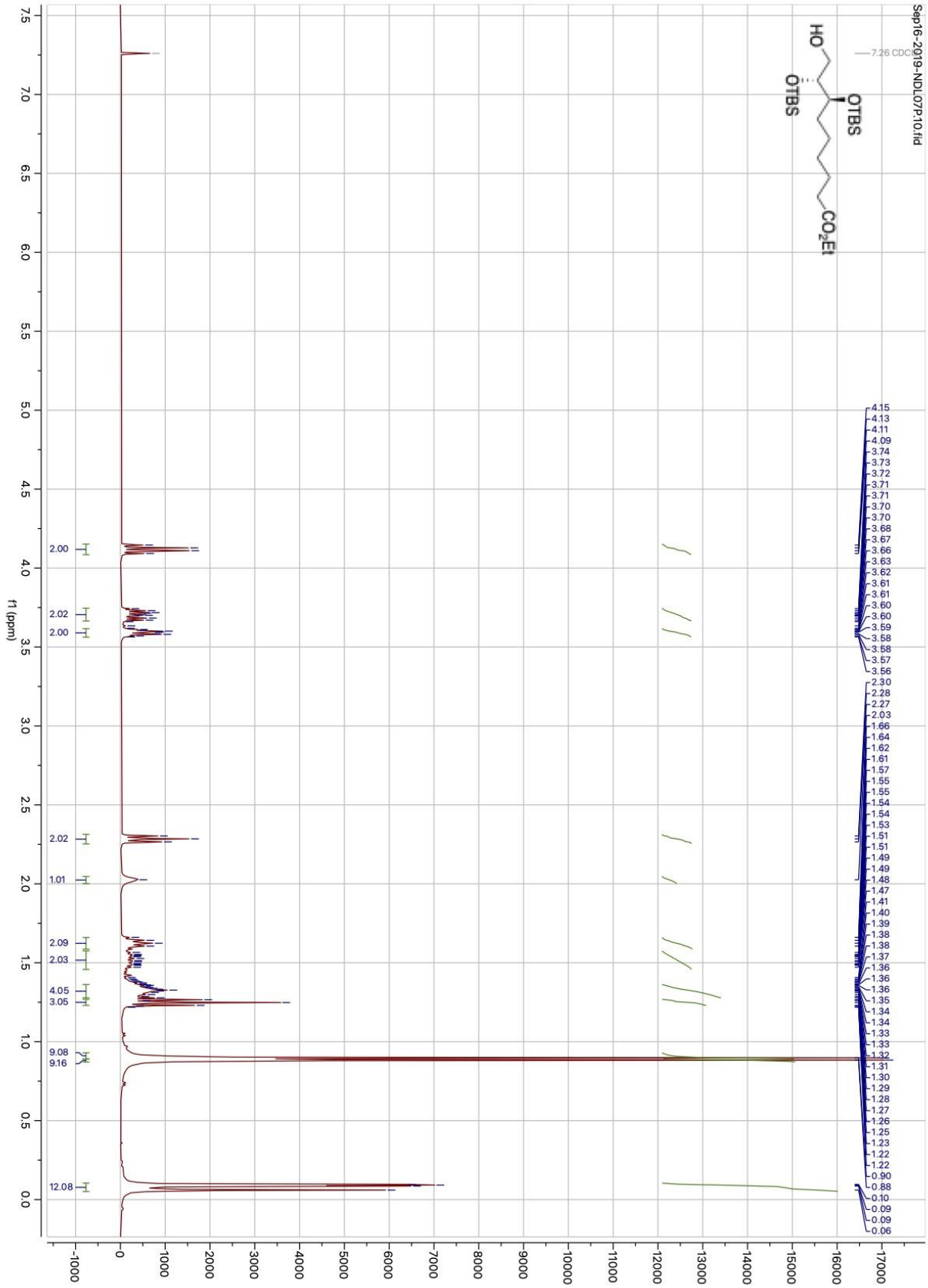

Figure 54: ^{1}H NMR spectrum of primary alcohol **67**.

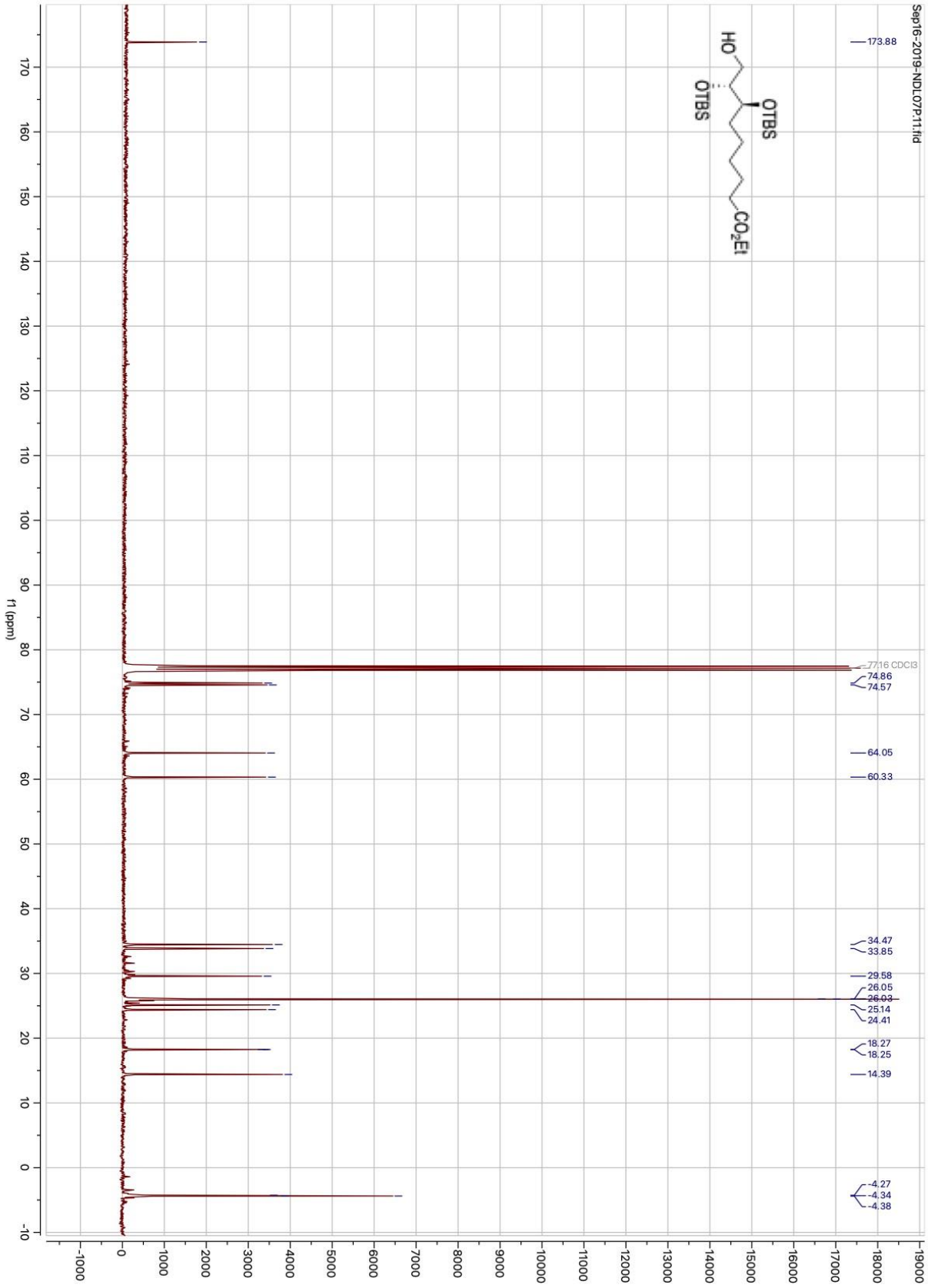

Figure 55: ^{13}C NMR spectrum of primary alcohol **67**.

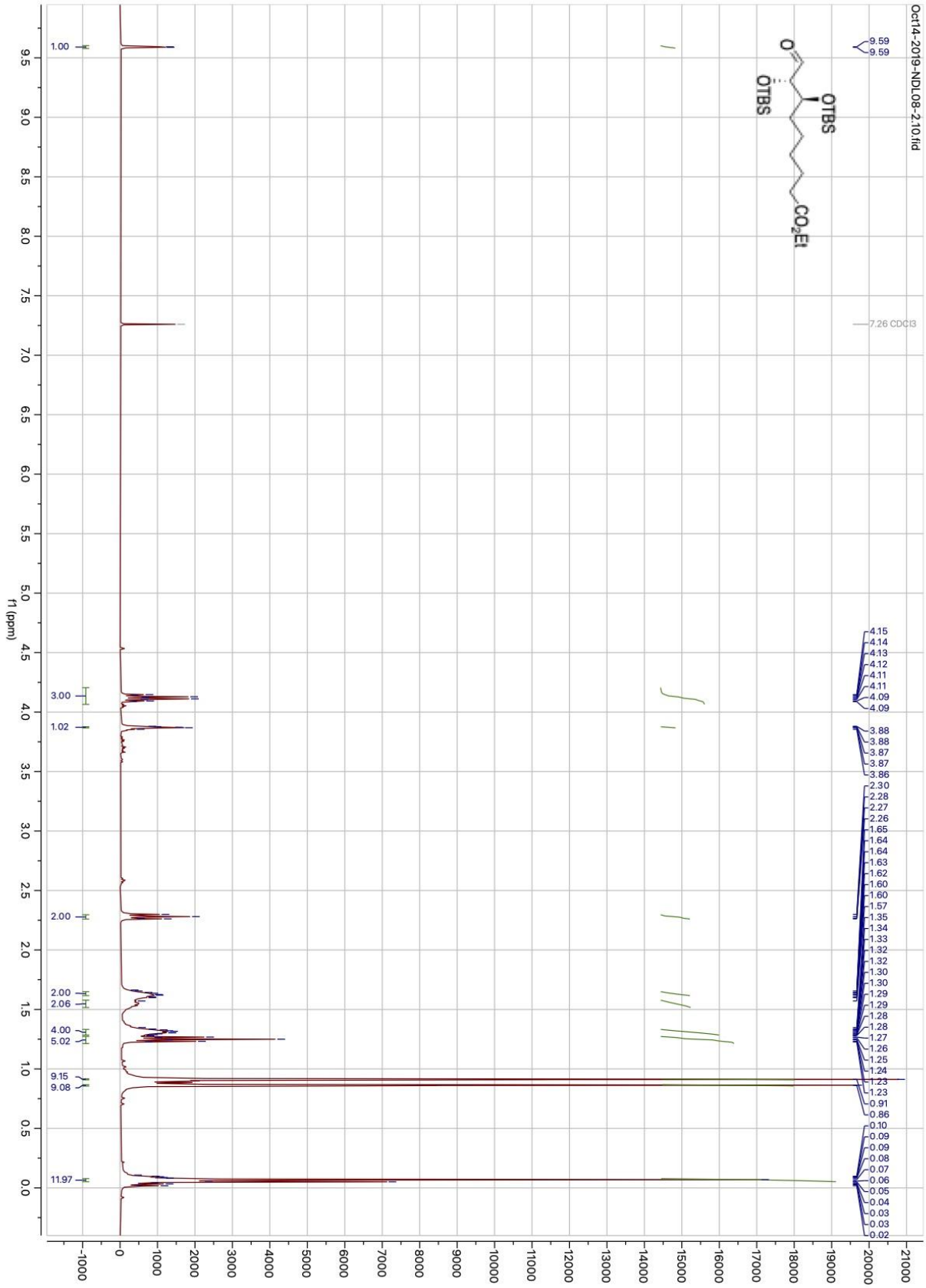

Figure 56: ^{1}H NMR spectrum of aldehyde **7**.

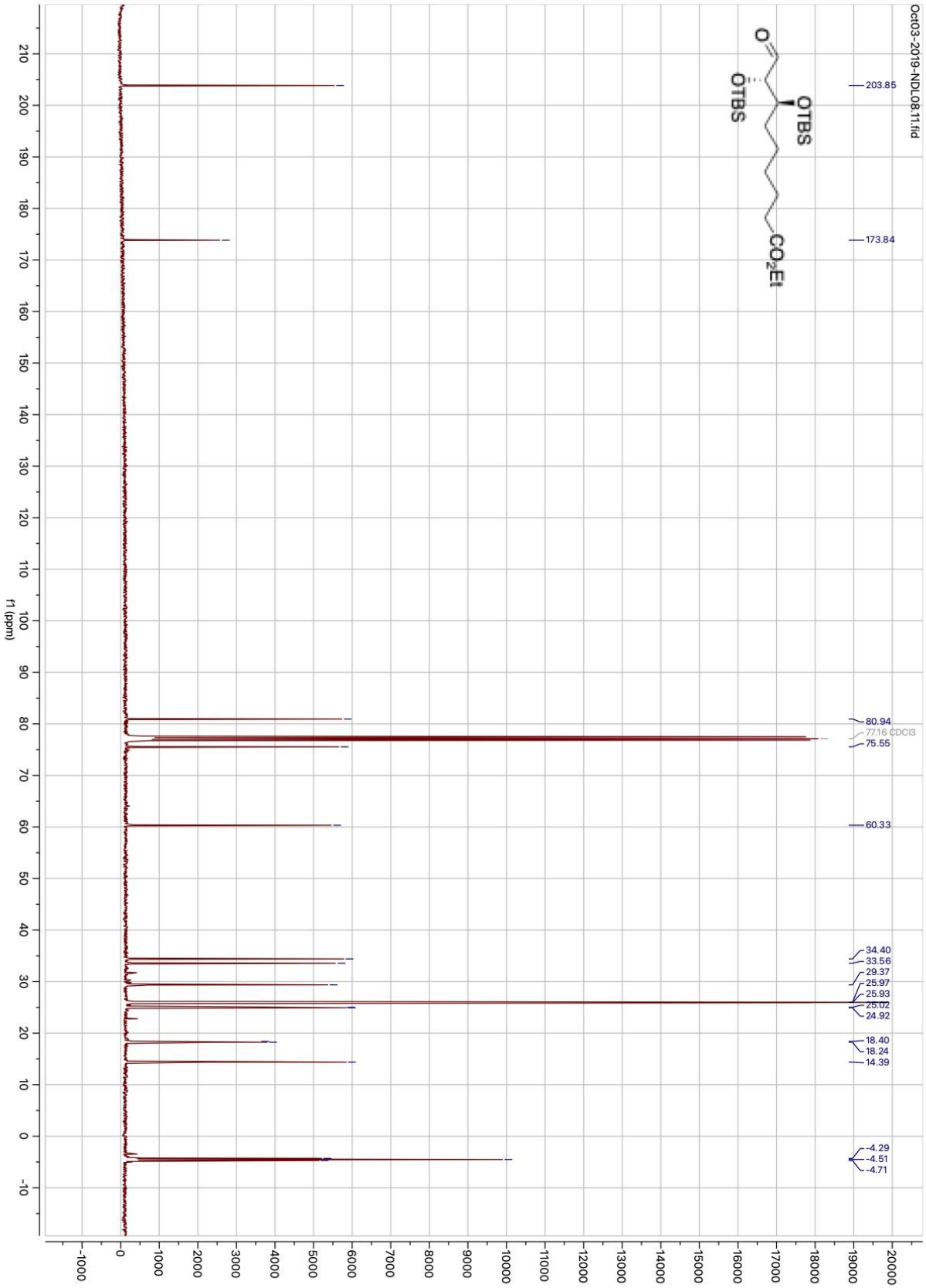

Figure 57: ^{13}C NMR spectrum of aldehyde **7**.

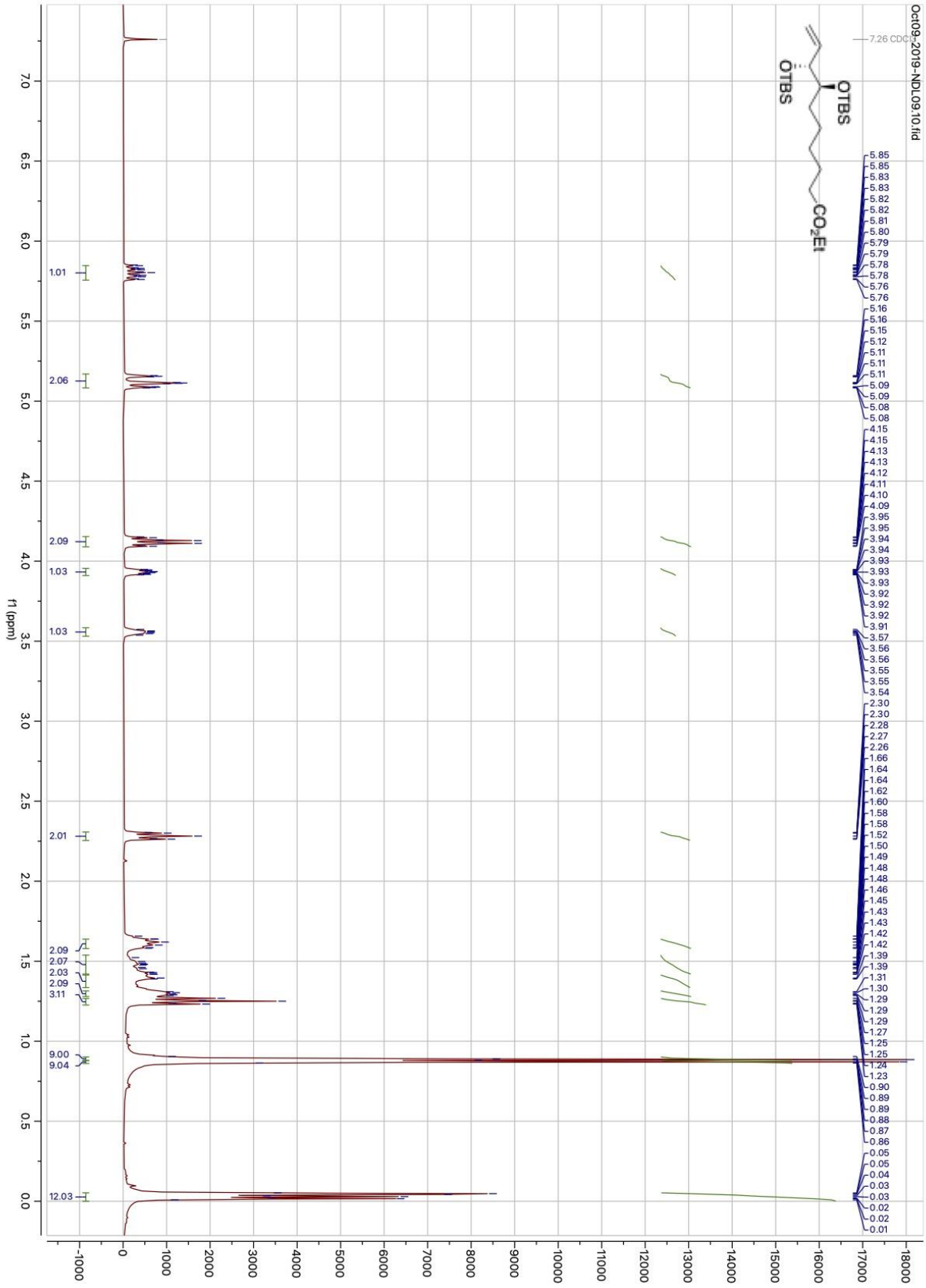

Figure 58: ^{1}H NMR spectrum of terminal alkene **6**.

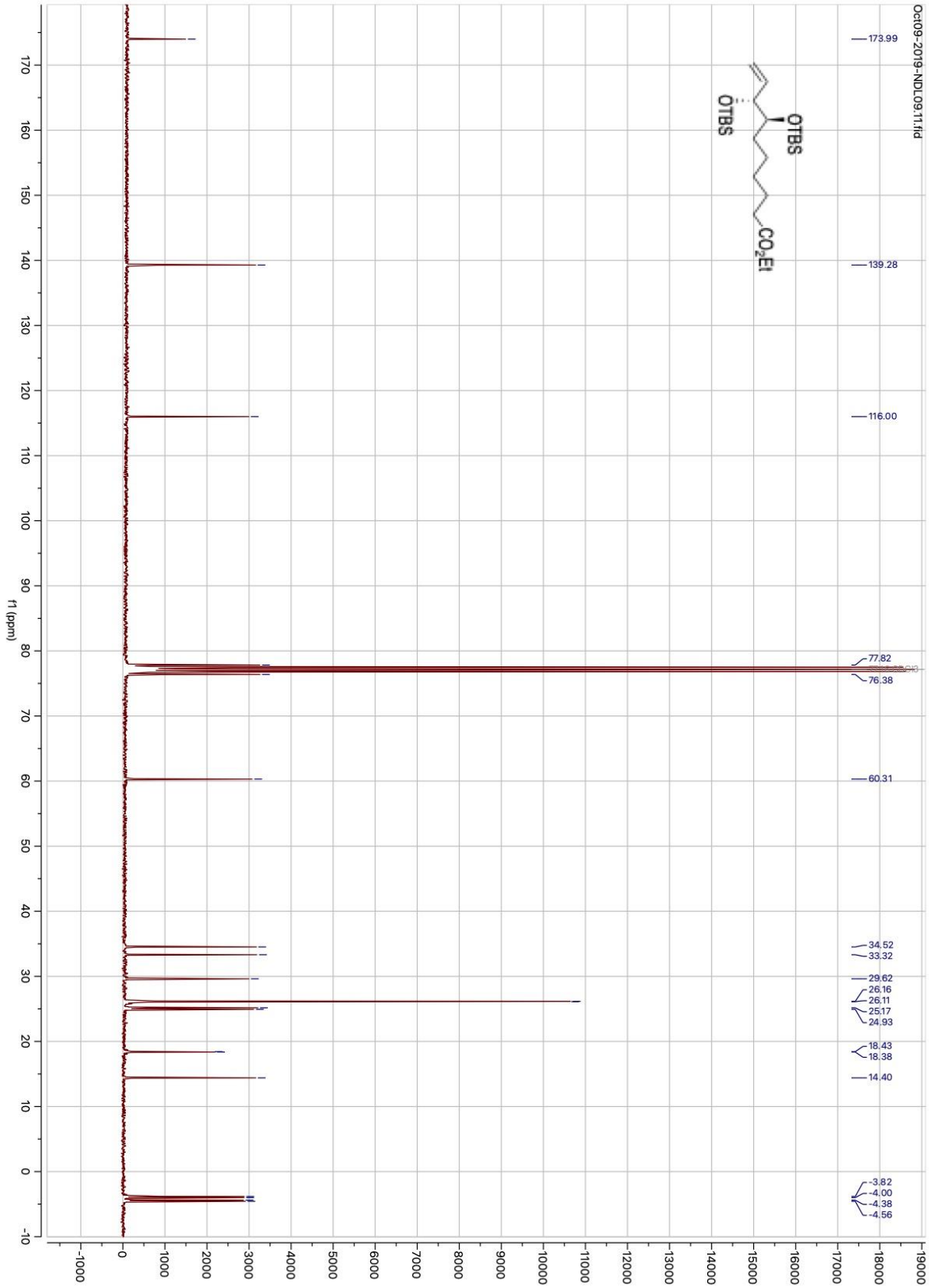

Figure 59: ^{13}C NMR spectrum of terminal alkene **6**.

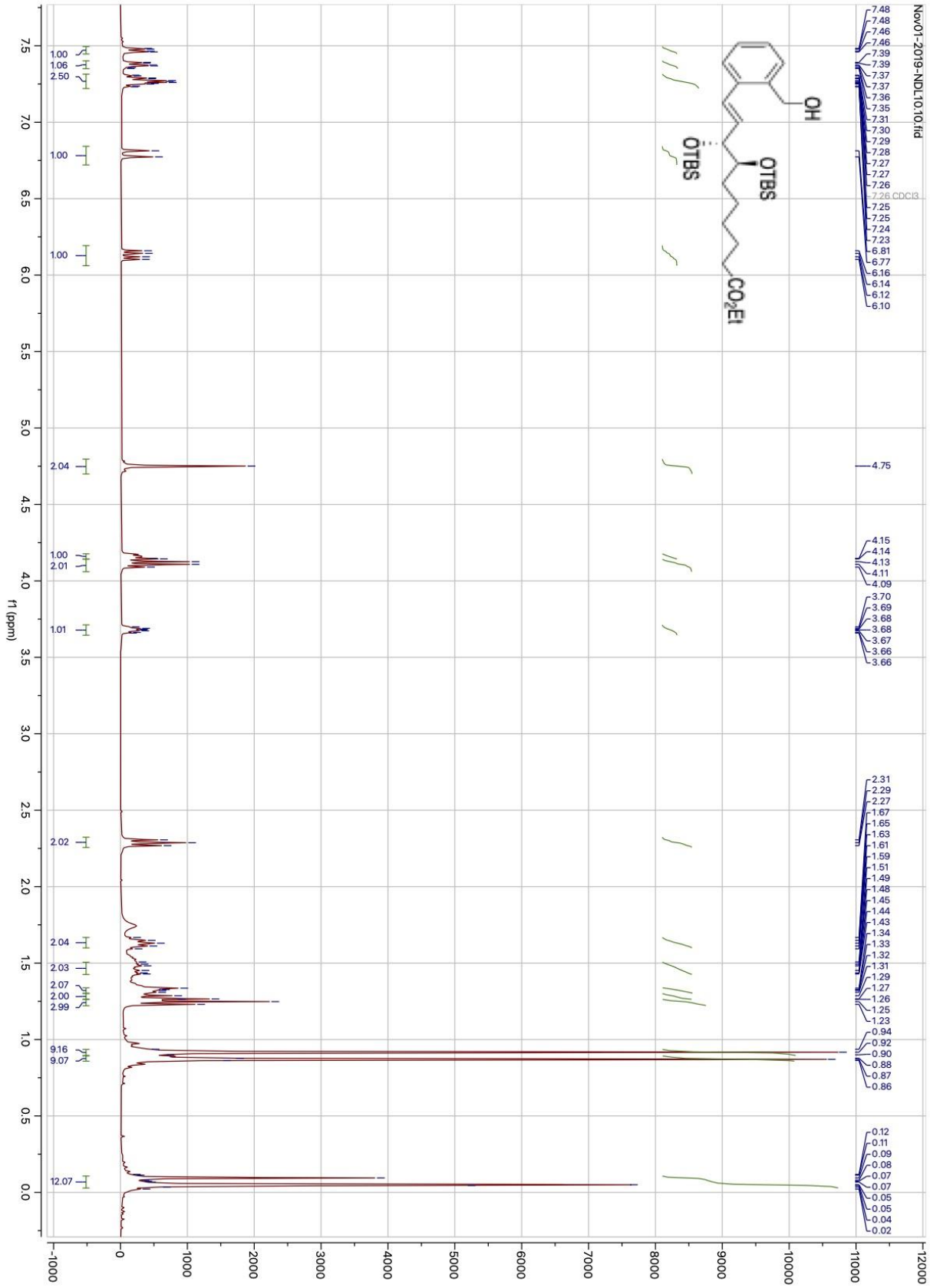

Figure 60: ^{1}H NMR spectrum of *ortho*-benzyl alcohol **57**.

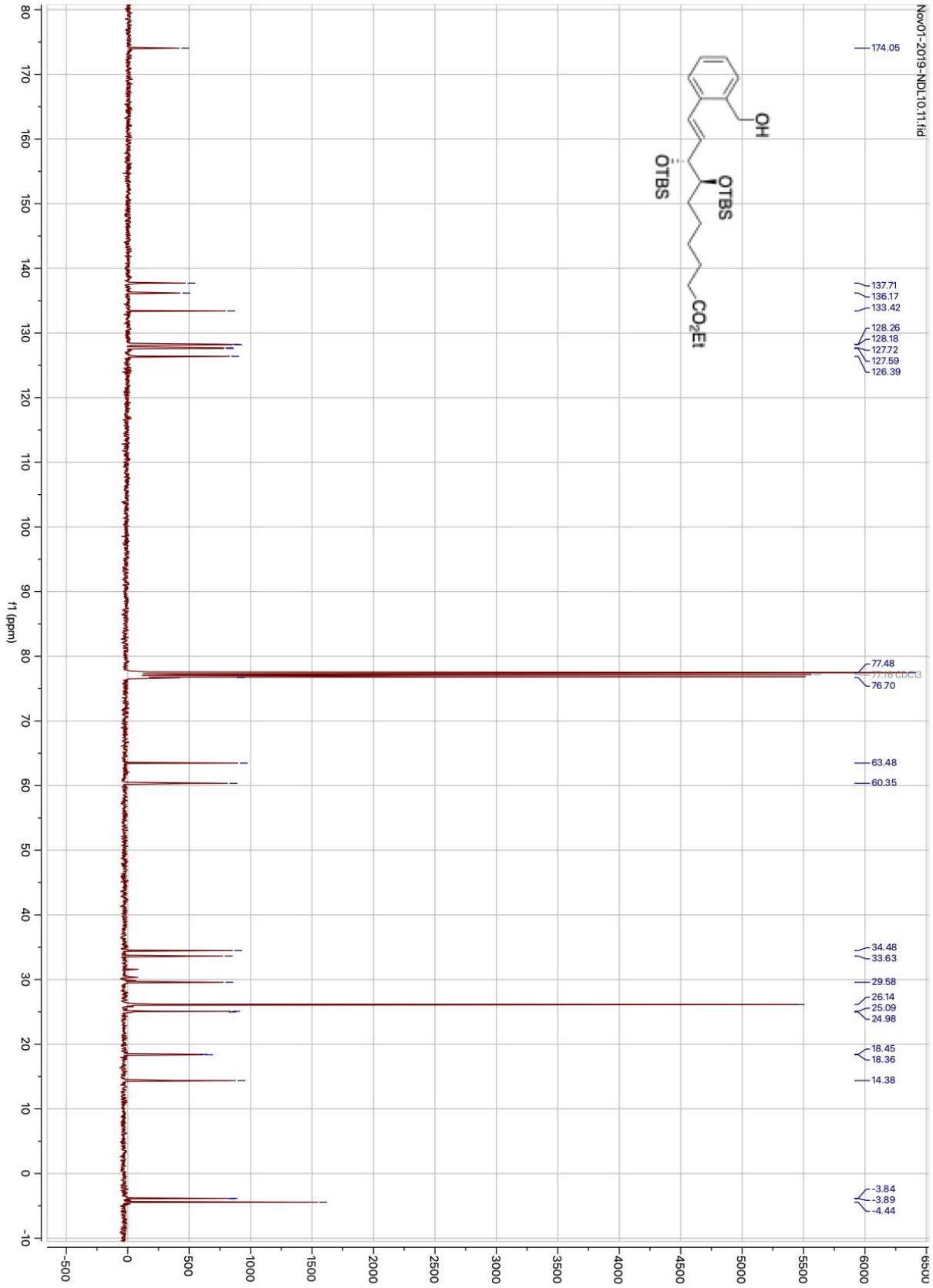

Figure 61: ^{13}C NMR spectrum of *ortho*-benzyl alcohol **57**.

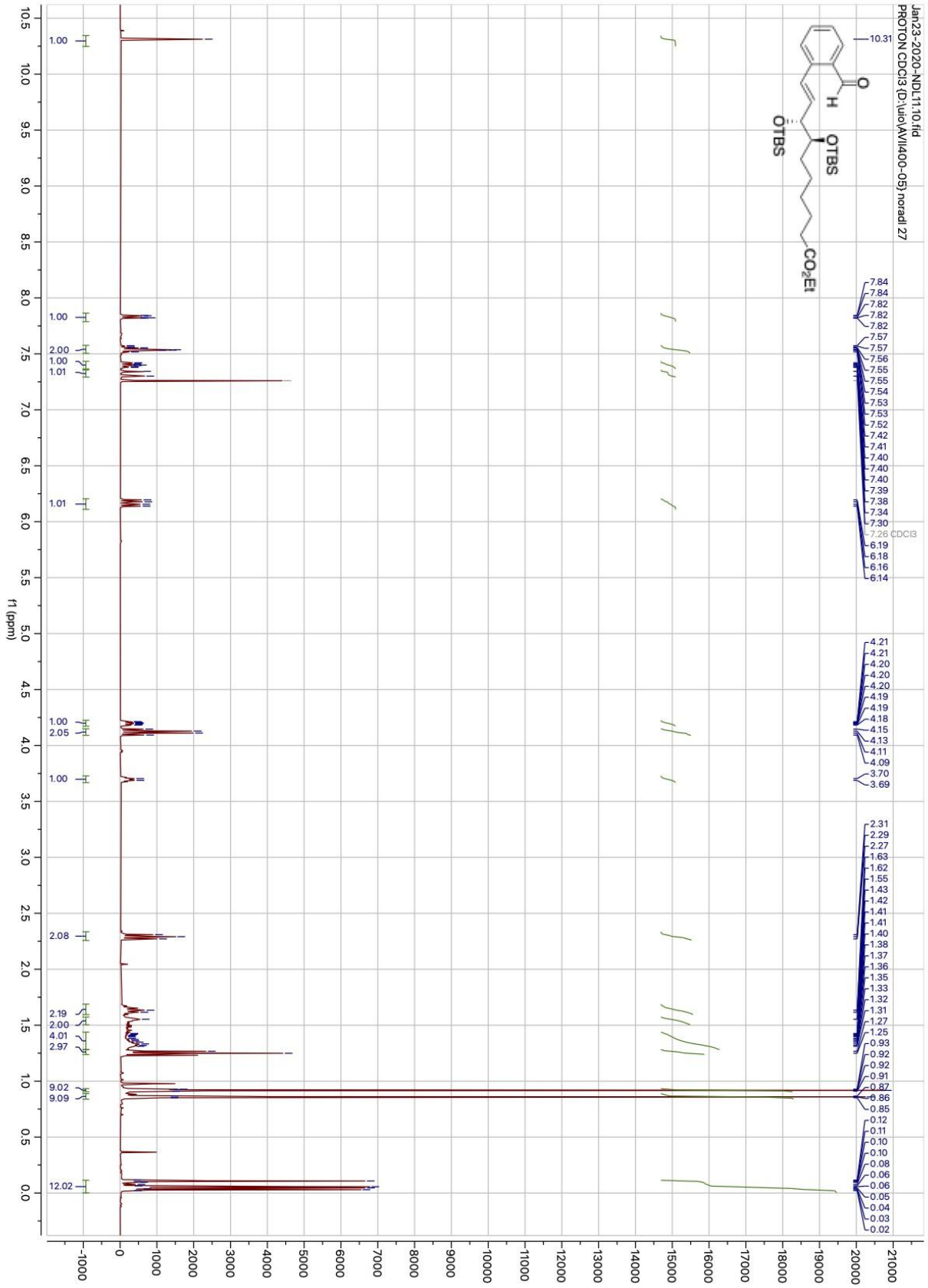

Figure 62: ^{1}H NMR spectrum of *ortho*-benzaldehyde **4**.

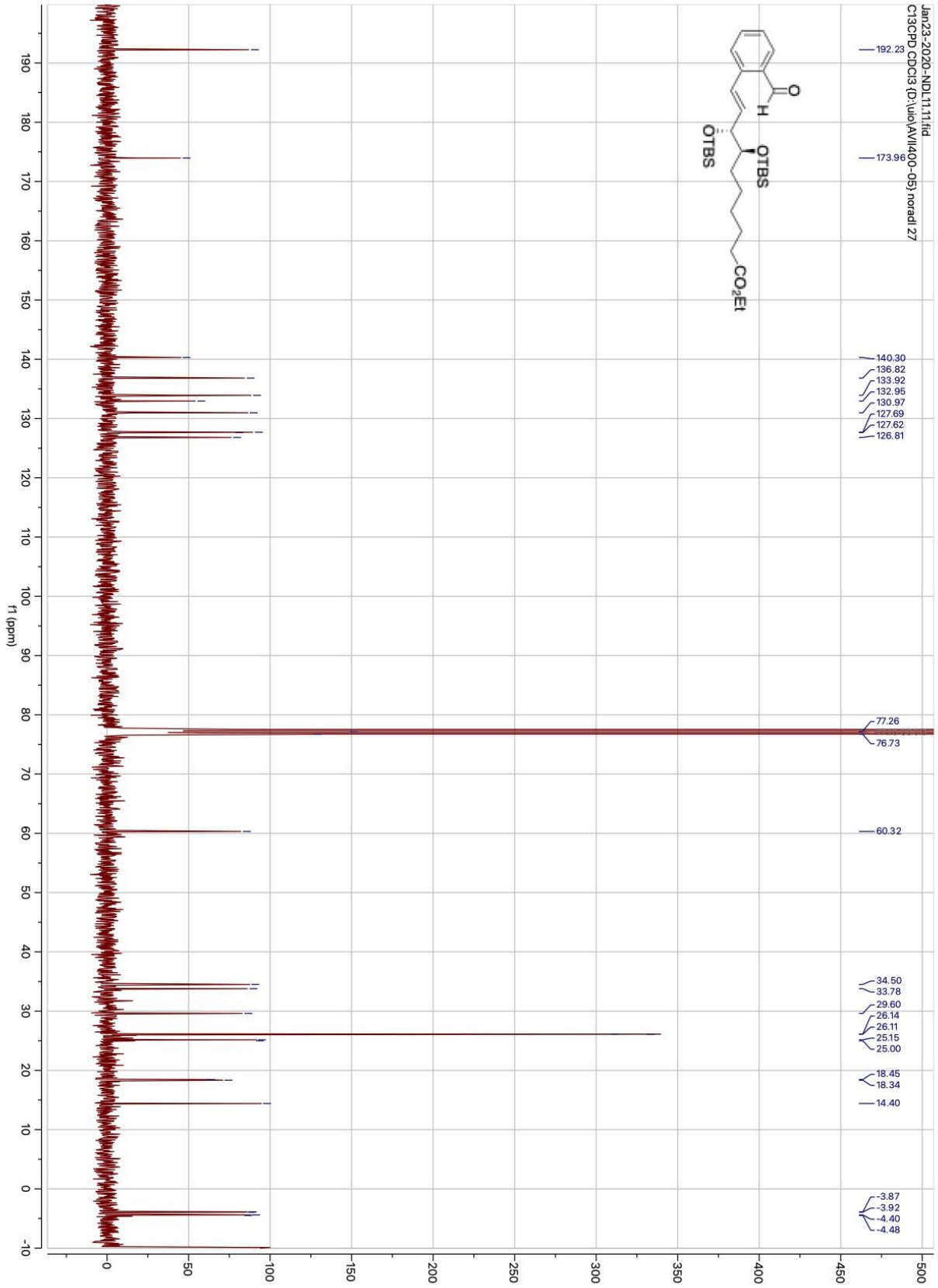

Figure 63: ^{13}C NMR spectrum of *ortho*-benzaldehyde **4**.

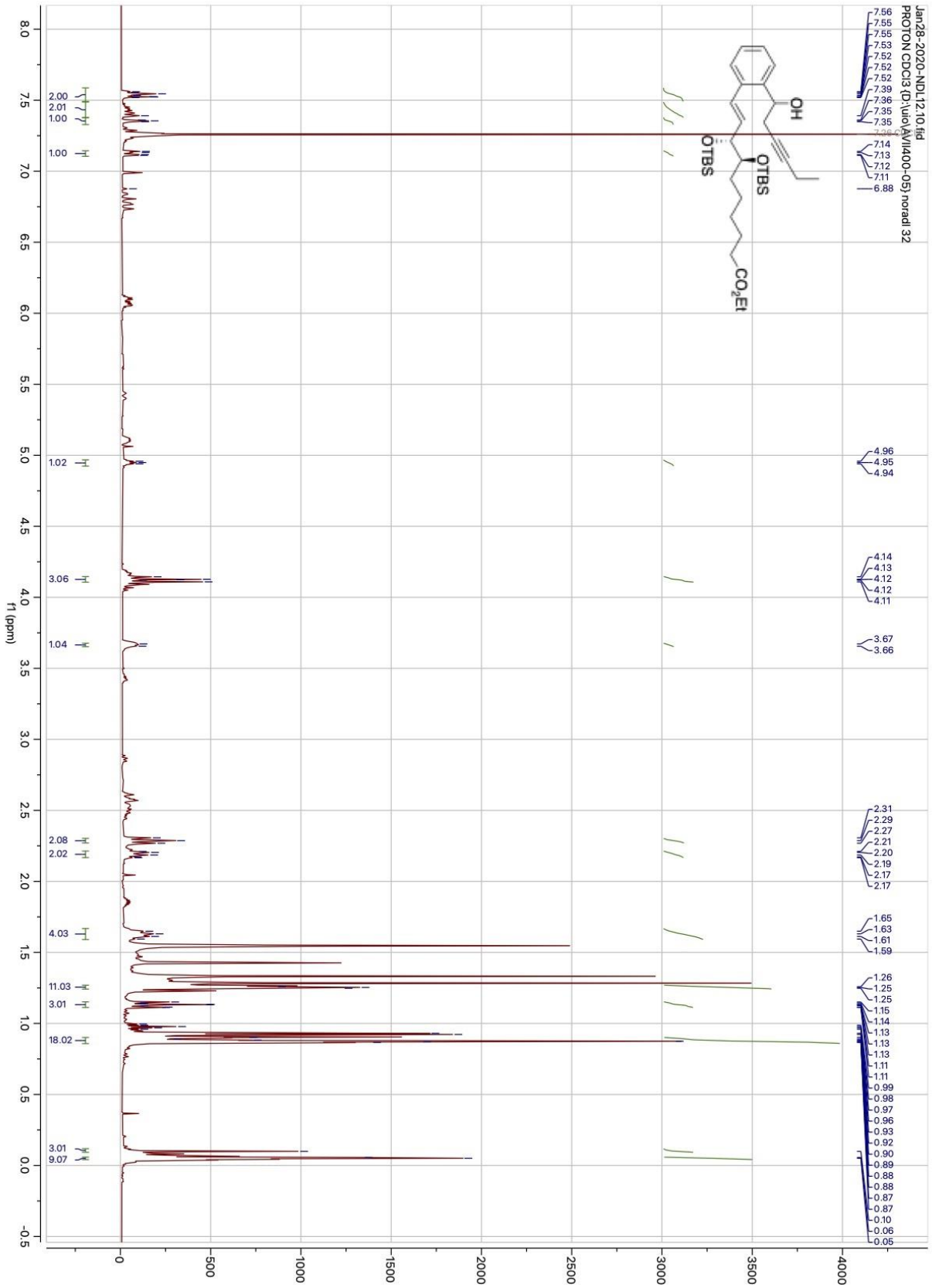

Figure 64: ^{1}H NMR spectrum for alkyne **63**.

6.2 MS and HRMS spectra

Terminal alkene 6 as sodium adduct, exact mass = 481.3140 *m/z*

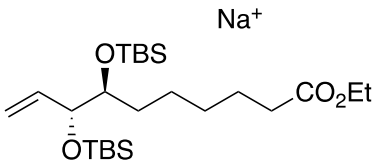

6

Figure 65: Structure of terminal alkene **6** as sodium adduct.

MS Spectrum Report

Analysis Info

Sample Name	AFR-41	Acquisition Date	8/27/2019 9:42:33 AM
Method	ESI_pos_50_1500_os.m	Analysis Name	D:\Data\maxis2019\15757.d

Acquisition Parameter

Source Type	ESI	Ion Polarity	Positive	Set Nebulizer	0.4 Bar
Focus	Not active	Set Capillary	3500 V	Set Dry Heater	200 °C
Scan Begin	50 m/z	Set End Plate Offset	-500 V	Set Dry Gas	4.0 l/min
Scan End	1500 m/z	Set Charging Voltage	2000 V	Set Divert Valve	Waste
		Set Corona	0 nA	Set APCI Heater	0 °C

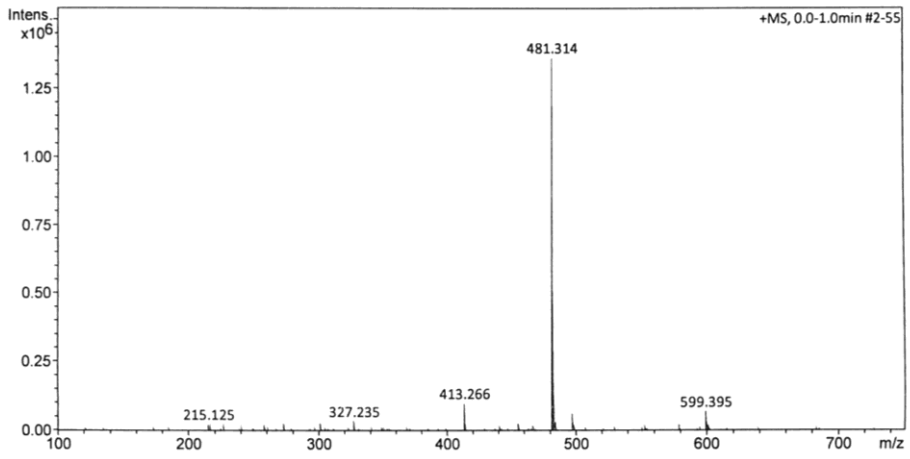

#	m/z	I %
1	215.125	1.7
2	217.105	1.2
3	227.125	1.3
4	258.149	1.6
5	273.167	1.8
6	301.141	2.2
7	327.235	2.5
8	413.266	7.4
9	414.270	2.0
10	455.298	1.9
11	481.314	100.0
12	482.316	34.0
13	483.314	9.5
14	484.315	2.3
15	497.288	4.7
16	498.290	1.6
17	553.459	1.0
18	579.312	1.6
19	599.395	5.0
20	600.398	2.3

Figure 66: MS spectrum of terminal alkene **6** as sodium adduct.

Elemental Analysis Report

Analysis Info

Sample Name	AFR-41	Acquisition Date	8/27/2019 9:42:33 AM
Method	ESI_pos_50_1500_os.m	Analysis Name	D:\Data\maxis2019\15757.d

Acquisition Parameter

Source Type	ESI	Ion Polarity	Positive	Set Nebulizer	0.4 Bar
Focus	Not active	Set Capillary	3500 V	Set Dry Heater	200 °C
Scan Begin	50 m/z	Set End Plate Offset	-500 V	Set Dry Gas	4.0 l/min
Scan End	1500 m/z	Set Charging Voltage	2000 V	Set Divert Valve	Waste
		Set Corona	0 nA	Set APCI Heater	0 °C

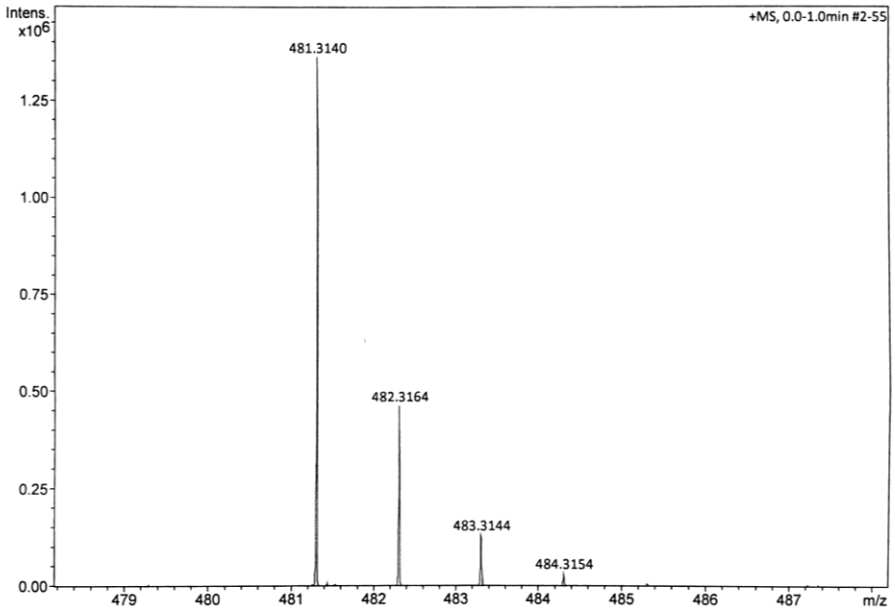

Meas. m/z	Ion Formula	m/z	err [ppm]
481.3140	C30H45O3Si	481.3132	-1.5
	C24H50NaO4Si2	481.3140	-0.0
	C27H45O7	481.3160	4.1
	C26H42N4NaO3	481.3149	1.9
	C25H46N4NaSi2	481.3153	2.8
	C26H49O4Si2	481.3164	5.0
	C24H37N10O	481.3146	1.3
	C25H46NaO7	481.3136	-0.9

Figure 67: HRMS of terminal alkene **6** as sodium adduct.

Ortho*-benzyl alcohol 57 as sodium adduct, exact mass = 587.3558 *m/z

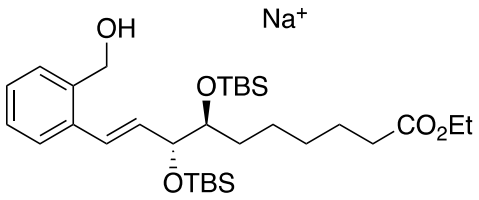

57

Figure 68: Structure of *ortho*-benzyl alcohol **57** as sodium adduct.

MS Spectrum Report

Analysis Info

Sample Name	NOL10	Acquisition Date	11/4/2019 12:51:48 PM
Method	ESI_pos_50_1500_os.m	Analysis Name	D:\Data\maxis2019\16085.d

Acquisition Parameter

Source Type	ESI	Ion Polarity	Positive	Set Nebulizer	0.4 Bar
Focus	Not active	Set Capillary	3500 V	Set Dry Heater	200 °C
Scan Begin	50 m/z	Set End Plate Offset	-500 V	Set Dry Gas	4.0 l/min
Scan End	1500 m/z	Set Charging Voltage	2000 V	Set Divert Valve	Waste
		Set Corona	0 nA	Set APCI Heater	0 °C

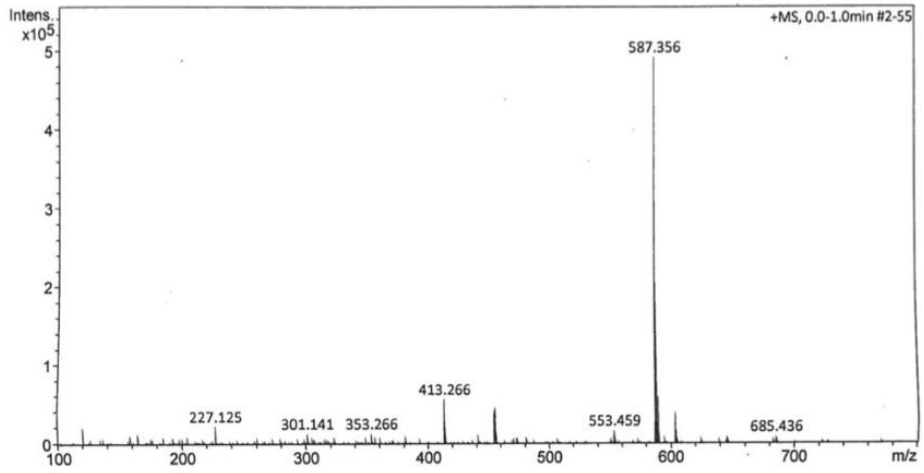

#	m/z	I %
1	120.987	4.1
2	158.903	2.1
3	164.920	2.6
4	204.913	1.9
5	227.125	4.5
6	301.141	2.6
7	301.180	1.8
8	353.266	2.7
9	413.266	11.6
10	414.270	3.1
11	455.259	9.1
12	456.262	2.8
13	553.459	3.4
14	587.356	100.0
15	588.358	42.1
16	589.358	12.2
17	590.358	3.3
18	603.330	8.0
19	604.332	3.5
20	685.436	1.8

Figure 69: MS spectrum of *ortho*-benzyl alcohol **57** as sodium adduct.

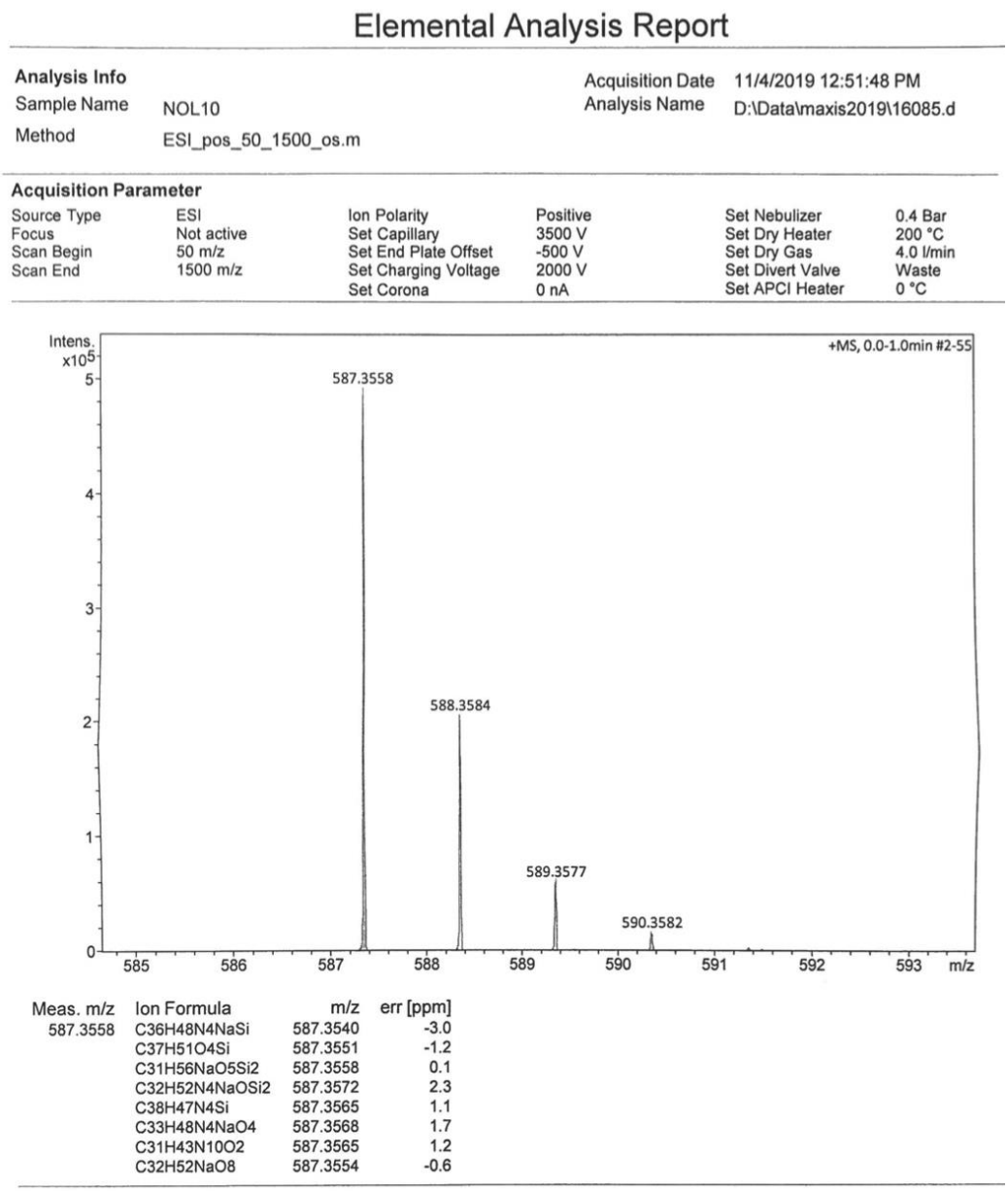

Figure 70: HRMS spectrum of *ortho*-benzyl alcohol **57** as sodium adduct.

Ortho*-benzaldehyde 4 as sodium adduct, exact mass = 585.3402 *m/z

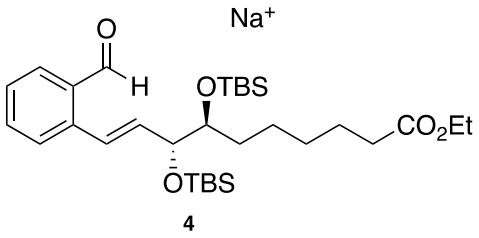

4

Figure 71: Structure of *ortho*-benzaldehyde **4** as sodium adduct.

MS Spectrum Report

Analysis Info

Sample Name	NDL11	Acquisition Date	1/29/2020 9:44:49 AM
Method	ESI_pos_50_1500_os.m	Analysis Name	D:\Data\maxis2020\16420.d

Acquisition Parameter

Source Type	ESI	Ion Polarity	Positive	Set Nebulizer	0.4 Bar
Focus	Not active	Set Capillary	3500 V	Set Dry Heater	200 °C
Scan Begin	50 m/z	Set End Plate Offset	-500 V	Set Dry Gas	4.0 l/min
Scan End	1500 m/z	Set Charging Voltage	2000 V	Set Divert Valve	Waste
		Set Corona	0 nA	Set APCI Heater	0 °C

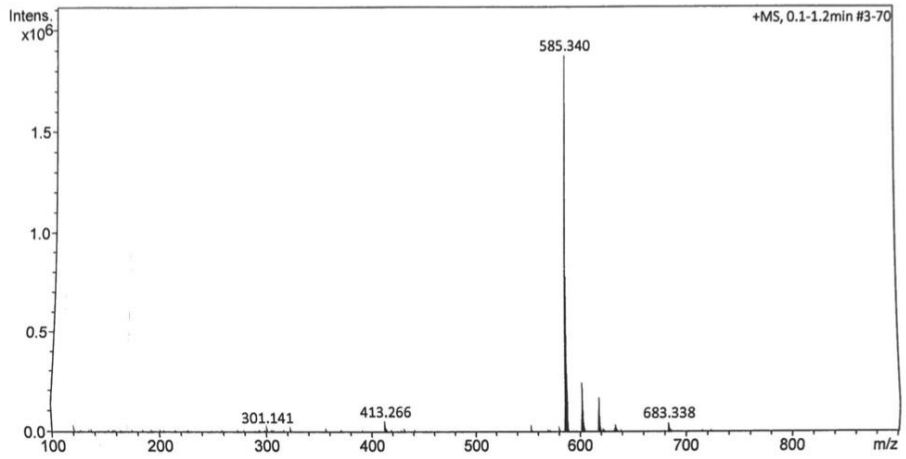

#	m/z	I %
1	120.987	1.0
2	301.141	1.2
3	413.266	2.8
4	553.459	1.0
5	580.385	0.9
6	585.340	100.0
7	585.485	1.0
8	586.343	41.8
9	587.342	12.5
10	588.343	3.4
11	601.314	13.0
12	602.317	5.5
13	603.314	2.5
14	604.316	0.9
15	617.366	9.1
16	618.369	4.1
17	619.369	1.2
18	633.340	1.8
19	683.338	2.4
20	684.341	1.0

Figure 72: MS spectrum of *ortho*-benzaldehyde **4** as sodium adduct.

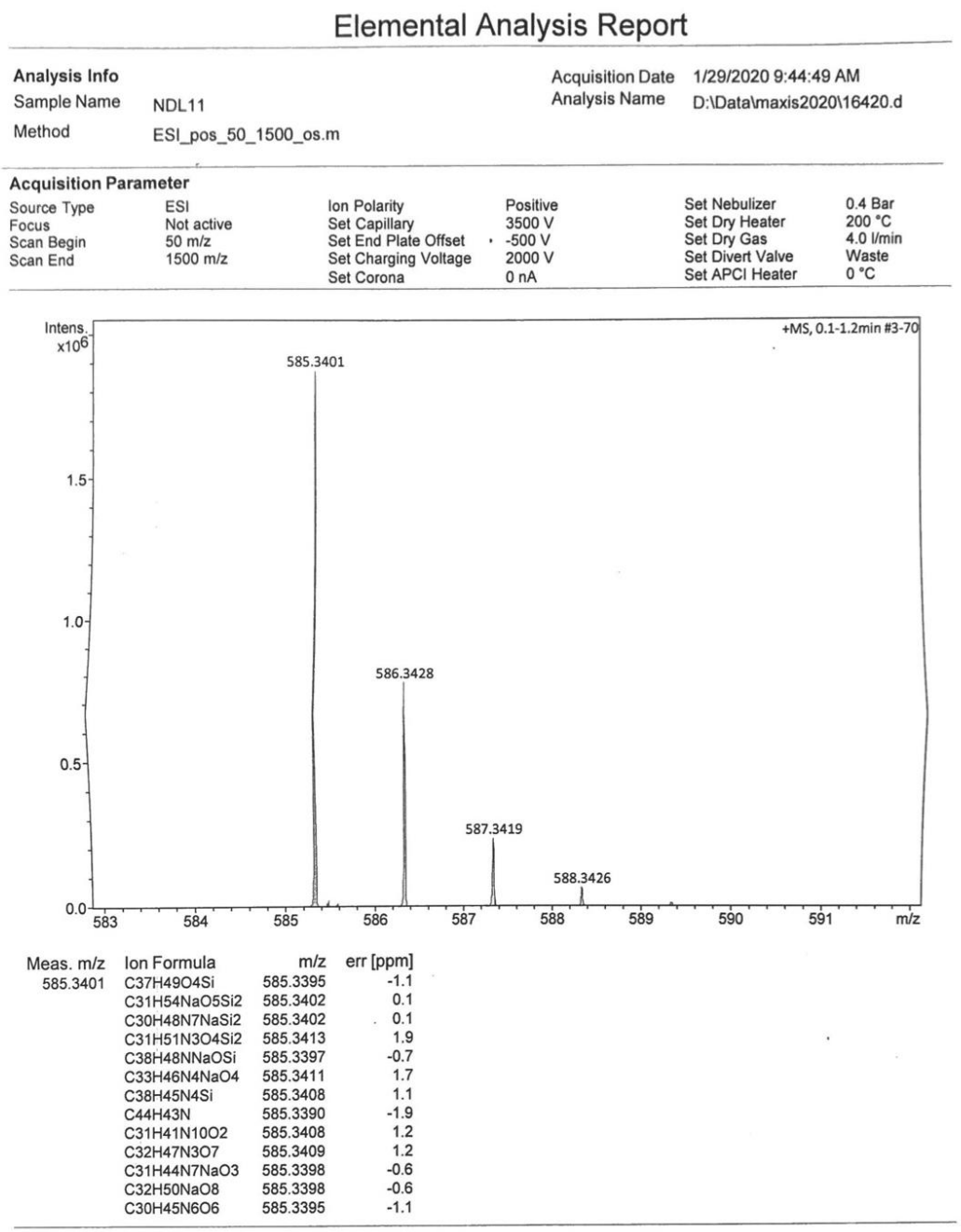

Elemental Analysis Report

Analysis Info

Sample Name	NDL11	Acquisition Date	1/29/2020 9:44:49 AM
Method	ESI_pos_50_1500_os.m	Analysis Name	D:\Data\maxis2020\16420.d

Acquisition Parameter

Source Type	ESI	Ion Polarity	Positive	Set Nebulizer	0.4 Bar
Focus	Not active	Set Capillary	3500 V	Set Dry Heater	200 °C
Scan Begin	50 m/z	Set End Plate Offset	-500 V	Set Dry Gas	4.0 l/min
Scan End	1500 m/z	Set Charging Voltage	2000 V	Set Divert Valve	Waste
		Set Corona	0 nA	Set APCI Heater	0 °C

Meas. m/z	Ion Formula	m/z	err [ppm]
585.3401	C37H49O4Si	585.3395	-1.1
	C31H54NaO5Si2	585.3402	0.1
	C30H48N7NaSi2	585.3402	0.1
	C31H51N3O4Si2	585.3413	1.9
	C38H48NNaOSi	585.3397	-0.7
	C33H46N4NaO4	585.3411	1.7
	C38H45N4Si	585.3408	1.1
	C44H43N	585.3390	-1.9
	C31H41N10O2	585.3408	1.2
	C32H47N3O7	585.3409	1.2
	C31H44N7NaO3	585.3398	-0.6
	C32H50NaO8	585.3398	-0.6
	C30H45N6O6	585.3395	-1.1

Figure 73: HRMS spectrum of *ortho*-benzaldehyde **4** as sodium adduct.

Alkyne 63 as sodium adduct, exact mass = 653.4028 *m/z*

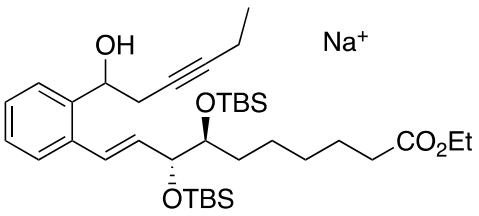

63

Figure 74: Structure of alkyne **63** as sodium adduct.

MS Spectrum Report

Analysis Info

Sample Name	NDL12	Acquisition Date	1/29/2020 8:07:14 AM
Method	ESI_pos_50_1500_os.m	Analysis Name	D:\Data\maxis2020\16414.d

Acquisition Parameter

Source Type	ESI	Ion Polarity	Positive	Set Nebulizer	0.4 Bar
Focus	Not active	Set Capillary	3500 V	Set Dry Heater	200 °C
Scan Begin	50 m/z	Set End Plate Offset	-500 V	Set Dry Gas	4.0 l/min
Scan End	1500 m/z	Set Charging Voltage	2000 V	Set Divert Valve	Waste
		Set Corona	0 nA	Set APCI Heater	0 °C

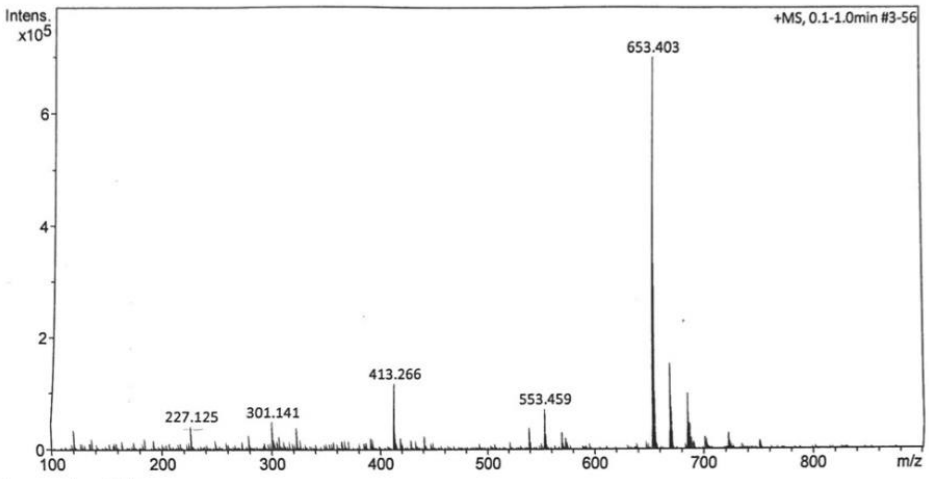

#	m/z	I %
1	120.987	4.9
2	227.125	5.9
3	301.141	7.0
4	323.256	5.6
5	413.266	17.1
6	414.270	4.4
7	539.316	5.4
8	553.459	10.3
9	569.433	4.3
10	653.403	100.0
11	654.406	47.8
12	655.405	14.7
13	656.406	4.1
14	669.377	22.1
15	670.379	10.9
16	671.378	4.8
17	685.436	14.2
18	686.439	6.6
19	687.364	6.5
20	722.527	4.0

Figure 75: MS spectrum of alkyne **63** as sodium adduct.

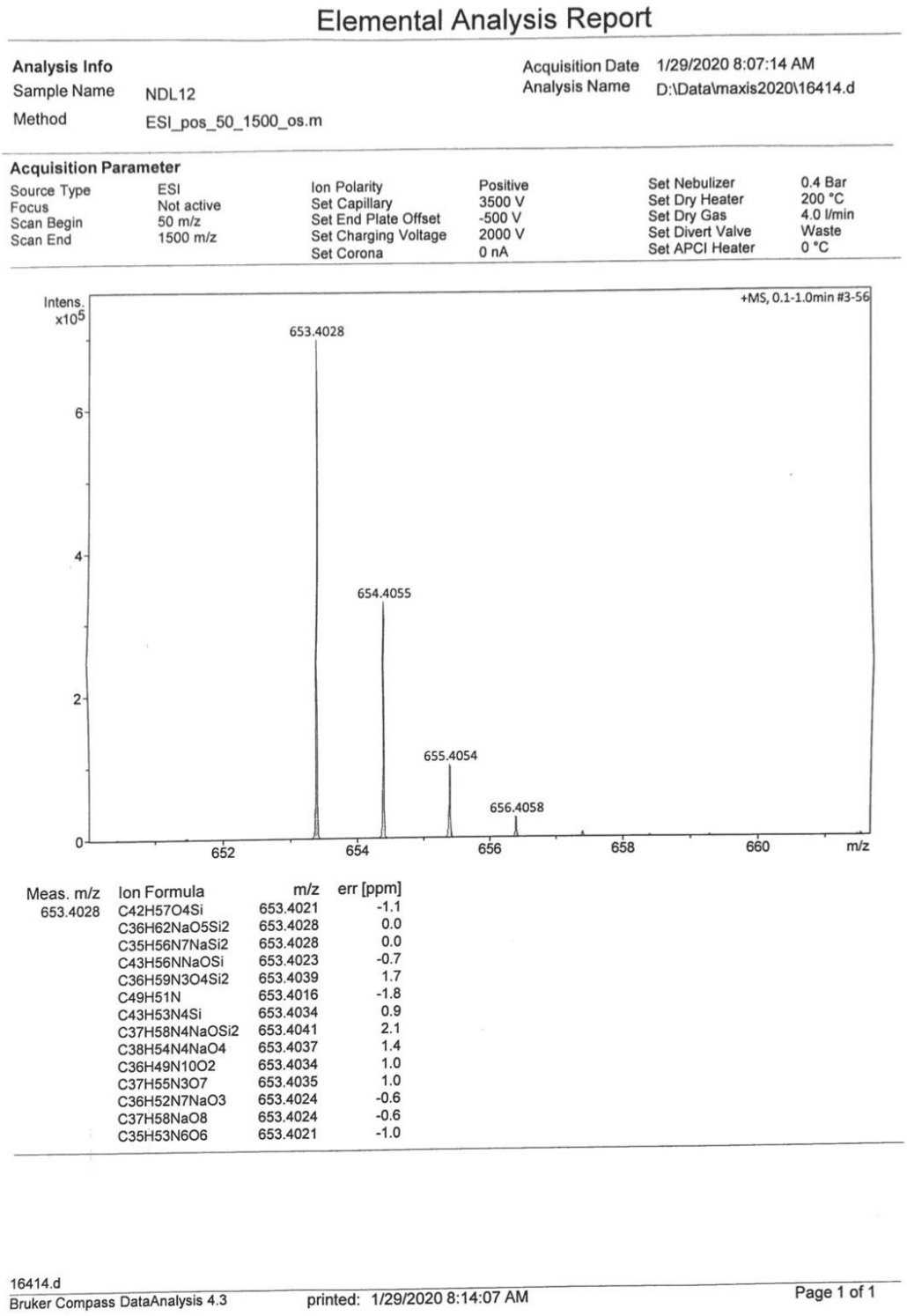

Figure 76: HRMS spectrum of alkyne **63** as sodium adduct.